

**University of Natural Resources  
and Life Sciences, Vienna**



**Department of Biotechnology**

(Head: Ao.Univ.Prof. Dipl.-Ing. Dr.nat.techn. Florian Rüker)



# **Heatprecipitation of homogenates: Scale-up study**

**Masterarbeit**

**zur Erlangung des akademischen Grades  
Diplom-Ingenieur**

**Verfasst von Christopher Zartler, BSc.**

Vorstand: Ao.Univ.Prof. Dipl.-Ing. Dr.nat.techn. Florian Rüker  
Supervisor: Assoc. Prof. Dipl.-Ing. Dr. Rainer Hahn  
Co-supervisor: Dipl.-Ing. Dr.nat.techn. Markus Luchner

## Eidesstattliche Erklärung

Ich erkläre ehrenwörtlich, dass ich die vorliegende Arbeit selbstständig und ohne fremde Hilfe verfasst habe, nicht andere als die angegebenen Quellen verwendet habe und die benutzten Quellen wörtlich oder inhaltlich entnommenen Stellen als solche kenntlich gemacht habe.

Tulln an der Donau, 26.02.2017  
Datum

Christopher Zoller  
Unterschrift

## Statutory declaration

I declare that I have authored this thesis independently, that I have not used other than the declared sources and that I have explicitly marked all material, quoted either literally or by content from the used sources.

Tulln an der Donau, 26.02.2017  
Date

Christopher Zoller  
Signature

0	Danksagung.....	3
1	Abstract.....	4
2	Introduction .....	5
2.1	History of GFP.....	5
2.2	Structure of GFP .....	5
2.3	Production of green fluorescent protein (GFP) .....	7
2.4	Heat precipitation step.....	7
3	Goals.....	8
4	Theory.....	9
4.1	Characterization of heat transfer in a jacketed stirred tank reactor .....	9
4.2	Dimensional analysis.....	10
4.3	Determination of the overall heat transfer coefficient $U$ .....	12
4.4	Heat precipitation .....	15
4.5	Separation of solids.....	15
4.6	Homogenization .....	17
4.7	Quantification of GFP .....	18
4.8	Turbidity .....	19
4.9	Solid fraction .....	19
4.10	Viscosity.....	19
4.11	Filtration .....	19
4.12	Particle sizes .....	22
4.13	SDS-PAGE .....	22
4.14	Adsorption isotherms.....	23
4.15	Quantification of DNA.....	23
5	Material and Methods .....	24
5.1	Cell line .....	24
5.2	Material .....	24
5.3	Chemicals .....	26
5.4	Methods .....	27
6	Results.....	36
6.1	Design and calculation of heat precipitation step.....	36
6.2	Heat precipitation in small scale .....	47
6.3	Heat precipitation in large scale.....	50
6.4	Homogenization trials.....	53
6.5	Separation.....	59
6.6	SDS-PAGE of large scale trials .....	62
6.7	Filtration .....	64
6.8	Production of GFP with implemented heat precipitation .....	68
7	Summary and conclusion .....	80
8	Symbols and mathematical notation.....	81

9	Abbreviations .....	83
10	Tables.....	84
11	Figures .....	85
12	Literaturverzeichnis.....	87
13	Appendix.....	89
13.1	Filtration trials in small scale.....	89

## 0 Danksagung

Ich möchte mich zu Beginn bei einigen Menschen bedanken, ohne die diese Arbeit nicht zustande gekommen wäre.

Zweifellos ist ein Studium mit einem erheblichen Arbeitsaufwand verknüpft. Genauso wichtig, wie die hineingesteckte Arbeit sind aber auch die Pausen. Diese Pausen in Gesellschaft von Menschen verbringen zu können, die mir nahe stehen war für mich immer eine Quelle der Kraft und Erholung.

Vor Allem danke ich meiner Familie für ihre außergewöhnliche moralische Unterstützung. Durch sie fand ich immer wieder die Kraft und Motivation weiterzumachen, sowohl was meine Ausbildung, als auch mein Privatleben betrifft. Ich möchte mich außerdem für die keinesfalls selbstverständliche finanzielle Unterstützung während meines gesamten Ausbildungswegs bedanken.

Genauso wichtig, wie meine Familie sind gute Freunde. Freunde, mit denen man sich über das Studium, das Private, über Gott und die Welt unterhalten kann. Mein besonderer Dank gilt Andreas Bayer, Philipp Andre und Domenik Ferstl. Gute bzw. echte Freunde erkennt man meiner Ansicht nach daran, dass der Kontakt und das Interesse auch dann bestehen bleibt, wenn man sich nicht mehr regelmäßig sieht. Ich bin froh, dass wir uns während unserer HTL Ausbildung kennen gelernt haben.

Bezüglich meiner Ausbildung möchte ich mich bei Dr. Wolfgang Kandler bedanken. Ich bin glücklich, die Gelegenheit bekommen zu haben, meine Bachelorarbeit unter seiner Betreuung zu verfassen. Dadurch konnte ich viel Nützliches über das Arbeiten im wissenschaftlichen Milieu lernen.

Weiters möchte ich mich bei Dr. Rainer Hahn und Dr. Markus Luchner für die Betreuung meiner Diplomarbeit bedanken. Die einmalige Möglichkeit, diese Arbeit in der Pilotanlage der Universität für Bodenkultur zu absolvieren empfand ich als sehr spannend und lehrreich. Die Tatsache, dass ihre Tür jederzeit für meine Fragen und Anliegen offen stand empfand ich als großartige Unterstützung.

Die Pilotanlage war für mich sehr beeindruckend und im ersten Moment auch etwas überfordernd. Ich möchte mich bei Clemens Keinprecht, Sabine Necina und Bernhard Sissolak bedanken, die mir mit Rat und Tat zur Seite standen, um mich dort zurechtzufinden.

Zuletzt möchte ich mich bei allen Teilnehmern der Lehrveranstaltung „Bioprocess Engineering Laboratory“ des Sommersemesters 2016 bedanken. In diesem Kurs wurden die Ergebnisse meiner Arbeit mit ihrer Unterstützung implementiert.

## 1 Abstract

In this work the process of heat transfer in a stirred tank reactor equipped with a jacket was characterized on a basis of water as modelling fluid. Heat transfer was split up into the different resistances of the thermal boundary layers on the jacket and the vessel side. These individual resistances were calculated by published correlations to obtain the theoretical overall heat transfer coefficient. Moreover an overall heat transfer coefficient was determined in practical experiments. Theoretical calculation yielded an overall heat transfer coefficient of 370.0 W/m<sup>2</sup>K for heating and 283.6 W/m<sup>2</sup>K for cooling. Practical determination yielded an overall heat transfer coefficient of 445.7 W/m<sup>2</sup>K for heating and 326.2 W/m<sup>2</sup>K for cooling.

The determined overall heat transfer coefficient was then used to model the heat precipitation process of a recombinant protein solution. The temperature profile prediction was compared to the actual heat precipitation of green fluorescent protein containing homogenate and the stability of green fluorescent protein to the heat treatment was assessed in small and large scale experiments.

Heat precipitation was investigated in small scale and was then scaled up to 50 kg homogenate. In order to provide the best material for heat precipitation, homogenization was investigated in detail with respect to release of green fluorescent protein, viscosity and cell debris particle size. Also the downstream steps after heat precipitation were investigated. These include separation of precipitate, depth and sterile filtration of supernatant in small scale and scale up, ultrafiltration and diafiltration, chromatography capture step (anionic exchange chromatography).

It could be shown, that the heat precipitation significantly improved the process. The separation of heat precipitate was shown to be more efficient. The obtained supernatant required less filter area for sterile filtration. The capacity on the anion exchanger *CaptoQ* was significantly higher.

## 2 Introduction

### 2.1 History of GFP

The first step in the discovery of GFP was a study of the jellyfish *Aequorea victoria* from Davenport and Nicol in 1955. They recognised, that the jellyfish was glowing due to a chemical reaction induced by light, which provides energy leading to the photon release responsible for the observed glowing. In the 1960s Shimomura et.al. discovered GFP as an associate to aequorin and noticed, that  $\text{Ca}^{2+}$  is needed in order to observe fluorescence. They found out, that  $\text{Ca}^{2+}$  leads to a conformational change of aequorin (Shimomura, The discovery of aequorin and green fluorescent protein, 2005). This induces a chemical reaction in which the chromophore undergoes an excitation state. During relaxation of aequorin some of the energy is transferred in a radiationless manner to GFP. As a consequence, the emitted light appears green. 1970 Shimomura postulated, that the chromophore of GFP was 4-(p-hydroxybenzylidene)imidazole-5 attached to a peptide backbone via the one and two positions of the ring. In 1974 Morise et.al. (Morise, Shimomura, Johnson, & Winant, 1974) managed to purify and crystallize GFP for the first time and confirmed the energy transfer from aequorin to GFP. Later the exact structure and mechanism of the chromophore was elucidated in 1979 by Shimomura. He described the type of energy transfer as a Förster-type-energy-transfer (Shimomura, Structure of the Chromophore of Aequorea Green Fluorescent Protein, 1979).

The idea arised to use GFP as a marker in cell biology by fusing it to other proteins in the cell. Due to the fluorescence properties one could map the occurrence of the targeted proteins in the cell or even whole cells specific to e.g. a certain organ. In 1992 it was Prasher (Prasher, Eckenrode, Ward, & Prendergast, 1992), who firstly identified the nucleotide sequence of wild-type GFP and only two years later Chalfie was able to express the coding sequence in *E.coli* and *C.elegans*. Tsuji reported the expression of recombinant GFP in 1994 (Inouye & Tsuji, 1994).

Since the wild-type GFP was shown to have several weaknesses, many groups started efforts in engineering of the protein. Targets were to improve its thermal stability, pH sensitivity and quantum yield. Especially the aminoacids associated directly to the chromophore were investigated closely. With increasing understanding several GFP-like variants were engineered by Tsien et.al. even emitting other light colours than green (Roda, 2010), (Tsien, 2010), (Sanders & Jackson, 2009).

Nowadays GFP is used for a variety of applications including e.g. the use as fusion tags, reporter gene or for photobleaching (Zimmer, 2002).

### 2.2 Structure of GFP

GFP stands for green fluorescent protein. Its wild-type form is composed of 238 aminoacids, which are arranged in 11  $\beta$ -strands protecting a central  $\alpha$ -helical structure containing the chromophore. The  $\beta$ -strands are arranged in the fashion of a  $\beta$ -barrel.

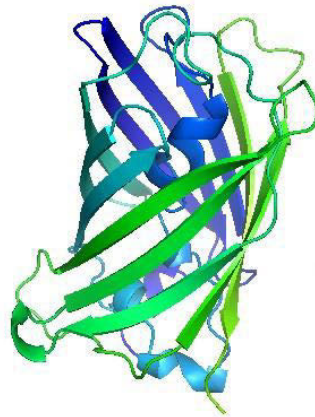


Figure 1: Structure of wild-type GFP (taken from PDB database, Code: 1GFL)

During the formation of GFP the folding is very important for its fluorescence properties. The chromophore is formed from the aminoacids *Ser65*, *Tyr66* and *Gly67*, which are covalently linked. In presence of oxygen they are oxidized to make the chromophore functional. If the group was alone, no fluorescence would be observed but at this point the protein fold comes into play. All known fluorescent proteins consist of two rings with a double bond derived from the dipeptide *Tyr-Gly*. These rings are usually arranged coplanar in the ground state. If the chromophore would then be supplied with excitation energy the arrangement of the rings would simply change to a perpendicular state. However the tight structure of GFP restrains the freedom of the rings in a way that they have to stay coplanar. Therefore the excitation energy, taken up by the electrons, has to be dissipated as light. There are two local absorbance maxima, since the chromophore can exist in an anionic or neutral form (Remington, 2011).

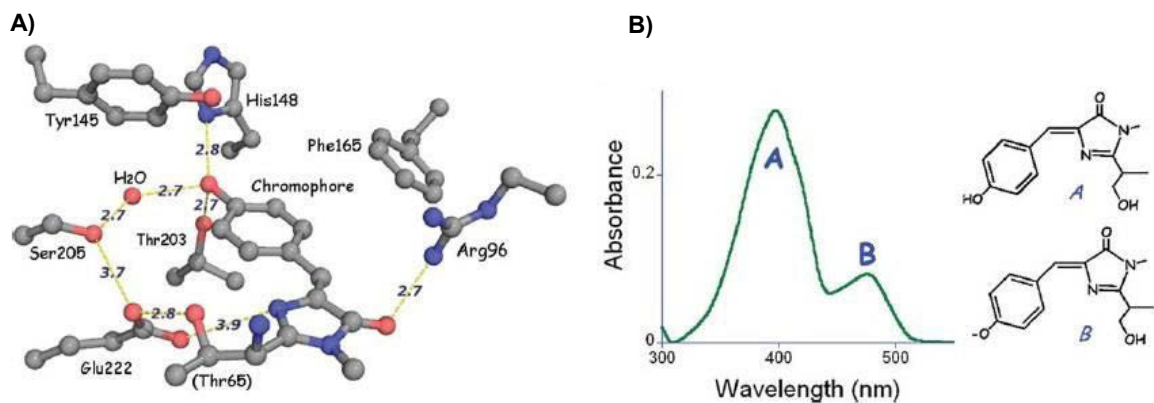


Figure 2: A) Structure of the chromophore of the S65T variant of GFP (red = oxygen, blue = nitrogen, other interactions = yellow, dashed); B) emission wavelengths of and their chromophore structure at the emission peaks of natural GFP

This chemical structure is utilized in nature in phenomena like bioluminescence. For bioluminescence GFP has the function of an acceptor for energy supplied by either  $\text{Ca}^{2+}$  activated photoproteins like the above mentioned aequorin or the well-known luciferase-oxyluciferine-system (Prasher, Eckenrode, Ward, & Prendergast, 1992).

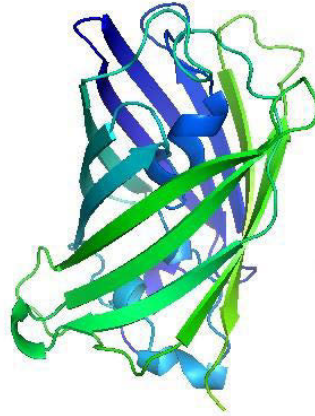


Figure 1: Structure of wild-type GFP (taken from PDB database, Code: 1GFL)

During the formation of GFP the folding is very important for its fluorescence properties. The chromophore is formed from the aminoacids *Ser65*, *Tyr66* and *Gly67*, which are covalently linked. In presence of oxygen they are oxidized to make the chromophore functional. If the group was alone, no fluorescence would be observed but at this point the protein fold comes into play. All known fluorescent proteins consist of two rings with a double bond derived from the dipeptide *Tyr-Gly*. These rings are usually arranged coplanar in the ground state. If the chromophore would then be supplied with excitation energy the arrangement of the rings would simply change to a perpendicular state. However the tight structure of GFP restrains the freedom of the rings in a way that they have to stay coplanar. Therefore the excitation energy, taken up by the electrons, has to be dissipated as light. There are two local absorbance maxima, since the chromophore can exist in an anionic or neutral form (Remington, 2011).

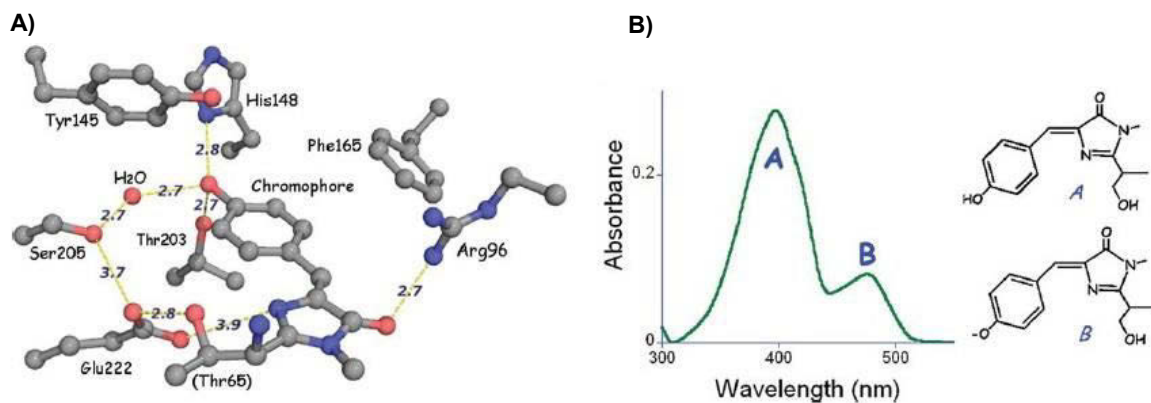


Figure 2: A) Structure of the chromophore of the S65T variant of GFP (red = oxygen, blue = nitrogen, other interactions = yellow, dashed); B) emission wavelengths of and their chromophore structure at the emission peaks of natural GFP

This chemical structure is utilized in nature in phenomena like bioluminescence. For bioluminescence GFP has the function of an acceptor for energy supplied by either  $\text{Ca}^{2+}$  activated photoproteins like the above mentioned aequorin or the well-known luciferase-oxyluciferine-system (Prasher, Eckenrode, Ward, & Prendergast, 1992).

### **2.3 Production of green fluorescent protein (GFP)**

The following protocol is used in the students laboratory course “Bioprocess Engineering Laboratory”:

For production of recombinant GFP the organism *E.coli HMS174(DE3) pET11a GFPmut3.1* is used. This is done by fed batch fermentation at 37°C at pH 7.0 with an oxygen saturation of 30%. The product is formed in soluble form in the cytosol. For primary harvest, the cells are separated from the media by a centrifugation step. The resulting cell paste is resuspended in homogenization buffer and undergoes a cell break up step in a homogenizer. During this step, the product is released from the cells by disrupting their cell walls by mechanical stress resulting from high pressure. In the following step, the debris are removed. The supernatant then is filtrated through a depth filter to remove bigger particles. The filtrate then is filtrated through a sterile filter and is then ultrafiltrated for concentration of product, if necessary. For removal of salt a diafiltration step follows. In an anion exchange chromatography the product gets captured. The product containing fraction is then applied to a hydrophobic interaction chromatography for purification. Then the product is further purified by a size exclusion chromatography and sterile filtrated.

### **2.4 Heat precipitation step**

In a previous study it was shown that especially the filtration step after debris removal has been problematic. The homogenate includes many undesired components of disintegrated cells like proteins and DNA which lead to formation of a precipitate. This process is slow at room temperature and therefore the filtrated solution forms precipitate right after filtration again. The precipitation can be accelerated by applying heat to the homogenate. Since GFP is quite stable at higher temperatures the solution can be heated above many proteins' melting points. As a result these proteins precipitate and GFP stays in the supernatant in its active form (Fink, 2015).

### 3 Goals

In this work the process of heat precipitation should be investigated. This will involve different steps:

#### Modelling of heat transfer with water

- Characterization of heat transfer in the available stirred tank reactor with the modelling fluid water
- Calculation of the theoretical overall heat transfer coefficient  $U$  from the individual resistances involved in heat transfer by use of published correlations; the individual resistances will be calculated for the vessel side and the jacket side and then will be used for the calculation of  $U$
- Determination of  $U$  from experiments with water

#### Heat precipitation of homogenate for GFP production

- Precipitation will be investigated in small scale and large scale
- Predicted temperature profile of heat precipitation with determined  $U$  for the modelling liquid water will be compared to experimental temperature profile
- Downstream processing for the purification of GFP will be investigated with a focus on homogenization parameters and their effects on heat precipitation and further downstream steps like filtration and chromatography
- Stability of GFP to heat will be investigated by SDS-PAGE

#### Implementation of heat precipitation into the downstream of GFP

The whole downstream process will be investigated with an included heat precipitation step. All steps will be analyzed with respect to their GFP yield and functionality. The process steps will be (chronologically) fermentation, cell harvest, cell homogenization, heat precipitation, separation of precipitate, depth and sterile filtration of supernatant in small scale and scale up, ultrafiltration and diafiltration, chromatography steps (AIEX, HIC, SEC) and final sterile filtration.

## 4 Theory

### 4.1 Characterization of heat transfer in a jacketed stirred tank reactor

The aim of the characterization of a system of heat transfer is to be able to predict the intended process as exact as possible. One is interested in the costs arising from the process step, which e.g. involve the amount of heat transfer media needed. This depends on the properties of the media and the process solution which determine the energy necessary. Another important parameter is the time needed for the process step. It is possible to predict the time of the heating and cooling step by calculating an overall heat transfer coefficient from model trials with a similar solution to the intended solution to be processed.

The overall heat transfer coefficient depends on the whole system of heat transfer. That includes:

- Temperatures of the media (bulk inside the vessel, heating/cooling media)
- Flow velocity of heating/cooling media and geometry of inlets/outlets (function of geometry of the vessel and the stirrer – characterized by Reynolds-number)
- Material properties of the vessel

These influences allow to segregate the overall heat transfer coefficient into a sum of individual resistances. These are the resistances of the thermal boundary layers at the jacket's wall and the resistance of the wall itself. This relationship can be expressed as

$$\frac{1}{UA_m} = \frac{1}{h_c A_c} + \frac{B}{\lambda_w A_m} + \frac{1}{h_h A_h} \quad \text{Eq.(4-1)}$$

where  $U$  is the overall heat transfer coefficient in  $[W/m^2K]$ ,  $h_c$  and  $h_h$  are the individual heat transfer coefficients of the thermal boundary layers in  $[W/m^2K]$ ,  $\lambda_w$  is the thermal conductivity of the wall in  $[W/mK]$ ,  $B$  is the thickness of the wall in  $[m]$ ,  $A_m$  is the area involved in heat transfer in  $[m^2]$  and the indices  $c$  and  $h$  represent the cold and the hot side of the system respectively and the index  $m$  represents the average area involved in heat transfer.  $U$  is the amount of energy transferred per unit time per unit temperature difference between hot and cold side and unit area involved in heat transfer.

The evaluation of  $U$  depends on whether the temperature of the leaving heating/cooling media is a function of time or remains constant.

If  $U$  and the properties of involved solutions are known, one can easily calculate the time needed for heating up or cooling down a certain amount of process solution. Since the homogenates in the process are aqueous solutions, trials with water allow a good estimate of  $U$ .

To identify low transfer zones in the heat transfer system, it is possible to determine the individual resistances ( $h$ ) to heat transfer by published correlations. It is possible to start the calculations from both sides. There are correlations for the inside of a cylindrical vessel to estimate the individual heat transfer coefficient of the thermal boundary layer on the inside, but also procedures to estimate the individual heat transfer coefficient of the thermal boundary layer on the side of the jacket.

In this work the procedure of Lehrer and a correlation for cylindrical vessels without baffles will be used and compared.

## 4.2 Dimensional analysis

### 4.2.1 Base quantities

For dimensional analysis there are seven base quantities. These quantities are used in dimensional analysis to reduce the amount of variables influencing the process, which should be investigated.

Table 1: Base quantities

Quantity	SI unit	Symbol	Dimension
Length	meter	m	L
Time	second	s	T
Mass	kilogram	kg	M
Temperature	kelvin	K	$\Theta$
Amount of substance	mole	mol	N
Electric current	ampere	A	I
Luminous intensity	candela	cd	J
Plane angle	radian	rad	1
Solid angle	steradian	sr	1

### 4.2.2 Dimensionless quantities

Efficiency in heat transfer involving fluid phases is dependent on many different variables. These are on the one hand the properties of involved media like viscosity, density, thermal conductivity, heat capacity and heat expansion. On the other hand the geometry of the device where heat transfer is occurring is important. Heat transfer is also dependent on the motion of the fluid media. Varying all those variables in experiments would be enormous effort. Therefore one uses model theory, which is based on the assumption, that velocity fields and temperature fields can be described in the form of dimensionless variables. These variables are independent of the applied system of units, because they are related to a reference magnitude like e.g. a specific temperature difference or a specific length. As a result it is possible to sum up more than one influencing variable in a dimensionless quantity. If this quantity is equal in two systems, then the systems are said to be similar. If the dimensionless quantity  $K$  depends on  $n$  variables and  $K$  is a power product, then  $K$  is a function of those variables with the form of

$$K = f(x_1, x_2, \dots, x_n) = \prod (x_1, x_2, \dots, x_n) \quad \text{Eq.(4-2)}$$

Proceeding like this, reduces the variables in the problem to a few resulting in a manageable amount of experiments necessary. From Eq.(4-2) it follows, that if the quantity shall be dimensionless, the sum of exponents of the base quantities has to be zero.

#### 4.2.2.1 Nusselt number = $Nu$

The Nusselt number links the local heat transfer coefficient  $h$  to the temperature field. The characteristic length for the problem is  $L_0$  which could be the diameter of a pipe or a vessel.  $L_0$  depends on the type of problem investigated. The heat transfer coefficient  $h$  is defined as the slope of the temperature profile near the wall and is determined by the temperature difference between the wall and the fluid.

$$h = -\lambda \frac{(\partial \vartheta / \partial y)_w}{\vartheta_w - \vartheta_F} \quad \text{Eq.(4-3)}$$

To obtain  $Nu$  the distance from the wall  $y$  is made dimensionless by relating it to  $L_0$  and  $\vartheta$  is made dimensionless by fixing a reference temperature  $\vartheta_0$  and relating it to a characteristic temperature difference (wall and fluid).

$$\mathcal{G}^+ = \frac{\vartheta - \vartheta_0}{\Delta\vartheta} \quad \text{Eq.(4-4)}$$

Inserting the dimensionless temperature into Eq.(4-3) the equation for  $h$  can be rearranged to

$$h = -\frac{\lambda}{L_0} \frac{(\partial\mathcal{G}^+/\partial y^+)_W}{\mathcal{G}^+_W - \mathcal{G}^+_F} \Rightarrow Nu = \frac{hL_0}{\lambda} = -\frac{(\partial\mathcal{G}^+/\partial y^+)_W}{\mathcal{G}^+_W - \mathcal{G}^+_F} \quad \text{Eq.(4-5)}$$

$Nu$  can be determined by experimental correlations, which depend on the geometry of the investigated system of heat transfer. It is dependent on several variables:

The fluid velocity field is influenced by the characteristic length  $L_0$  and the characteristic velocity  $u_0$  of fluid entering. The velocity of fluid entering depends on the density  $\rho$  and the viscosity  $\mu$  of the fluid. The latter influences frictional processes and is therefore responsible for the formation of the fluids boundary layer.

The temperature field is dependent on the characteristic temperature difference  $\Delta\vartheta_0$ , the specific heat capacity  $C_p$  and the thermal conductivity  $\lambda$  of the fluid.  $C_p$  links the enthalpy of the fluid to its temperature.

Summarizing the dependencies  $Nu$  can be written as

$$Nu = f(L_0, u_0, \rho, \mu, \Delta\vartheta, \lambda, C_p) = \frac{hD_T}{\lambda_b} \quad \text{Eq.(4-6)}$$

Since there are seven variables determining  $Nu$ , the temperature field and the velocity field can be broken down further to summarize them in other dimensionless quantities. It can be seen, that  $Nu$  is influenced by the base quantities  $M$ ,  $T$ ,  $\vartheta$  and  $L$ . This yields a system of four equations for seven variables and therefore three independent dimensionless quantities. Two of them ( $Re$ ,  $Pr$ ) are discussed below because the third one ( $Ec$ ) can be neglected in this work.  $Ec$  is called the Eckert number and represents the influences on the temperature field arising due to friction within the observed fluids.

At high  $Nu$  the heat transfer is fast, since the individual heat transfer through the thermal boundary layer is high. (Baehr & Stephan, 2013).

#### 4.2.2.2 Reynolds number = $Re$

The Reynolds number characterizes the velocity field of the fluid.

$Re$  relates inertial forces to viscous forces in the velocity field. It is used to characterize flow regimes in fluid dynamics. In this work it was used to calculate whether or not turbulence in the stirred vessel and the double jacket was reached respectively. For stirred vessels  $Re$  is defined as  $Re_i$

$$Re_i = \frac{N_i D_i^2 \rho}{\mu} \quad \text{Eq.(4-7)}$$

where  $N_i$  is the impeller speed [ $s^{-1}$ ],  $D_i$  is the impeller diameter [m],  $\rho$  is the density [ $kg/m^3$ ] and  $\mu$  is the viscosity [ $kg/ms$ ]. If  $Re_i$  is greater than  $10^4$  the flow regime is turbulent. This is favorable for heat transfer, because higher turbulence ensures a thinner stagnant thermal

boundary layer at the surface through which heat is transferred. As a result heat transfer is improved. It should be noted, that also the pattern of agitation is important. This can't be covered by  $Re$ , and has to be investigated by methods of CFD.

The same concept can also be applied to other geometries like the geometry of the double jacket. This changes the formula slightly to

$$Re_s = \frac{u_h d_g \rho}{\mu} \quad \text{Eq.(4-8)}$$

where  $u_h$  is the characteristic fluid velocity [m/s],  $d_g$  is the characteristic diameter [m],  $\rho$  is the density [kg/m<sup>3</sup>] and  $\mu$  is the viscosity [kg/ms].

$Re$  is dependent on the temperature because  $\rho$  and  $\mu$  are functions of temperature and is therefore changing during the course of heating/cooling.

#### 4.2.2.3 Prandtl number = $Pr$

The Prandtl number relates the velocity field of a fluid to the temperature field. It is only dependent on the properties of the fluid.

$$Pr = \frac{C_p \mu}{\lambda} \quad \text{Eq.(4-9)}$$

The numerator represents the viscous diffusion rate, while the denominator represents the thermal diffusion rate.

If  $Pr \ll 1$  the heat transfer process is limited by viscous diffusivity because thermal diffusivity is large. That means, that heat transfer due to conduction dominates over the heat transfer due to convection. In this case heat is diffusing more quickly than momentum.

If  $Pr \gg 1$  the heat transfer process is limited by thermal diffusivity because viscous diffusivity is large. Now the heat transfer process is dominated by the heat transfer due to convection rather than conduction and momentum is transferred faster than heat.

$Pr$  gives a statement over the thickness of the boundary layers of the fluid. It shows if the thermal boundary layer or the momentum boundary layer is dominating heat transfer.

For heat transfer a low  $Pr$  is desirable because of the faster thermal diffusion (Baehr & Stephan, 2013).

### 4.3 Determination of the overall heat transfer coefficient $U$

#### 4.3.1 Practical determination of $U$

A certain amount of water is heated by use of tap water or the tempering unit and then cooled with ice water. All temperatures needed for calculation are recorded. These are:

- Temperature of heating/cooling media at the inlet
- Temperature of heating/cooling media at the outlet
- Temperature of the bulk inside the vessel

It is then determined if the heating/cooling medias temperatures are a function of time or they are constant during the process. This influences the selection of the procedure to calculate  $U$ .

For time dependent outlet temperature  $U$  is calculated for heating and cooling (Perry, 2007).

For heating Eq.(4-10) is used.

$$\ln\left(\frac{T_1 - t_1}{T_1 - t_2}\right) = \frac{WC_p}{Mc_p} \left(\frac{K_1 - 1}{K_1}\right) \theta \quad \text{Eq.(4-10)}$$

For cooling Eq.(4-11) is used.

$$\ln\left(\frac{T_1 - t_1}{T_2 - t_1}\right) = \frac{WC_p}{Mc_p} \left(\frac{K_1 - 1}{K_1}\right) \theta \quad \text{Eq.(4-11)}$$

In Eq.(4-10) and Eq.(4-11)  $K_1$  is

$$K_1 = \exp\left(\frac{UA_m}{WC_p}\right) \quad \text{Eq.(4-12)}$$

For time independent outlet temperature  $U$  is calculated by

$$\frac{T_1 - t_2}{T_1 - t_1} = \exp\left\{-\left(\frac{UA_m}{Mc_p}\right) \theta\right\} \quad \text{Eq.(4-13)}$$

The abbreviations can be found in the glossary. The isobaric heat capacities  $c_p$  and  $C_p$  are calculated for the mean temperatures. For the bulk fluid that is the average of the temperature at start ( $t_1$ ) and the end ( $t_2$ ). For the heating/cooling media every two minutes during heat transfer the temperature is measured and the average of all points is used as the mean temperature. For the area  $A_m$  involved in heat transfer, the mean of the outer and the inner surface is used.

## 4.3.2 Theoretical determination of $U$

### 4.3.2.1 Jacket-side: Procedure of Lehrer

This procedure is used to estimate the resistance to heat transfer due to the thermal boundary layer at the wall of the jacket with heating or cooling medium. It is based on the Prandtl analogy between impulse transfer and heat transfer. For the calculation of the individual heat transfer coefficient of the thermal boundary layer Lehrer suggests the following correlations using dimensionless quantities.

$$Nu_{s,L} = \left[ \frac{0.03 * Re_s^{0.75} Pr}{1 + \frac{1.74(Pr-1)}{Re_s^{0.125}}} \right] * \left( \frac{\mu}{\mu_w} \right)^{0.14} = \frac{hd_g}{\lambda} \quad \text{Eq.(4-14)}$$

In Eq.(4-14)  $Re$  and  $Pr$  are evaluated by Eq.(4-8) and Eq.(4-9) respectively.

In the correlation  $d_g$  is the characteristic length of the jacket geometry for  $Nu_{s,L}$  and  $Re_s$ . It is evaluated from the width of the annular space  $\delta$  by

$$d_g = \delta * \sqrt{(8/3)} \quad \text{Eq.(4-15)}$$

The fluid velocity  $u_h$  is the characteristic fluid velocity of the jacket geometry for  $Re_S$ . It is a combination of the fluid velocity at the inlet  $u_O$ , fluid velocity in the annular space  $u_S$  of the jacket and fluid velocity arising due to free convection  $u_A$ . It was calculated by

$$u_h = \sqrt{(u_S u_O)} + u_A = \sqrt{(u_S u_O)} \quad \text{Eq.(4-16)}$$

The contribution of free convection is small compared to forced convection and is neglected by setting it to zero. The velocities  $u_S$  and  $u_O$  are evaluated for tangential inlets by

$$u_S = \frac{\dot{V}_M}{h_S \delta} \quad \text{Eq.(4-17)}$$

$$u_O = \frac{\dot{V}_M}{\left(\frac{\pi d_O^2}{4}\right)} \quad \text{Eq.(4-18)}$$

For calculation of the individual heat transfer coefficient at first the characteristic length  $d_g$  and the characteristic velocity  $u_h$  are calculated. From these values  $Pr$  and  $Re_S$  are obtained to evaluate  $Nu_{S,L}$ . From  $Nu_{S,L}$  the individual heat transfer coefficient  $h$  is calculated. The procedure of Lehrer can be found in (Verein deutscher Ingenieure, 2013).

#### 4.3.2.2 Vessel-side: Correlation for stirred liquids

For heat transferred to a stirred liquid by a jacket the individual heat transfer coefficient is calculated from the correlation (Doran P. M., 2013).

$$Nu = 0.36 * Re_i^{0.67} Pr^{0.33} \left(\frac{\mu}{\mu_w}\right)^{0.14} = \frac{hD_T}{\lambda_b} \quad \text{Eq.(4-19)}$$

In Eq.(4-19)  $Re$  and  $Pr$  are evaluated by Eq.(4-7) and Eq.(4-9) respectively.

For calculation of the individual heat transfer coefficient  $Pr$  and  $Re_i$  are calculated at the arithmetic average temperature of start and end temperature.  $Nu$  is evaluated and the individual heat transfer coefficient  $h$  is calculated.

#### 4.3.2.3 Wall separating vessel and jacket

The thermal resistance of the wall is evaluated by Eq.(4-20).

$$R_w = \frac{B}{\lambda_w A_m} \quad \text{Eq.(4-20)}$$

#### 4.3.2.4 Combination of theoretical resistances

The resistances are combined by Eq.(4-1). Adding up the resistances due to the jacket-side, the wall and the vessel-side the theoretical overall heat transfer coefficient  $U$  is calculated.

#### 4.4 Heat precipitation

In a heat precipitation step one uses the different melting temperatures of proteins. Many proteins become denatured at temperatures above ~40°C. This is because they usually must employ their function at the temperatures where the organism it belongs to lives. However there are some exceptions of proteins which are stable at higher temperatures too. GFP is one of these exceptions and is unusually stable up to 50°C (Fink, 2015). Its stability was also challenged in the work of Alkaabi, who showed, that even in presence of 8 M urea incubation at 50°C led to a time dependent decrease of fluorescence only at a pH of 6.5. At pH 7.5 and 8.5 GFP was stable. If only heat was applied to GFP, denaturation was only a function of pH (Alkaabi, Yafea, & Ashraf, 2005). Its stability is even applicable to use it as a biological indicator (BI) for the success of heat treatment of certain equipment (Vessoni, Ishii, Cholewa, & de Souza, 2004). After fermentation, the cells can be separated and used for homogenization. Unfortunately homogenization frees many undesired species like debris, DNA, proteins and so on. The homogenate can then be heated to a certain temperature, where most proteins precipitate but the desired product (in this work: GFP) does not.

The basic mechanism can be explained in terms of an equilibrium state between natural (N) and denatured (D) state of the respective proteins. For the transition from N → D irreversibility is considered. In the N state, the protein is limited in its freedom because of the rigid organization of the protein. In the D state these structure is resolved and the aminoacid chains are far more mobile (more available states of arrangement). At a certain temperature the entropy change compensates the enthalpy change of the denaturation reaction. This temperature is called the melting point of the protein.

By further increase of temperature the equilibrium shifts to D because the Gibb's free energy becomes negative, and therefore unfolding is highly favorable.

Precipitation also affects the species in the homogenate, which are not directly influenced or damaged by heat. This is because the precipitate can include other species in its structure and thereby remove those species.

#### 4.5 Separation of solids

For separation of solids the differences in density are used. In bioprocessing it is applied downstream for e.g. removal of cells, debris, different precipitates or phase separation after extraction processes. For this tasks the physical law of Stoke is used, which describes the settlement velocity of a particle in suspension.

$$u_g = \frac{\rho_P - \rho_L}{18\mu} D_p^2 g \quad \text{Eq.(4-21)}$$

Eq.(4-21) applies for the gravitational acceleration. In separation processes the settlement velocity in the centrifugal acceleration field is of greater interest. It can be calculated by replacing  $g$  to obtain:

$$u_c = \frac{\rho_P - \rho_L}{18\mu} D_p^2 \omega^2 r \quad \text{Eq.(4-22)}$$

Most commonly used are tubular bowl centrifuges and disc stack centrifuges. In this work both were applied and will be discussed next (Doran P. M., 2013).

### 4.5.1 Tubular bowl centrifuge

The tubular bowl centrifuge is the simplest way for separation tasks. The suspension is supplied on the one end of the bowl with a certain flow rate (semicontinuous operation). This flow rate is chosen in a way, that the particles to be separated, have enough time to settle at the wall of the bowl. The clarified supernatant is removed from the center of the bowl.

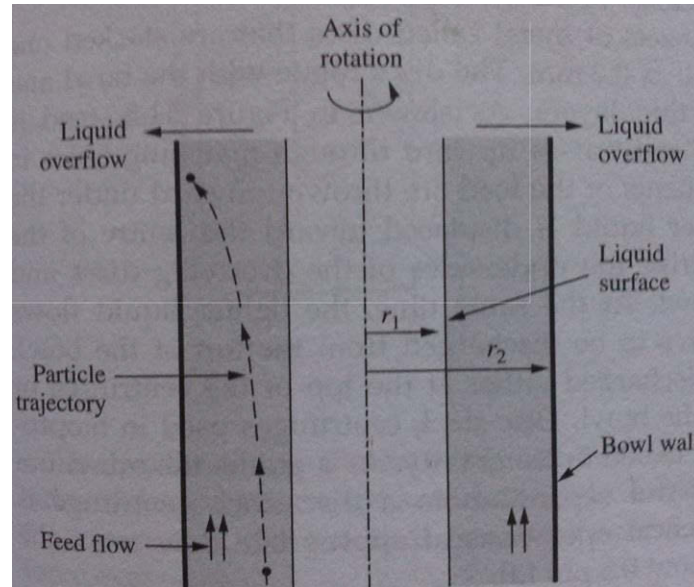


Figure 3: Tubular bowl centrifuge (Doran, 2<sup>nd</sup>, edition p.461, Figure 11.6)

In Figure 3 the feed is supplied from below and travels upwards. Over the way the particle settles and the supernatant is removed at the upper side. The maximum thickness of the solid layer is  $(r_1 - r_2)$ .

### 4.5.2 Disc stack centrifuge

In a disc stack centrifuge a density difference from 0.01 to 0.03 g/L is sufficient to separate solids from the liquid. The operation is semicontinuous and the discharge of separated solids can be performed at the top of the centrifugation bowl or through nozzles in the wall.

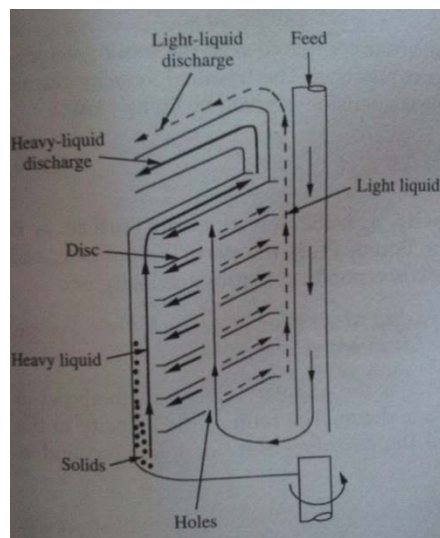


Figure 4: Disc stack centrifuge (Doran, 2<sup>nd</sup> edition, p.463, Figure 11.8)

As shown in Figure 4 the feed is supplied continuously from the upper side and is transported to the bottom of the bowl. From there it travels upwards through several metal discs. They are conically shaped and stacked above each other with a clearance of about around 3 mm. The discs fulfill the purpose to separate the suspension in many thin liquid films to enhance separation. By centrifugation the lighter liquid phase is travelling towards the inside and can be drained from there. The heavier solids slip down the discs and accumulate at the bottom of the centrifuge bowl.

#### 4.6 Homogenization

Since many products (like antibodies, medicinal proteins,... or GFP) obtained by fermentation are intercellular this step is necessary to free them in order to make them available for further downstream. This is achieved by breaking up the cell wall to free the desired product (Kelly & Muske, 2004). A typical homogenization valve is shown in Figure 5. For homogenization, the feed is promoted axially in the direction of the valve through the valve seat. From there the feed is distributed radially onto the impact ring and is forced through the gap between the seat and the impact ring. The width of the gap determines the pressure applied to the cells and therefore is one key parameter determining the yield.

Generally there are four different types of force responsible for cell break up. These are the inlet pressure gradient, channel shear stress, post channel turbulence and impact ring impingement forces. They are all a form of mechanical stress. Another important effect causing cell disruption is cavitation. Due to high pressure gradients arising during homogenization it is possible, that small zones emerge, which are free of liquid and under low pressure. These cavities are susceptible to collapsing under the surrounding high pressure, therefore creating a shock wave leading to cell disruption (Kelly & Muske, 2004) (Kleinig & Middelberg, 1998). When performing homogenization it is important to find a compromise between applied pressure and obtained yield. Too much mechanical stress may cause thermal degradation or mechanical damage of the product. Moreover it can introduce cell debris, which may be so small, that they interfere with further downstream steps like centrifugation and filtration. Depending on the flow velocity one distinguishes between acting viscous forces, which dominate at low  $Re$  number and acting inertial forces, which dominate at high  $Re$ . The latter are arising due to the high inlet pressure gradient at higher flow velocity (Kleinig & Middelberg, 1998).

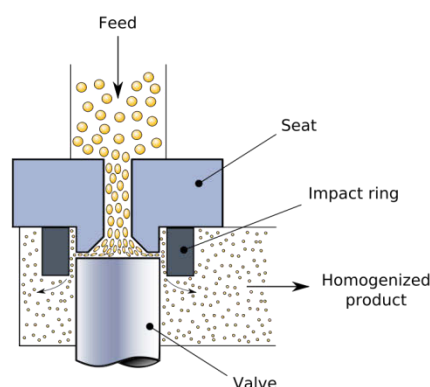


Figure 5: Homogenization valve

([https://en.wikipedia.org/wiki/Homogenization\\_\(chemistry\)#/media/File:Homogenizing\\_valve.svg](https://en.wikipedia.org/wiki/Homogenization_(chemistry)#/media/File:Homogenizing_valve.svg); 06.12.2016)

Homogenization is usually performed over one stage or two stages. If one e.g. homogenizes with 70/700 bar pressure, this means that the cell suspension is forced through a ring slit applying 700 bar pressure on the cells, which is called the first stage. In the example the

solution is not expanded to zero bar directly but undergoes an applied pressure of 70 bar afterwards, which is called the second stage. Using two stages provides the advantage, that firstly cell walls are disrupted at high pressure and by not expanding directly to zero bar freed DNA is fragmented. Due to the fragmentation of DNA viscosity is lowered, making processing of the solution easier.

The last screw, one can adjust for homogenization is the number of passages. It may be more favorable to apply less pressure, but to do this twice or more in a row (Wong, O'Neill, & Middelberg, 1997).

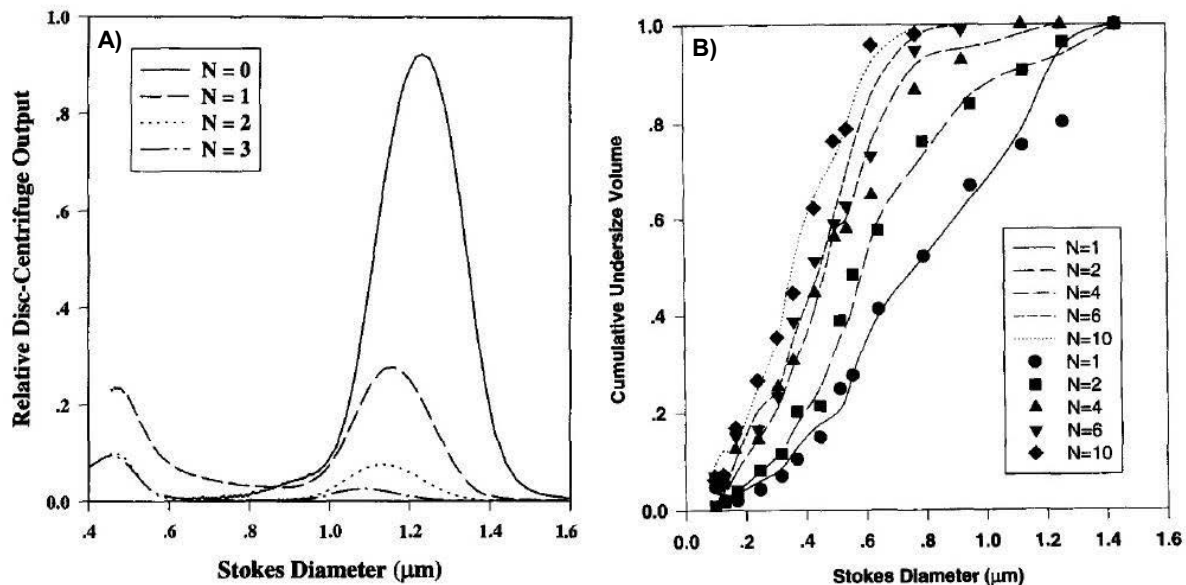


Figure 6: (A) Influence of the number of passages on cell break up; (B) influence of the number of passages on particle size

Figure 6 shows, that the fewer passages are applied, the fewer cells are broken up (large peak at  $\sim 1.2 \mu\text{m}$  in A) represent intact cells). In B) it is indicated, that the more passages are performed, the particle size distribution shifts to particles of smaller size.

## 4.7 Quantification of GFP

### 4.7.1 Fluorescence

Fluorescence is the physical phenomenon used for quantification of GFP.

Electrons are organized in atoms in the form of different discrete energy levels. This means an electron can only have the energy of  $E_1$  or  $E_2$ , but it could never have an energy level in between  $E_1$  and  $E_2$ .

It is possible, that an electron takes up a certain amount of energy to jump from  $E_1$  to  $E_2$ . This energy is supplied in the form of light. This process is called excitation. When the electron after excitation falls back down from  $E_2$  to its original energy level  $E_1$  the energy difference  $E_2 - E_1$  is dissipated. To the dissipation the emission of light of a higher wavelength (less energy than the excitation wavelength) is associated. The intensity of the emitted light can be measured.

### **4.7.2 GFP**

The basics of the fluorescence properties of GFP were explained above (see 2.2). Since the absorbance maximum is higher at the first peak around ~395 nm, this peak is used for the excitation. The concentration is determined by setting up a standard curve and measurement of the respective sample.

### **4.8 Turbidity**

Turbidity is measured by nephelometry. The method is based on the tyndall-effect. The effect is observed, when a light source hits a suspension containing small particles. A part of the light is scattered sideways due to the tyndall-effect. The scattered light is measured and expressed in terms of NTU (nephelometric turbidity units).

### **4.9 Solid fraction**

The fraction of solids in different solutions can be determined by centrifugation. The volume of the pellet is determined by calibration and comparison with a reference tube. The pellet size with reference to the sample volume gives the solid fraction in % (v/v).

### **4.10 Viscosity**

Viscosity is measured with a rotational viscosimeter (Rheometer). It is build up from a measurement chamber which can be tempered and a spindle applying shear stress to the sample to be measured. The chamber is filled with sample, shear stress is applied and the momentum necessary to apply the stress is measured. The viscosity is the proportionality constant relating shear stress and momentum. If viscosity does not depend on the applied shear stress, a fluid is called Newtonian. For the evaluation of measured viscosities Newtonian behavior is assumed (Doran P. M., 2013).

### **4.11 Filtration**

#### **4.11.1 Modes of filtration**

Filtration is used for removing of particles from a suspension with a porous membrane. Depending on the purpose of filtration one distinguishes depth-filtration and sterile-filtration.

Depth-filtration intends to remove particles in the dimension of ~0.5 to 2  $\mu\text{m}$  like cells and cell-debris from homogenates. A typical material for depth-filters are glass fibers. These are organized as a webbed structure. As a result a depth filter doesn't have a uniform pore size, but a distribution of pore sizes. Care has to be taken regarding pressure, because high pressure damages the structure resulting in filter blocking.

Sterile-filtration uses even smaller pore sizes of ~0.2 to 0.4  $\mu\text{m}$ . Most sterile filters are composed of membranes. Several materials can be used like e.g. cellulose-acetate. Sterile filters are supposed to remove all microorganisms. Because of this, the pore size is uniform. Since there is not a complex web-like-structure involved, membrane filters are quite pressure resistant.

Filtration can be performed in two modes. These are dead-end-filtration and cross-flow-filtration.

Dead-end-filtrations means the suspension hits the filter device vertically. During the course of filtration a cake is building up on the filter, resulting in a decline of flux until the filter is completely blocked. During filtration there are two resistances determining the procedure:

- resistance of filter device (depending on the filter material)
- resistance of filter cake (depending on nature of filtrated particles, pressure,..)

Dead-end-filtration can therefore only be operated in a discontinuous fashion.

Cross-flow-filtration means that the suspension is pumped tangentially to the filtration area. This can be performed with different kinds of membrane modules. Due to the tangential flow mode, filter cake is building up only to a certain degree. It can't get thicker because it is removed by the flow velocity of the stream. Therefore long operation intervals and cleaning of the filter devices by flushing backwards is possible. Cross-flow-filtrations are used for e.g.:

- desalting of solutions (diafiltration)
- concentration of a product (ultrafiltration)

For ultrafiltration (UF) the solution to be concentrated is continuously pumped through a membrane. The concentrate is then collected again in the reservoir, while the ultrafiltrate is discarded. The UF is conducted at a constant level of liquid. To achieve this fresh solution is continuously added to the reservoir to maintain the level. The membrane used has a cut-off, which only allows impurities to cross, but retains the product within the concentrate. An important parameter in UF is the factor of concentration.

For diafiltration (DF) the mode of operation is principally the same as in UF. The difference lies in the buffer which is added to keep the liquid level constant. DF is often used to prepare the product containing solution for e.g. a chromatographic step like ALEX. For this purpose ALEX equilibration buffer is used to achieve low conductivity to allow the product to bind to the resin. In DF the salt is crossing the membrane and is discarded with the diafiltrate, while the product is retained in the retentate. An important parameter in DF is the number of changes of volume.

Both modes are characterized by the trans-membrane pressure (TMP), which is calculated from the pressures before and after the membrane (Doran P. M., 2013).

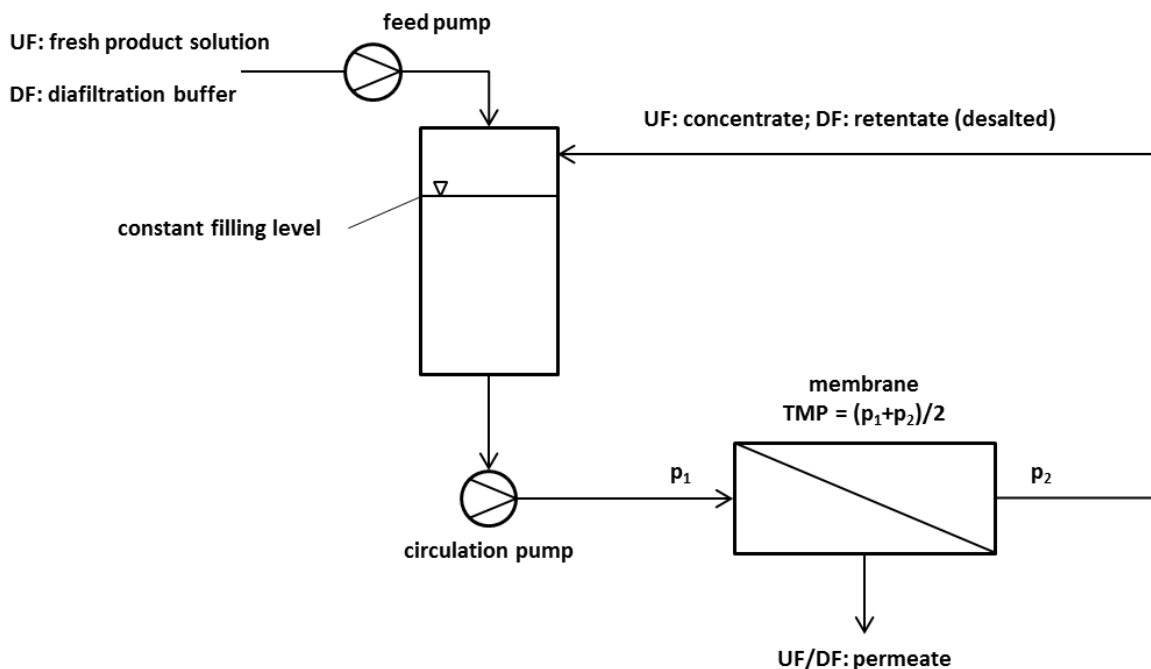


Figure 7: Scheme of an ultrafiltration/diafiltration process

#### 4.11.2 Scale up of dead-end-filtration

For scale up only the theory of the standard blocking case shall be covered in this section. Other cases than that are derived analogous. The only difference arises due to the changed exponent  $n$ .

For estimation of the required filter area for dead-end-filtration the method of “ $V_{\max}$ -analysis” was used (Zydney & Ho, 2002), (Honig & Schwartz, 1997). The filter sizing is done by considering the filtration pressure as constant. Then the flux decline can be written in the general form of

$$\frac{d^2t}{dV^2} = k \left( \frac{dt}{dV} \right)^n \quad \text{Eq.(4-23)}$$

Eq.(4-23) can also be expressed in terms of flux  $J$

$$\frac{dJ}{dt} = -kJ(J)^{2-n} = -kJ^{3-n} \quad \text{Eq.(4-24)}$$

$J$  is the flux [ $\text{m}^3/\text{s}$ ],  $V$  is the accumulated volume [ $\text{m}^3$ ],  $k$  is the resistance coefficient [ $\text{s}^{1-n}\text{m}^{3n-6}$ ],  $t$  is the filtration time [ $\text{s}$ ] and  $n$  is the blocking index.

#### Standard blocking ( $n = 3/2$ )

If standard blocking is assumed, the following equation is obtained

$$\frac{d^2t}{dV^2} = K_s J_0^{1/2} \left( \frac{dt}{dV} \right)^{3/2} \quad \text{Eq.(4-25)}$$

$K_s$  is called the kinetic constant of flux decline [ $\text{s}^{-1}$ ]. The equation can be linearized to

$$\frac{t}{V} = \frac{K_s}{2} t + \frac{1}{J_0} = \frac{1}{V_{\max}} + \frac{1}{J_0} \quad \text{Eq.(4-26)}$$

$V_{\max}$  is the maximum volume [ $\text{m}^3$ ] which can be filtrated and  $J_0$  is the flux at filtration time  $t = 0$  [ $\text{m}^3/\text{s}$ ]. By plotting  $t/V$  against filtration time  $t$  one can determine  $V_{\max}$  from the slope and  $J_0$  from the intercept.

$$V_{\max} = \frac{1}{\text{slope}} \quad \text{Eq.(4-27)}$$

$$J_0 = \frac{1}{\text{intercept}} \quad \text{Eq.(4-28)}$$

Since the filtration should practically be ended in a feasible time, one sizes the filter based on a maximum allowable flux decline  $J_{\min}/J_0$ . Introducing and rearranging gives

$$\frac{J_{\min}}{J_0} = \left( 1 + \frac{J_0 t}{V_{\max}} \right)^{-2} = \left( 1 + \frac{V}{V_{\max}} \right)^{-2} \quad \text{Eq.(4-29)}$$

From Eq.(4-29), the capacity volume  $V_{cap}$  [m<sup>3</sup>], which can be filtrated until the allowable flux decline is reached can be calculated by

$$V_{cap} = V_{max} \left( 1 - \sqrt{\frac{J_{min}}{J_0}} \right) \quad Eq.(4-30)$$

If  $V_{max}$  is known the required filter area can be estimated by

$$A = \frac{V_B}{V_{max}} + \frac{V_B}{J_0 t} \quad Eq.(4-31)$$

$A$  is the required filter area [m<sup>2</sup>] for the batch volume  $V_B$  [m<sup>3</sup>]. If the initial flux is large and filtration time is considered long, the second term can be neglected.

#### 4.12 Particle sizes

The measurement is based on the settling behavior of the particles of interest. This behavior is characterized by Stokes' law as it was discussed above (4.5; Eq.(4-21) and Eq.(4-22)).

If viscosity and density of the particles are known and their settling velocity is determined it is possible to calculate the particle size.

The determination of the settling velocity is done by measurement of transmission during centrifugation. At every point on the length of the cuvette transmission is measured. Due to the centrifugal force the particles settle in the direction of the bottom of the cuvette. This leads to increasing transmission in the cuvette and one gets a time-dependent course of clearance of sample. For calculation fixed points of the cuvette are chosen. For these points the change of transmission over centrifugation time allows to determine the settling velocity.

#### 4.13 SDS-PAGE

SDS-PAGE stands for sodium dodecyl sulfate (SDS) polyacrylamide gel electrophoresis (PAGE). An SDS-PAGE serves many different purposes like determination of molar mass, separation of different proteins to determined purity of a solution or to determine the identity of proteins.

For SDS-PAGE the protein is denatured and treated with the anionic detergent SDS. This charges the protein negatively. The charged protein is then loaded onto a polyacrylamide gel with varying degree of crosslinking (directly under the loading slots, the gel is less crosslinked to obtain a sharp gel front). To the gel a voltage is applied and therefore an electric field is created. The charged protein then travels towards the positively charged anode. The path travelled is only dependent on the size of the protein. Small proteins are travelling faster, than big proteins because big proteins are hindered by the polyacrylamide gel.

After the proteins are separated on the gel, the protein bands have to be dyed to make them visible. This can be achieved in different ways. In this work the dyeing with Coomassie Brilliant Blue R250 was used. The dye binds to the protein bands by formation of a complex with the protein. Since the staining solution also stains the gel, the gel is treated with destaining solution containing methanol and acetic acid.

Besides the samples, a protein ladder with known molar masses is always run on the gel. From the known masses and their distance travelled a calibration is obtained. The calibration is used to evaluate the molar masses of the protein bands of the unknown proteins from the samples.

#### 4.14 Adsorption isotherms

The first step after diafiltration is the capture of GFP on a resin for anionic exchange chromatography. For the trials *CaptoQ* resin was used. To estimate the resin's binding capacity for GFP adsorption isotherms are recorded. For the isotherms the Langmuir model is used.

$$q = \frac{q_m K_a C}{1 + K_a C} \quad \text{Eq.(4-32)}$$

In Eq.(4-32)  $q$  is the binding capacity [mg/mL],  $q_m$  is the maximum binding capacity [mg/mL],  $C$  is the equilibrium concentration in the supernatant [mg/mL] and  $K_a$  is the association constant [mL/mg]. The Langmuir model is applied to all systems where adsorbed molecules form only a monolayer, each site is equivalent with respect to the adsorption energy and no interactions take place between adjacent adsorbed molecules (Doran P. M., 2013).

Different amounts of resin are mixed with defined volumes of sample with a known GFP concentration. After incubation equilibrium between bound (to the resin) and free GFP (in the supernatant) is reached. The equilibrium concentration in the supernatant is measured. From the mass balance it is determined how much GFP is bound, and furthermore the load of mg GFP per mL resin can be calculated. Therefore to each equilibrium concentration in the supernatant belongs a loading on the resin. The loading is plotted on the y-axis versus the equilibrium concentration on the x-axis.

The determination of the binding behavior of DNA is done in the same way.

#### 4.15 Quantification of DNA

DNA can be quantified in various ways like simple measurement of absorbance at 260 nm. This method is susceptible to contaminations like RNA or other proteins, which absorb at 260 nm. Due to this the quantification with a fluorochrome was used in this work. This quantification is based on fluorescence like described in 4.7.1.

The fluorochrome used was Hoechst 33258. This chemical binds to the minor groove of DNA, where it favors sequences containing AT (Labarca & Paigen, 1980), (Daxhelet, Coene, Hoet, & Cocito, 1989). The binding shifts the fluorescence output of the dye and can be measured by an excitation wavelength of 360 nm and an emission wavelength of 460 nm. Hoechst 33258 binds to single stranded DNA less efficient, than it does to double stranded DNA. Moreover it does not bind to DNA small oligomers. It gives similar fluorescence intensities for linear and for circular DNA (Daxhelet, Coene, Hoet, & Cocito, 1989), (Moe, Garbarsch, & Kirkeby, 1994).

For quantification a calibration is prepared with calf thymus DNA. This DNA is double stranded and has an AT content of 58%.

## 5 Material and Methods

### 5.1 Cell line

For the production of GFP for downstream the organism *E.coli HMS174(DE3)* was used. It contained the plasmid *pET11a GFPmut3.1* for GFP expression.

### 5.2 Material

Device	Type	Manufacturer
Disc stack separator	Westfalia Separator, Nr.1729-791, Typ PSC-1-06-177	GEA
Continuous lab centrifuge and rotors	Heraeus Biofuge stratos	Thermo-Scientific
	Continuous Flow Through Rotor #3049 (Titanium) Eq.41573196 HCT 22.300	Thermo-Scientific
	HIGHConic™ Fixed Angle Rotor	Thermo-Scientific
Centrifuge	MultifugeX3Fr	Thermo-Scientific
	TX-750 4*750 mL Swinging Bucket Rotor	Thermo-Scientific
Lab centrifuge	Laboratory Centrifuge 2-16P, Serial no.120756	Sigma
Minifuge	Galaxy Mini Centrifuge, Serial no.0805 0894	VWR International
Pump	Masterflex® L/S® with Masterflex Easy Load® II; Modell no.77200-60	?
Rheometer	DV-II+ Pro	Brookfield
	CPA-41Z spindle	Brookfield
Homogenizer	NS1001L Panda, Serial No.120756	GEA
	Ariete NS3006, Serial No. 10185	GEA
Scales	M-Pad AX6202	Sartorius
	Midrics 1	Sartorius
	SIWDCP-2-35-HCE	Sartorius
	Precisa 30100DG-FR SCS	Swiss Quality+
Magnetic stirrer	IKA® C-Mag HS10	
	RZR2052 Control	Heidolph
pH-Meter	WTW pH7110	Ino Lab
pH/temperature sensor	Easy Ferm Plus ARC120	Hamilton
ÄKTA	ÄKTA explorer Serial no.001892	amersham pharmacia biotech
Stirred tank reactor	Double jacketed stirred tank reactor	-
	BMR 30 DC agitator	Zeta
SDS-PAGE equipment	XCell Sure Lock™	Invitrogen
	Novex Mini-Cell	Invitrogen
	Electrophoresis Power Supply EPS600	Pharmacia Biotech
	Mini-Protean® Tetra-System	BIO-RAD
	Power Pac Basic	BIO-RAD
Thermomixer	Eppendorf™ Thermomixer™ R	Thermo-Scientific
Nephelometer	2100Q	Hach-Lange
Fluorescence microtiter plate 96-well (black)	Nunclon 96 Flat Bottom Black Polystyrol LumiNunc FluoroNunc	Thermo-Scientific
Plate reader	Hardware: infinite 200pro	Tecan
	Software: Tecan i-control, 1.10.4.0	Tecan
Filter Discs	Sartopore PP3 0.65µm Order No.50505P-47-----B; Lot 0315 50505P 500211099	Sartorius stedim biotech
	Sartopore PP3 0.45µm Order No.505056P-47-----B; Lot 0315 50506P 500211100	Sartorius stedim biotech
	54707F 500199562	
	Sartopore 2 0.8/0.2µm Order No.54407G-47-----B; Lot 101354407G 500095407	Sartorius stedim biotech
	Sartopore 2 0.35/0.2µm Order No. 54407I-47-----B; Lot 0914 54407I 500173297	
	Sartoguard PES 1.2/0.2µm Order No.54707F-47-----B; Lot 0115	Sartorius stedim biotech
	Sartoguard PES 0.8/0.2µm Order No. 54758G-47-----B; Lot 1013 54758G 500095408	Sartorius stedim biotech
	Sartobran P 0.45/0.2µm Order No. 52307H-47----P-B; Lot 0414 52307H 500133350	Sartorius stedim biotech

	Sartobran P150 0.45/0.2µm Order No. 52313074H—SS; Lot 315000203	Sartorius stedim biotech
	Sartoguard GF 0.2/0.1µm Order No. 54858M-47-----B; Lot 0216 54858M 500303247	Sartorius stedim biotech
	Sartobran P 0.45µm/0.2µm; filtration area 0.45 m <sup>2</sup> ; Order No. 5235307HO	Sartorius stedim biotech
Automated filterability and scale up system	Zero-T	Sartorius stedim biotech
LUMiSizer and cuvettes	LUMiSizer 6512-79	LUM GmbH
	LUM 10mm, PC, Rect. Synthetic Cell (110-132xx)	LUM GmbH
Ultrafiltration/Diafiltration device and membrane	Sartoflow® Advanced	Sartorius stedim biotech
	Sartocon® Hydrosart® Cassette	Sartorius stedim biotech
	17546SF418	Sartorius stedim biotech

### 5.2.1 Stirred tank reactor

A vessel made of 316L stainless steel was used. The cylindrical vessel was equipped with a double jacket for heating and cooling and one baffle. The bottom of the tank was curved. In the center a *BMR 30 DC* agitator was placed on the bottom without clearance. The *BMR 30 DC* is designed to remove temperature gradients rapidly and therefore provides good heat transfer attributes. It draws in the liquid from above and releases it radially against the wall of the vessel. On top, the vessel was equipped with a lid with six ports. Furthermore the vessel had four ports for *Hamilton* pH/temperature probes on the level of the agitator and three ports on different heights next to the baffle. The geometry is shown in Table 2.

Table 2: Geometry of the stirred tank reactor

Parameter	Value	Unit
Inner diameter	0.400	m
Outer diameter	0.508	m
Thickness of walls	0.003	m
Height of the vessel	1.220	m
Height of double jacket	0.840	m
Width of annular gap of double jacket	0.048	m
Diameter of inlet for heating/cooling media	0.0279	m
Diameter of outlet for heating/cooling media	0.0279	m
Agitator diameter	0.080	m
Volume of the ellipsoid bottom part*	3.877	L

\*) The volume in the ellipsoid part of the bottom is not in contact with the surface of the jacket. This is important for the calculation of the heat transfer in the system.

### 5.2.2 Tempering unit

For tempering of the vessel jacket a *Haake K20/DC10* unit was used like shown in Table 3. *K20* is the designation of the bath itself and *DC10* designates the tempering unit associated with the bath. The pump of the device allowed two different speeds.

Table 3: Data of tempering unit K20 DC10

Parameter	Value	Unit
Operating temperature	-30 to 100	°C
Heater capacity	2000	W
Max. pump pressure	300	mbar
Circulation capacity (open mode)	17	L/min
Circulation capacity (circulation mode, 12 mm hoses)	12.5	L/min
Immersion depth	85 to 140	mm
Voltage	230 ± 10%	V
Frequency	50 to 60	Hz
Total wattage consumption	2050	VA

### 5.3 Chemicals

<b>Chemical</b>	<b>Order No.</b>	<b>Manufacturer</b>
Di-potassiumhydrogenphosphate	1.05101	Merck
Potassium-dihydrogenphosphate	1.04877	Merck
Potassiumchloride	1.37009	Merck
Sodiumchloride	141659	Applichem
Tris	0497	Merck
Tween20	37470	Serva
TritonX100	-	Sigma Aldrich
Hydrochloric acid	-	Merck
Fluorescent DNA Quantification kit	170-2480	Bio-Rad
CaptoQ	17531604	GE Healthcare Lifesciences
Butylsepharose High Performance	17543260	GE Healthcare Lifesciences
Superdex 75 Prep Grade	17-5174-01	GE Healthcare Lifesciences
Precision Plus Protein <sup>TM</sup> Dual Color Standards 500 µL	161-0374	Bio-Rad
Ethanol, 96%	-	-
Glacial acetic acid	-	Sigma Aldrich
Coomassie Blue R250	Cat.No. 20278	Thermo Fisher
4x Laemmli Sample Buffer	161-0747	Bio-Rad

## 5.4 Methods

### 5.4.1 Flow of heating/cooling media

#### 5.4.1.1 Tempering unit (used for heating / keeping temperature)

The water bath was placed next to the vessel on a laboratory bench. After connecting the jacket of the vessel was filled with RO-water. The outlet hose was not connected to the bath but placed next to a bucket. After starting the pump the promoted water was collected at the outlet for one minute. The mass was determined and with the density the flowrate was calculated.

#### 5.4.1.2 Tap water (used for heating)

The procedure of flow determination was the same as for the tempering unit but with tap connected to the jacket. The flow was measured at maximum possible waterflow.

#### 5.4.1.3 Ice water circuit (used for cooling)

For cooling water from the ice-water circuit was used. The procedure of flow determination was the same as described above but with ice-water connected to the jacket.

### 5.4.2 Temperature measurement of involved media

For determination of the temperatures of heating and cooling media at the inlet they were switched on for 15 min. Then the temperatures were measured.

For determination of the temperatures of heating and cooling media at the outlet, the hose connected to it was equipped with a thermometer. This allowed continuous monitoring of the outlet temperature by use of a Pt100 thermometer.

The temperature of media in the vessel was monitored by an *Easy Ferm Plus ARC120 (Hamilton)* probe through a port at the height of the agitator.

### 5.4.3 Correlations for properties of water

To calculate the properties of the model fluid water, correlations were used based on the data for water provided in VDI Wärmeatlas (Verein deutscher Ingenieure, 2013). The correlations were calculated in the form of a polynomial

$$y = y_0 + aT + bT^2 + cT^3 + dT^4 + eT^5 \quad \text{Eq.(5-1)}$$

Table 4 shows the parameters for the different properties of water. For calculation the temperature was inserted in [°C].

Table 4: Properties of water

Parameter	Viscosity $\mu$ [kg/ms]	Thermal conductivity $\lambda$ [W/mK]	Isobaric heat capacity $C_p$ [J/kgK]	Density $\rho$ [kg/m <sup>3</sup> ]
$y_0$	1.786E-03	0.5627	4218.79	999.93
a	-5.575E-05	1.973E-03	-3.200	0.02075
b	9.955E-07	-8.354E-06	0.1038	-5.929E-03
c	-9.146E-09	0	-1.775E-03	1.575E-05
d	3.266E-11	0	1.611E-05	0
e	0	0	-5.585E-08	0

## 5.4.4 Heat precipitation

### 5.4.4.1 Small scale

Cell harvest for preparation of homogenate was separated by use of a continuous flow through rotor (*Continuous Flow Through Rotor #3049 (Titanium) Eq.41573196 HCT 22.300*; Thermo Scientific) at 25000 g with a flow rate of 120 mL/min.

Homogenates were obtained by resuspension of cells to a concentration of 25 g/L CDM and homogenization at 70/700 bar over one passage. Precipitation was performed with clarified homogenate and unclarified homogenate. The suspensions were filled into 1 L Schott-bottles. The bottles were heated by a circulating water bath, kept at 50°C. Samples were taken every 30 min for measurement of turbidity, solid content, GFP concentration and viscosity. At every sample time, the bottles were shaken prior to sampling. The solutions were exposed to heat for 3 h (measured from the point of putting the bottles into the bath).

Every separation step for homogenates and heat precipitate was done with a continuous flow through rotor (as above) at 25000 g and a flow rate of 90 mL/min.

### 5.4.4.2 Large Scale

#### Operation of the stirred tank reactor

For heating up by using the tempering unit the pressure side of the pump was connected to the bottom inlet of the jacket. From the top inlet the water was promoted back to the bath, where it was reheated. For the connections silicone hoses with a diameter of 12 mm and a strength of 4 mm were used. They were fixed with hose clamps at the bath and with clamps at the vessel's inlets. Since the inlets only had a screw thread two adapters were used to be able to establish a clamp connection.

When tap water was used for heating, the tap water was connected to the bottom inlet and the water was removed through the top inlet.

Before cooling of the precipitate, the jacket was emptied and then connected to the ice-water-circuit.

Before starting heat precipitation it was made sure, that the jacket with the media was sufficiently preheated.

#### Precipitation process

The solution to treat was filled into the tank with a pump. As soon as the bottom was covered with liquid, the stirrer was set to 600 rpm. After pumping in all the liquid, the lid was closed and sealed.

The process was monitored by recording the temperature with the probe *Easy Ferm Plus ARC120 (Hamilton)*. Moreover samples were taken for measurement of turbidity, solid content, GFP concentration and viscosity.

## 5.4.5 Homogenization

### 5.4.5.1 Small scale

For homogenization of small volumes (up to 10 L) a small homogenizer (*NS1001L Panda, Serial No.120756; GEA Niro Soavi*) was used with a flow of 170 mL/min. For larger volumes a *Ariete NS3006, Serial No. 10185; GEA Niro Soavi* was used with a flow of 50 – 75 L/h.

For small scale heat precipitation trials 7.42 L of a cell suspension with a concentration of 25.96 g/L CDM in homogenization buffer was used. The homogenization buffer used

consisted of 20 mM Tris, 100 mM NaCl and 0.1 % (v/v) Tween20 with a pH of 8.5 (adjusted with 25% HCl). The cell suspension was resuspended with a propeller shaped stirrer for 20 min. The homogenization was performed at 70/700 bar over one passage.

For homogenization trials 6.83 L of a cell suspension with a concentration of 24.93 g/L CDM and 3.42 L of a cell suspension with a concentration of 49.93 g/L CDM in homogenization buffer were prepared respectively. The homogenization buffer used consisted of 20 mM TRIS, 100 mM NaCl, 0.1 % (v/v) Tween20 with a pH of 8.5 (adjusted with 25% HCl). The lower concentrated suspension was resuspended for 2 h at room temperature on an *IKA® C-Mag HS10* magnetic stirrer prior to homogenization. The higher concentrated suspension was resuspended on a magnetic stirrer (*IKA® C-Mag HS10*) over night prior to homogenization. For both concentrations different homogenization pressures were performed. After each passage samples were taken for analysis of particle size, GFP release and viscosity.

#### 5.4.5.2 Large scale

For preparation of the cell suspensions used for homogenization a homogenization buffer containing 20 mM Tris, 100 mM NaCl, 0.1% Tween20 with a pH of 8.5 (adjusted with 25% HCl) was used. The starting material for preparation was cell paste with a solid content of 62.5%. For conversion of WCM to CDM a factor of 5 was used. Homogenization was performed with a Homogenisator (*Ariete NS3006, Serial No. 10185*) at a flow rate of 60 L/h.

(1): 50 L of a cell suspension with a CDM concentration of 25 g/L were prepared. Therefore 10.00 kg of wet cell paste were filled up to 50.00 kg with homogenization buffer. The cell suspension was then homogenized at a pressure of 70/700 bar over one passage. The resulting suspension was then used for heat precipitation followed by separation with the disc stack centrifuge. The supernatant was used for further experiments like filtration trials.

(2): 20 L of a cell suspension with a CDM concentration of 25 g/L were prepared. Therefore 4.00 kg of wet cell paste were filled up to 20.00 kg with homogenization buffer. To this suspension 2% of TritonX100 were added. The suspension was incubated at 4°C over night before it was homogenized at 0/400 bar over one passage. The resulting suspension was then used for separation with the disc stack centrifuge. The supernatant was used for further experiments like filtration trials.

(3) and (4): 25 L of a cell suspension with a CDM concentration of 50 g/L were prepared. Therefore 10.00 kg of wet cell paste were filled up to 25.00 kg with homogenization buffer. The resulting suspension was homogenized at 50/500 bar over two passages. The suspension was then used for separation with the disc stack centrifuge, whereby (3) was separated once and (4) was separated twice. The supernatants were used for further experiments like filtration trials.

### 5.4.6 Measurement of GFP via fluorescence

#### 5.4.6.1 Calibration

For calibration pure GFP in a concentration of 11.5 mg/mL was used. The solution was diluted with PBS in order to obtain a linear relationship between concentration of GFP and relative fluorescence units. The standards were prepared in a 2 mL reaction tubes. After preparation they were mixed well with a vortex and were pipetted in the wells of a multiwell plate (*Nunclon 96 Flat Bottom Black Polystyrol LumiNunc FluoroNunc*). The standards were measured with the plate reader (*Tecan*).

Table 5: GFP calibration - parameters

Parameter	Value	Unit
Mode	Fluorescence top reading	-
Microtiter plate	Nunclon 96 Flat Bottom Black Polystyrol LumiNunc FluoroNunc	
Excitation wavelength	485	nm
Emission wavelength	520	nm
Excitation bandwidth	9	nm
Emission bandwidth	20	nm
Gain	53	-
Z-position	18811	µm
Number of flashes	40	-
Integration time	20	µs
Lag time	0	µs
Settle time	0	µs
Media for dilution	PBS	-
Volume for measurement	100	µL
Linear range of concentration	10 - 400	mg/L
Slope	35.34	rfu/(mg/L)
Intercept	67.84	rfu
Correlation coefficient	0.9993	-

Table 6: GFP calibration – calibration curve

GFP [mg/L]	Volume GFP-standard [µL]	Volume PBS [µL]	Fluorescence 1.measurement [rfu]	Fluorescence 2.measurement [rfu]	Fluorescence signal average [rfu]
400	347.8	652.2	330	332	331
200	173.9	826.1	857	865	861
100	869.6	130.4	1786	1874	1830
75	652.2	347.8	2680	2680	2680
50	434.8	565.2	3763	3721	3742
25	217.4	782.6	7225	7461	7343
10	87.0	913.0	14075	14088	14082

## GFP calibration in PBS

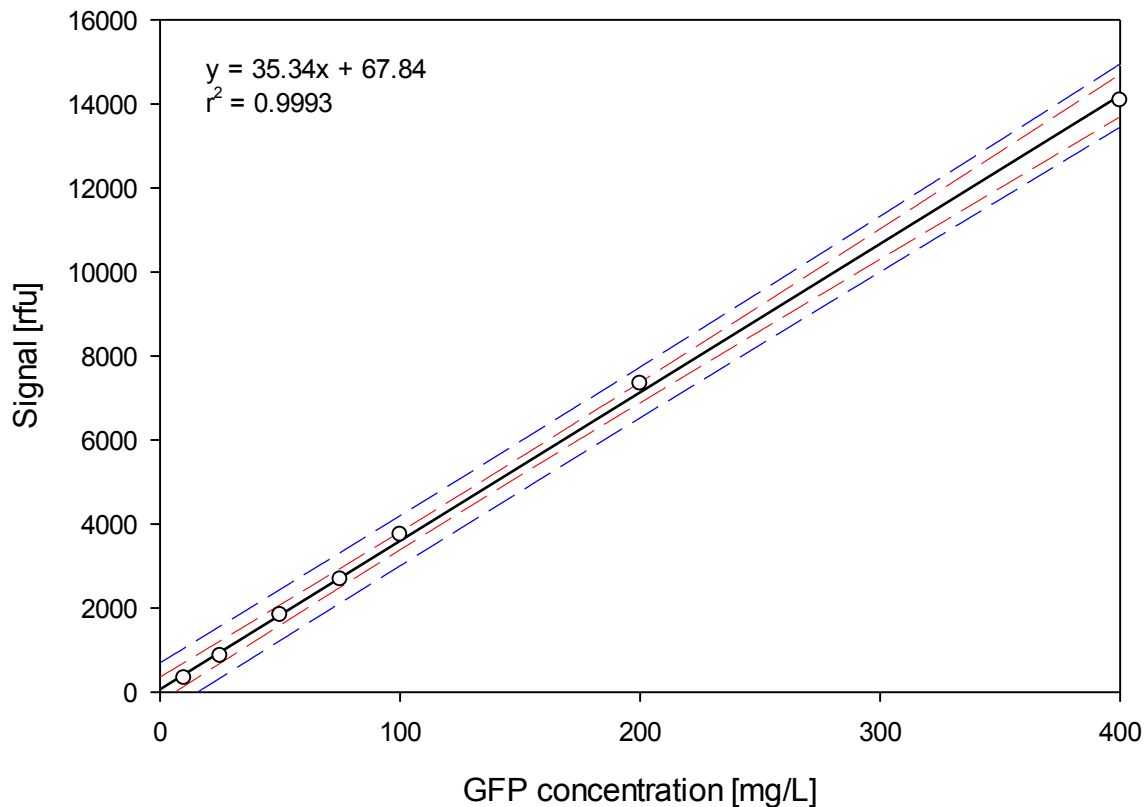


*Figure 8: GFP calibration in PBS*

In Figure 8 the correlation between GFP concentration and its fluorescence signal obtained by applying linear regression is shown as the black line. The dashed red lines represent the confidence interval chosen with a significance of  $\alpha = 0.01$ . The dashed blue lines represent the prediction interval.

### 5.4.6.2 GFP outside the cells

Samples were diluted in PBS to obtain fluorescence signals in the linear range of the calibration and to work in the same matrix in which the calibration was obtained. 100  $\mu$ L of diluted sample were pipetted into a well on the microtiter plate. Every measurement was done in duplicate. From each of the two signals the concentration was calculated from the linear regression. The average was used as the result.

### 5.4.6.3 GFP inside cells

For the measurement of GFP inside the cells, the procedure was the same as described in 5.4.6.2. The result was corrected, to the expected GFP content in homogenate. Therefore the resulting fluorescence from evaluation by the calibration shown in Figure 8 was converted by linear regression ( $r^2 = 0.9732$ ).

$$c(GFP)_{\text{homogenate}} = 0.7318 * c(GFP)_{\text{cellsuspension}} - 0.9030 \quad \text{Eq. (5-2)}$$

#### 5.4.7 Measurement of turbidity

For measurement a nephelometer (2100Q, Hach-Lange) was used. Before every measurement the calibration was checked with two standards (10 NTU and 800 NTU). For measurement of samples they were diluted in the cuvette with PBS so that the turbidity was in the range of 10 to 800 NTU. For the measurement 15 mL of sample (diluted if necessary) were used. In some cases there was not enough sample volume available for the measurement of 15 mL. If this was the case it is indicated.

#### 5.4.8 Measurement of solid fraction

15 mL tubes were filled with a defined volume of sample with a pipette. Samples were shaken or stirred prior to pipetting in order to obtain a representative result. The samples were centrifuged at 4500 rpm in a *Laboratory Centrifuge 2-16P (Sigma)* for 12 – 20 min. The time was chosen in a way that the supernatant was cleared as good as possible from solids.

#### 5.4.9 Measurement of viscosity

At first the rheometer (*DV-II+ Pro, Brookfield*) was zeroed. Therefore the spindle (*CPA-41Z, Brookfield*) was mounted and the slit between the bottom of the chamber and the spindle was adjusted. For zeroing the spindle was removed again.

For sample measurement, the measuring chamber was tempered to 20°C by use of the tempering unit *KC20 DC10*. The chamber was filled with 2 mL of sample and a shear rate of  $\dot{\gamma} = 150 \text{ s}^{-1}$  was applied for 30 s.

#### 5.4.10 Measurement of particle size

The samples were diluted with homogenization buffer in cuvettes (*LUM 10mm, PC, Rect. Synthetic Cell (110-132xx)*). For 25 g/L CDM the solutions were used diluted 1:10. They were centrifuged in the lumisizer (*LUMiSizer 6512-79*) with the parameters shown in Table 7.

Table 7: Parameters for the determination of particle sizes

Parameter	Value	Unit
Speed	4000	min <sup>-1</sup>
Number of measurements	1000	-
Measurement interval	5	s
Light factor	1.00	-

For evaluation and calculation of the particle sizes the viscosity of the continuous and the disperse phase was needed. They were measured with the rotational rheometer.

Furthermore the densities of both phases were needed. The density of the continuous phase was assumed to be the density of water at 20°C. This is legitimate since the measurement was made in a tempered measurement device, and the homogenization buffer was an aqueous solution.

The density of the dispersed particles had to be assumed. The heat precipitate is mostly protein. Proteins have a density of about 1400 kg/m<sup>3</sup>. In the precipitate they are hydrated, which lowers the density. Moreover they form a precipitate together with cell debris, which were assumed with a density of 1300 kg/m<sup>3</sup>. As a compromise the particle sizes of homogenates and heat precipitate were evaluated with a density of 1350 kg/m<sup>3</sup>. For evaluation of the particle size of cells their density was assumed to be 1090 kg/m<sup>3</sup>.

### 5.4.11 Adsorption isotherms

The resin was stored in 20% ethanol. It was spun down for two minutes at 400 rpm in a *Laboratory Centrifuge 2-16P (Sigma)* to remove the storage liquid. Then it was washed 5 times with the same buffer as the sample to be examined for equilibration. From the resin a 50% (v/v) slurry was prepared and different amounts were pipetted into 2 mL reaction tubes and filled up with sample to the final assay volume. The assay was incubated on a rotator over night at room temperature to reach equilibrium. Then the samples were spun down in a *Galaxy Mini Centrifuge (VWR)* for a short time to settle the resin with bound GFP. From the supernatant GFP was measured by fluorescence and from the mass balance the capacity  $q$  was calculated. Capacity and equilibrium concentration were plotted against each other like described above. The same was done for DNA.

Table 8: Adsorption isotherm of AIEX eluate diluted 1:2 with AIEX flow through on CaptoQ

CaptoQ slurry 50% [mL]	Volume of buffer [mL]	c(GFP) in assay [mg/mL]	m(GFP) in assay [mg]
0.050	0.950	12.29	11.94
0.100	0.900	12.00	11.31
0.150	0.850	11.69	10.68
0.200	0.800	11.36	10.05
0.300	0.700	10.63	8.80
0.400	0.600	9.79	7.54

Table 9: Adsorption isotherm of ultrafiltrate on CaptoQ

CaptoQ slurry 50% [mL]	Volume of buffer [mL]	c(GFP) in assay [mg/mL]	m(GFP) in assay [mg]
0.100	1.900	8.02	15.59
0.200	1.800	7.83	14.77
0.300	1.700	7.63	13.94
0.400	1.600	7.42	13.12
0.500	1.500	7.19	12.30
0.600	1.400	6.94	11.48
0.700	1.300	6.68	10.66
0.800	1.200	6.39	9.84

Table 10: Adsorption isotherm of diafiltrate on CaptoQ

CaptoQ slurry 50% [mL]	Volume of buffer [mL]	c(GFP) in assay [mg/mL]	m(GFP) in assay [mg]
0.050	1.950	8.27	16.31
0.100	1.900	8.18	15.89
0.150	1.850	8.08	15.47
0.200	1.800	7.99	15.05
0.400	1.600	7.56	13.38
0.600	1.400	7.07	11.71
0.700	1.300	6.81	10.87
0.800	1.200	6.52	10.04

### 5.4.12 SDS-PAGE

The samples were prepared by downspinning of 1 mL for 10 min. For analysis the supernatants were diluted as shown in Table 11. 15  $\mu$ L of supernatant were incubated with 45  $\mu$ L of sample buffer at 75°C for 15 min. The incubated solution was used for loading.

Table 11: Samples for SDS-PAGE in large scale trials

Sample	c(GFP) [mg/L]	Dilution	Solution loaded [ $\mu$ L]	m(GFP) loaded [ $\mu$ g]
Homogenate 70/700 bar Psg.1	1282.7	78.0 filled up to 500 $\mu$ L	10	0.50
Supernatant of heat precipitation	1390.1	71.9 filled up to 500 $\mu$ L	5; 10; 15	0.25; 0.50; 0.75
Homogenate 50/500 bar Psg.2	1211.0	82.6 filled up to 500 $\mu$ L	5; 10; 15	0.25; 0.50; 0.75
Homogenate 0/400 bar Psg.1 with TritonX100 added	1304.0	76.7 filled up to 500 $\mu$ L	5; 10; 15	0.25; 0.50; 0.75
Standard	-	-	5	-

The gel (*NuPAGE® 4-122% BT 1.0*, ) was flushed with water and was then inserted into the chamber (*Novex Mini-Cell, Invitrogen*). The chamber was filled with running buffer until the loading slots were covered and the slots were loaded as shown in Table 11. The chamber was assembled and the electrophoresis was started at 200 V and 400 mA (*Electrophoresis Power Supply EPS600, Pharmacia Biotech*). The gel was run for 50 min.

After the completed run, the gel was flushed with water and incubated for 30 min in fixing solution on a shaker at room temperature. After staining, the gel was flushed with water and incubated in staining solution for 10 min on a shaker at room temperature. After staining, the gel was flushed with water and incubated in destaining solution for 20 h on a shaker at room temperature. For every incubation step the volume of solution used was chosen in a way, that the gel was completely covered.

The stained bands were evaluated by measurement of their respective distance travelled. The distances were compared to a standard with known molar masses.

The solutions used were prepared according to Table 12.

Table 12: Solutions for SDS-PAGE

Chemical	Ethanol, 96%	Glacial acetic acid	Coomassie Blue R250
Fixing solution	500 mL	100 mL	-
Staining solution	200 mL	50 mL	1 g
Destaining solution	250 mL	80 mL	-

### 5.4.13 Filtration trials and scale up

For filtration trials the automated filterability and scale up system (*Zero-T, Sartorius stedim biotech*) was used. For all filtration trials a volume of 1 L was filled into the storage container. The storage container was equipped with a pressure transducer and an inlet for applying pressure to the filtration. The filter disc was placed in the filter housing, wetted with a few drops of water and the housing was closed. After the filter chamber was vented, the storage container was closed air tight. After applying the desired pressure, the valve to the filter was opened to start the trial. Filtration time and total mass of filtrate were recorded for evaluation of required filter size for scale up.

#### 5.4.13.1 Small scale

3 different suspensions were tested with different filter discs. The cells were resuspended with homogenization buffer pH 9.0 containing 20 mM Tris, 100 mM NaCl and 0.1% Tween20 to a CDM concentration of 25 g/L. Then they were homogenized at 70/700 bar over one passage.

(1) The reference suspension was homogenate, which was separated with a continuous rotor. The resulting suspension was used for filtration trials.

(2) The debris containing homogenate was directly used for heat precipitation. It was precipitated at 50°C for 3 h. Then it was separated with a continuous rotor. The resulting suspension was used for filtration trials.

(3) The homogenate was first separated with a continuous rotor. Then it was heat precipitated at 50°C for 3 h for heat precipitation. The heat treated suspension was then separated with a continuous rotor. The resulting suspension was used for filtration trials.

For removing debris for (1) and (3) a centrifugation speed of 25000 g and a flow rate of 90 mL/min were used.

For separation of the heat precipitates a speed of 25000 g and a flow rate of 90 mL/min were used.

#### 5.4.13.2 *Large Scale*

For filtration trials in large scale four different homogenates were prepared. The preparation of these suspensions is described above (5.4.5.2). After further treatment (heat precipitation, separation of debris, separation of heat precipitate) the obtained supernatants were used for filtration trials.

## 6 Results

### 6.1 Design and calculation of heat precipitation step

#### 6.1.1 Design of equipment

At first the volumetric flows and temperatures of heating/cooling media were determined as described in 5.4.1. The results are summarized in Table 13.

Table 13: Flow and temperature of heating/cooling media

Source of heating/cooling media	Flow $W$ [L/min]	Temperature $T$ [°C]
Tempering unit (heating/keeping temperature)	8.98	50.0
Tap water (heating)	21.8	54.3
Ice-water circuit (cooling)	45.3	4.5

To guarantee turbulence the stirrer speed was fixed with 600 rpm. For the calculation of the minimum Reynolds number  $Re_i$  a viscosity of 1.56 mPas at 4.5°C was considered, since this was the most unfavorable point with respect to turbulence. At the given geometry  $Re_i$  is:

$$Re_i = \frac{N_i D_i^2 \rho}{\mu} = \frac{10s^{-1} * 0.08m * 999.91kg/m^3}{15.6 * 10^{-4} kg/ms} = 4.12 * 10^4$$

Since  $Re_i > 10^4$  the flow regime in the vessel is turbulent at every point of operation justifying the assumption of a well-mixed system with uniform bulk temperature.

##### 6.1.1.1 Energy demand

For raising the temperature from  $T_1$  to  $T_2$ , a certain amount of energy in the form of heat has to be transferred by the heating media. The same amount has to be removed when cooling from  $T_2$  to  $T_1$ . Assuming that heating is started at room temperature 20°C and 50°C is the desired temperature the energy demand was calculated by Eq.(6-1).

$$Q = C_p M \Delta T \quad \text{Eq.(6-1)}$$

$Q$  is the energy demand [J],  $C_p$  is the isobaric heat capacity in [J/kgK],  $m$  [kg] is the mass of fluid to be heated and  $\Delta T$  [K] is the temperature difference between start and end point. For  $C_p$  the value at the average temperature of heated water (35°C) was used (4179.2 J/kgK). Table 14 shows the energy demand for different filling volumes.

Table 14: Flow and temperature of heating/cooling media

Mass of water $M$ [kg]	Heat energy demand $Q$ [kJ]
20	2507
50	6268
80	10030

#### 6.1.2 Theoretical calculation of $U$

The calculation of the individual resistances and therefore the theoretical  $U$  was carried out as described in 4.3.2 for heating and cooling. Since the tubings used for heating and cooling were not identical, for the inlet diameter an arithmetic average of the tubing diameter and the inlet diameter was used.

For heating and cooling medium temperature and mass flow the measured values from Table 13 were used.

For the calculations the properties of water at different temperatures were needed. These were

- Temperature of heating and cooling medium respectively (the temperature at the inlet was used)
- Temperature of the bulk fluid in the vessel (the arithmetic average of start and end temperature was used)
- Temperature of wall between bulk fluid and heating or cooling medium (the arithmetic average of the average temperature of bulk fluid and the temperature of heating or cooling medium was used)

The calculation was carried out based on measured values of the equipment used as shown in Table 15 and on a working volume of 50 kg water in the vessel.

Table 15: Values for estimation of individual heat transfer resistances

Parameter	Value	Unit
Temperature of heating medium	54.3	°C
Temperature of cooling medium	4.5	°C
Average temperature of bulk fluid (heating)	30.79	°C
Average temperature of bulk fluid (cooling)	27.98	°C
Average temperature of the wall (heating)	42.54	°C
Average temperature of the wall (cooling)	16.24	°C
Diameter of inlet and outlet (heating)	0.01992	m
Diameter of inlet and outlet (cooling)	0.02306	m
Mass flow of heating medium	0.358	kg/s
Mass flow of cooling medium	0.755	kg/s
Area involved in heat transfer – jacket side (heating/cooling)	0.468 / 0.461	m <sup>2</sup>
Area involved in heat transfer – wall (heating/cooling)	0.465 / 0.458	m <sup>2</sup>
Area involved in heat transfer – vessel side (heating/cooling)	0.461 / 0.454	m <sup>2</sup>
Stirrer speed	600	min <sup>-1</sup>

The different areas for heating and cooling are a result of the average temperature of the bulk water used for the determination of  $U$ .

#### 6.1.2.1 Jacket side

The procedure of Lehrer was used (see 4.3.2.1) to calculate the resistance of the thermal boundary layer on the jacket side. In Table 16 the properties of water of media involved in heating and cooling are shown. These properties were used in the calculation. The corresponding temperatures were taken from the measured values during practical determination (see 6.1.3).

Table 16: Properties of water for calculation of individual heat transfer resistances

Properties of water at the temperature of	Temperature [°C]	Density [kg/m <sup>3</sup> ]	Viscosity *10 <sup>-4</sup> [kg/ms]	Heat capacity [J/kgK]	Thermal conductivity [W/mK]
Heating medium	54.3	986.1	5.14	4180.9	0.645
Bulk fluid (heating)	30.79	995.4	7.76	4179.9	0.616
Wall (heating)	42.54	991.3	6.19	4179.0	0.632
Cooling medium	4.5	999.9	15.6	4206.3	0.572
Bulk fluid (cooling)	27.98	996.2	8.25	4180.6	0.611
Wall (cooling)	16.24	998.8	11.1	4187.7	0.593

In Table 17 and Table 18 the results of the Lehrer procedure are shown for heating and cooling respectively. The tables show the characteristic velocities needed to calculate the dimensionless numbers needed to calculate  $Nu_{S,L}$ . From  $Nu_{S,L}$  the individual heat transfer coefficients  $h_h$  and  $h_c$  were calculated. Then  $h_h$  and  $h_c$  were used to calculate the resistance due to the thermal boundary layers.

Table 17: Jacket side – individual heat transfer - heating

Variable	Value	Unit
$d_g$	0.0784	m
$u_O$	1.165	m/s
$u_S$	0.0090	m/s
$u_h$	0.1024	m/s
$Pr$	3.328	-
$Re_S$	$1.54 \cdot 10^4$	-
$\mu/\mu_w$	0.830	-
$Nu_{S,L}$	60.77	-
$h_h$	500.3	W/m <sup>2</sup> K
$R_{J,heat} = 1/(h_h \cdot A_o)$	$4.27 \cdot 10^{-3}$	K/W

Table 18: Jacket side – individual heat transfer - cooling

Variable	Value	Unit
$d_g$	0.0784	m
$u_O$	1.783	m/s
$u_S$	0.0185	m/s
$u_h$	0.1814	m/s
$Pr$	11.44	-
$Re_S$	$9.15 \cdot 10^3$	-
$\mu/\mu_w$	1.405	-
$Nu_{S,L}$	49.44	-
$h_c$	360.5	W/m <sup>2</sup> K
$R_{J,cool} = 1/(h_c \cdot A_o)$	$6.01 \cdot 10^{-3}$	K/W

### 6.1.2.2 Wall

The thermal resistance of the wall was calculated as described in 6.1.2.2. It yielded a thermal resistance of  $4.30 \cdot 10^{-4}$  K/W for heating and  $4.37 \cdot 10^{-4}$  K/W for cooling.

### 6.1.2.3 Vessel side

For the calculation of the individual heat transfer coefficient of the thermal boundary layer at the vessel side Eq.(4-19) was used. From the individual heat transfer coefficient the thermal resistance of the thermal boundary layer was calculated. Table 19 and

Table 20 show the dimensionless numbers required for the correlation to calculate Nu. From Nu  $h_c$  and  $h_h$  were calculated from which the thermal resistances were calculated.

Table 19: Vessel side – individual heat transfer - heating

Variable	Value	Unit
$Re_i$	$8.21 \cdot 10^4$	-
$Pr$	5.268	-
$Nu$	1261	-
$h_c$	1941	W/m <sup>2</sup> K
$R_{V,heat} = 1/(h_c \cdot A_i)$	$1.12 \cdot 10^{-3}$	K/W

Table 20: Vessel side – individual heat transfer - cooling

Variable	Value	Unit
$Re_i$	$7.72 \cdot 10^4$	-
$Pr$	5.643	-
$Nu$	1151	-
$h_h$	1760	W/m <sup>2</sup> K
$R_{V,cool} = 1/(h_h \cdot A_i)$	$1.25 \cdot 10^{-3}$	K/W

### 6.1.2.4 Overall resistance to heat transfer

From the individual thermal resistances the overall thermal resistance and the overall heat transfer coefficient  $U$  was calculated.

Table 21: Theoretical overall heat transfer coefficient  $U$

Thermal resistance $R$	Heating (*10 <sup>-4</sup> )	Cooling (*10 <sup>-4</sup> )
Jacket side $R_J$	42.7 K/W	60.1 K/W
Wall $R_W$	4.30 K/W	4.37 K/W
Vessel side $R_V$	11.2 K/W	12.5 K/W
Overall thermal resistance $R_T$	58.2 K/W	77.0 K/W
theoretical overall heat transfer coefficient $U$	370.0 W/m <sup>2</sup> K	283.6 W/m <sup>2</sup> K

The calculated thermal resistances are shown in Figure 9.

### Thermal resistances in the heat transfer system

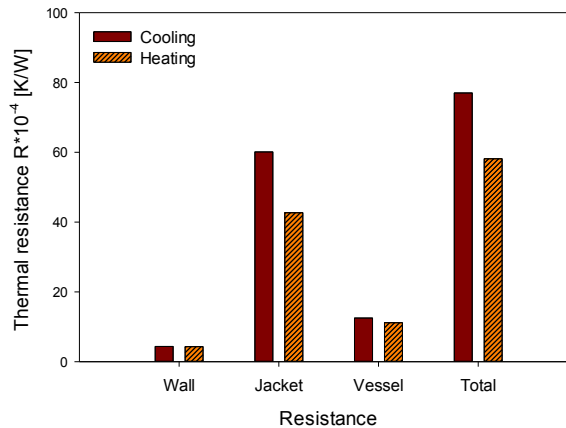


Figure 9: Theoretical thermal resistances of the tested system of heat transfer

Figure 9 shows, that the jacket had the highest thermal resistance in the process of heat transfer in the given system. Therefore the transfer of heat through the boundary layer on the side of the jacket is the limiting step of the whole heat transfer process. This is the case for both, heating and cooling.

The thermal resistance of the jacket side for heating was lower, than for cooling. This can be explained from the properties of water. Since the temperature of the cooling media is lower than of the heating media, the heat transfer is worse. This is also shown by the  $Pr$ , which is significantly increased by the high viscosity of cold water. A high  $Pr$  number means, that the process of heat transfer is limited by thermal diffusion and therefore by convective heat transfer. The lower  $Re$  for the cooling process increases the thermal boundary layer and therefore heat transfer is worse.

## 6.1.3 Practical determination of $U$

### 6.1.3.1 Heating

#### Tempering unit as heating source

To determine which amount of solution can be handled by the system equipped with the tempering unit, trials with 20 L, 50 L and 80 L water were made respectively. Water was heated up from room temperature to 47°C.

When the temperature of heating media was reached, the water was poured into the vessel. As soon as the temperature of the bulk began to rise, the recording of temperature was started. From that point on every minute temperatures of inlet, outlet and bulk were recorded.

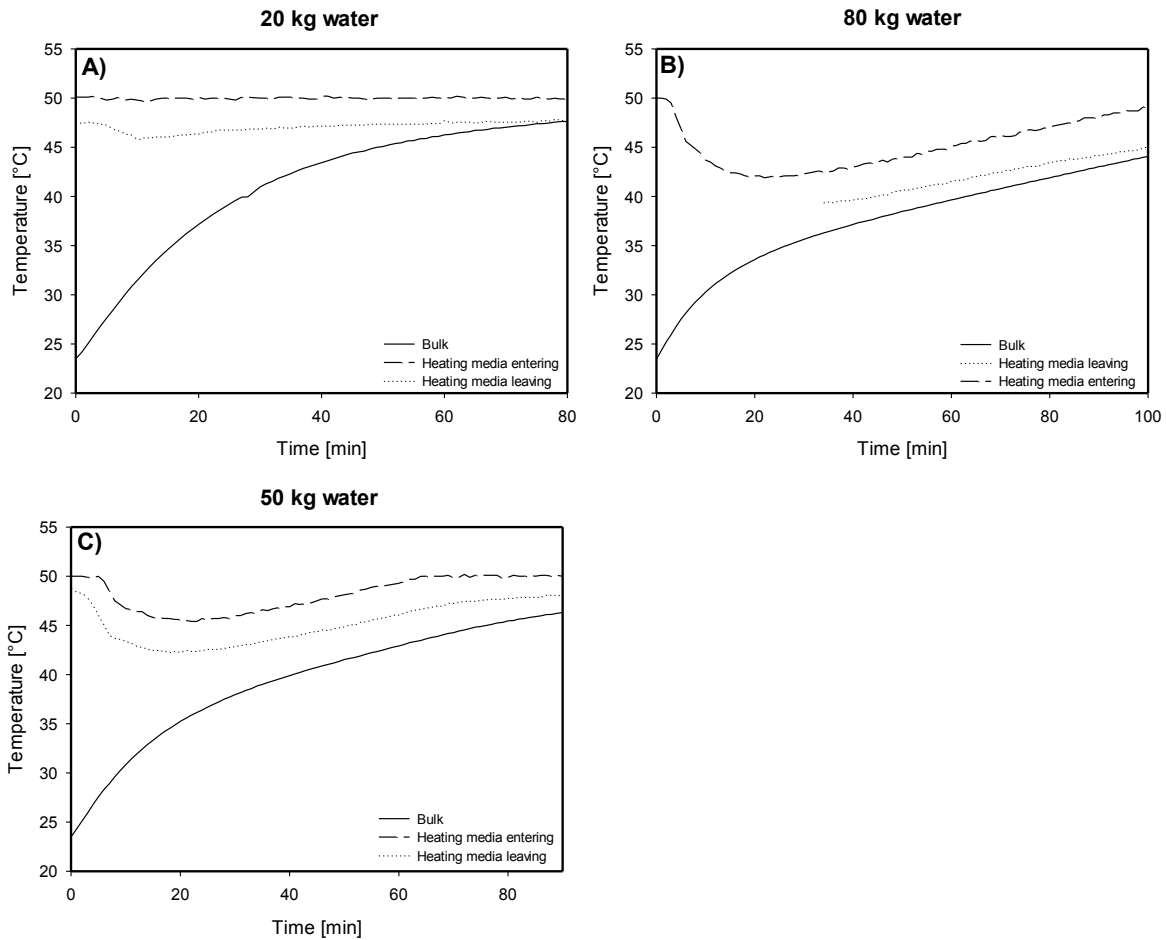


Figure 10: Heating trials with tempering unit. The red line is the temperature of heating media at the inlet; the blue line is the temperature of the heating media at the outlet; the black line is the temperature of the bulk. A) 20 kg of water heated; B) 50 kg of water heated; C) 80 kg of water heated

Figure 10 shows, that the temperature of leaving heating media was a function of time, when applying 50 or 80 kg of water. For 20 kg of water the temperature of leaving heating media was constant. With 50 kg and 80 kg of water respectively the device couldn't compensate for the loss of heat due to transfer. Therefore the temperature of heating media entering the jacket became lower. As a result the process of heating took longer.

The overall heat transfer coefficients were calculated. Trials with 50 kg and 80 kg water were evaluated by Eq.(4-10) and Eq.(4-11) because of the time dependent outlet temperature. As the mean temperature of the heating media an average of one minute time increments was used. The trial with 20 kg water was evaluated by Eq.(4-13) because the outlet temperature was constant.

Table 22: Overall heat transfer coefficients – tempering unit

Mass of water [kg]	Start temperature [°C]	End temperature [°C]	Temperature heating media [°C]	Time [min]	$U$ [W/m <sup>2</sup> K]
20	24.49	47.00	50.00	70	210.1
50	23.49	46.31	48.15	90	216.3
80	23.45	44.07	45.14	100	241.9

The results showed that the overall heat transfer coefficient for the used system was around 200 W/m<sup>2</sup>K. For 20 kg and 50 kg water respectively the overall heat transfer coefficient was approximately equal. For 80 kg it was slightly higher. The average temperature was only an estimation which contributed to the uncertainty of the result. It is also visible, that higher filling volumes increased the necessary time for heating significantly.

The results suggested using tap water as a more time efficient way for heating the bulk fluid in the vessel. Advantages were

- Temperature does not exceed the heat stability of GFP (see 6.2)
- Allows a higher flowrate of heating media and therefore higher turbulence
- Temperature at the inlet is constant allowing calculation of  $U$

For maintaining the temperature of the bulk, the tempering unit seemed sufficient.

### Tap water as heating source

The volume to treat was fixed to 50 L. The volume was restricted to this value to guarantee adequate mixing, since the homogenate was more viscous than water. For practical determination of the overall heat transfer coefficient a heating trial was made, where bulk temperature and temperature of heating media at the outlet were measured every two minutes.

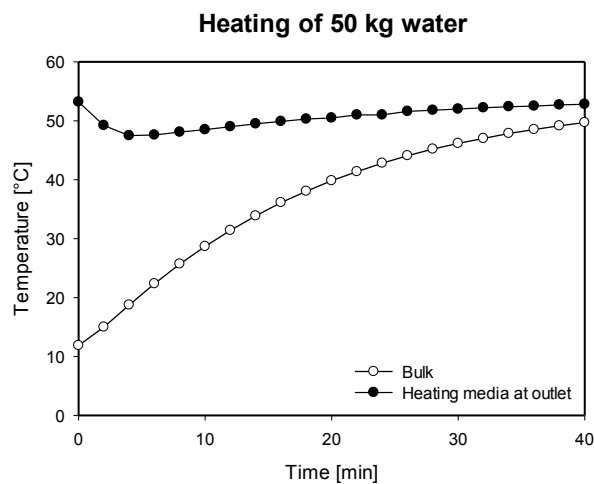


Figure 11: Heating of 50 kg of water; heating media was tap water with a temperature of 54.3°C and a flow through the annular space of 21.8 L/min

The trial showed, that the temperature at the outlet was a function of time. The process of heating  $M = 50$  kg water from  $t_1 = 11.87^\circ\text{C}$  to  $t_2 = 49.70^\circ\text{C}$  took  $\theta = 40$  min. From the properties of water and the measured parameters the overall heat transfer coefficient for heating was calculated using Eq.(4-10) for heating with time dependent outlet temperature. The temperatures and properties of water from Table 15 and **Fehler! Verweisquelle konnte nicht gefunden werden.** were used.

In Eq.(4-10) the only unknown was  $K_1$ , from which  $U$  was calculated. For cylindrical geometry the surface involved in heat transfer was calculated by

$$A_m = 2r\pi * H_L = D_m\pi * H_L \quad \text{Eq.(6-2)}$$

$H_L$  was calculated from the filling volume  $V_{fill}$ . The ellipsoid shape of the bottom of the tank was taken into account.

$$H_L = \frac{V}{A} = \frac{V_{fill} - V_{ellipsoid}}{(D_T/2)^2 \pi} = \frac{(0.0502 - 0.00388)m^3}{(0.200m)^2 \pi} = 0.37m \quad Eq.(6-3)$$

For the diameter to calculate the surface the average diameter  $D_m$  was used.

$$D_m = D_T + B = 0.400m + 0.003m = 0.403m \quad Eq.(6-4)$$

Rearranging of Eq.(4-10) gives an expression for  $K_1$

$$K_1 = \frac{1}{1 - \frac{Mc_p}{WC_p \theta} * \ln\left(\frac{T_1 - t_1}{T_1 - t_2}\right)} \quad Eq.(6-5)$$

Inserting the result from Eq.(6-5) into Eq.(4-12),  $U$  was calculated by

$$U = \frac{WC_p * \ln K_1}{A_m} \quad Eq.(6-6)$$

Evaluation yielded  $K_1 = 1.148$  and  $U = 445.7 \text{ W/m}^2\text{K}$ .

Therefore for the given system of heat transfer, the overall heat transfer coefficient  $U$  for the process of heating was **445.7 W/m<sup>2</sup>K**.

### 6.1.3.2 Cooling

The determination of  $U$  for the cooling process was done as described above.

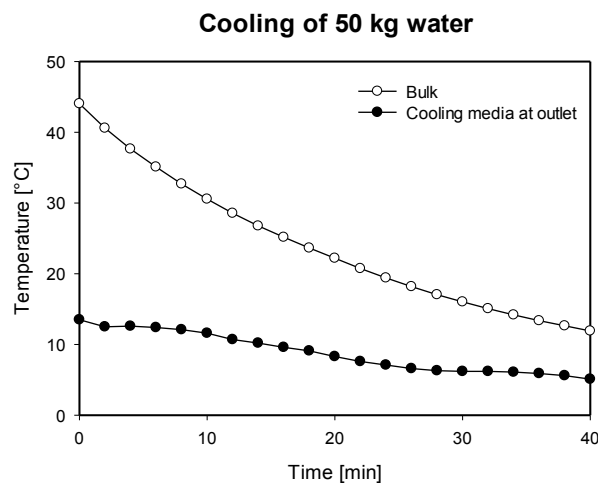


Figure 12: Heating of 50 kg of water; cooling media was ice water with a temperature of 4.5°C and a flow through the annular space of 45.3 L/min

The trial showed, that the temperature at the outlet was a function of time. The process of cooling  $M = 50 \text{ kg}$  water from  $T_1 = 44.04^\circ\text{C}$  to  $T_2 = 11.91^\circ\text{C}$  took  $\theta = 40 \text{ min}$ . From the properties of water and the measured parameters the overall heat transfer coefficient for

cooling was calculated using Eq.(4-11) and Eq.(4-12). The temperatures and properties of water from Table 15 and **Fehler! Verweisquelle konnte nicht gefunden werden.** were used.

Rearrangement as done above yielded  $K_1 = 1.049$  and an overall heat transfer coefficient for the process of cooling  $U$  of **326.2 W/m<sup>2</sup>K**.

#### 6.1.4 Theoretical vs. practical $U$

In Figure 13 practically determined and theoretically determined  $U$  are compared.

The practically determined  $U$  was obtained from the trial of heating and cooling 50 kg of water. Temperatures were recorded and  $U$  was calculated from Eq.(4-10) and Eq.(4-11).

The theoretically determined  $U$  was obtained from combination of the different resistances contributing to the process of heat transfer. For the jacket Eq.(4-14) was used. For the wall Eq.(4-20) was used. For the vessel Eq.(4-19) was used. For evaluation of the correlations used measured values from the practical experiments were used as a basis.

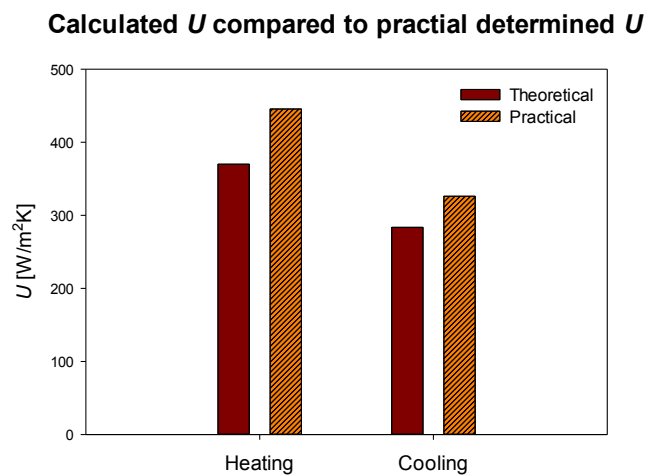


Figure 13: Comparison of theoretical and practical determined overall heat transfer coefficient  $U$  for heating and cooling process

The differences between the theoretical and the practical values of  $U$  can be explained by the calculation procedure. The correlation used for the vessel side was designed for vessels without baffles. Since the vessel contained one baffle, the correlation yielded a result, which is associated with an error in prediction. This error arises due to the higher degree of turbulence produced by the baffle. Therefore the calculation may underestimate the individual heat transfer coefficient in the thermal boundary layer on the vessel side.

The correlation for the jacket side proposed by Lehrer was originally investigated for a range of  $5 < Pr < 7$  and  $2.2 \cdot 10^4 < Re_s < 8.0 \cdot 10^4$ . Cooling and heating were both not fulfilling these requirements.  $Re_s$  for heating was  $1.54 \cdot 10^4$  and for cooling  $Re_s$  was  $9.28 \cdot 10^3$ .  $Pr$  of the heating media was 3.328 and  $Pr$  for cooling media was 11.44. Since  $Re_s$  always was below the lower limit of the correlation, the procedure may underestimate the thermal boundary layer on the jacket side. The underestimation may be increased for the cooling process because of the highly unfavorable  $Pr$ , where convective heat transfer is dominating. This is also the case for heating but to a weaker extent.

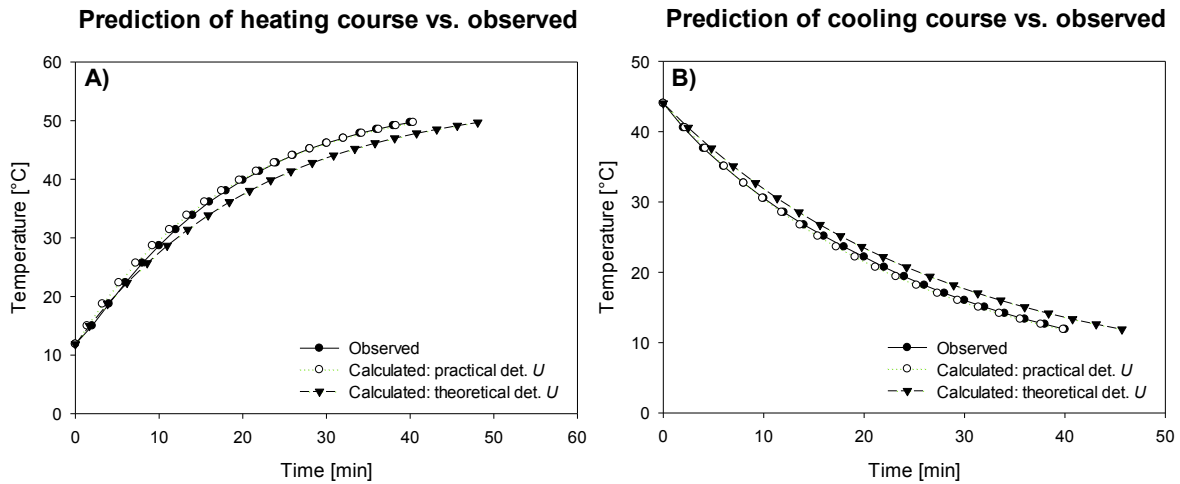


Figure 14: A) prediction of the course of bulk temperature for water and heating process with practically determined and theoretically determined  $U$ ; B) prediction of the course of bulk temperature for water and cooling process with practically determined and theoretically determined  $U$

Figure 14 the profiles of heating and cooling are shown. The profiles, which were obtained in the practical determination of the overall heat transfer coefficients were compared to the predicted profiles. Therefore two ways of prediction were used:

- 1) The values for  $U$  from the practical determination were used to predict the profile.
- 2) The theoretical calculated values for  $U$  from the correlations were used to predict the profile.

For both, heating and cooling, the differences from the obtained profiles and the predicted profiles were small, when the practically determined  $U$  was used. Calculation using the theoretically determined  $U$  estimated a longer time for heating and cooling, than the observed time. This is shown in Figure 15, where the residues calculated by Eq.(6-7), are shown.

$$r_{T_i} = t_{T_i,calc} - t_{T_i,obs} \quad Eq.(6-7)$$

The index  $T_i$  refers to the temperature, which was reached after the observed time interval. The index  $calc$  refers to the predicted time to reach  $T_i$ , the index  $obs$  refers to the measured time to reach  $T_i$ .

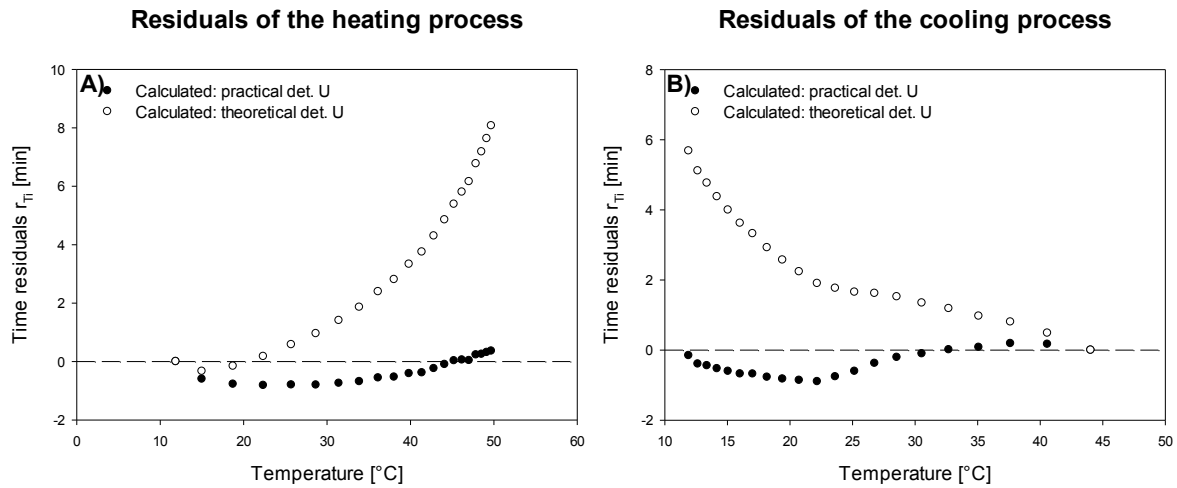


Figure 15: A) time residuals with respect to the observed temperature course of bulk temperature for water and heating process with practically determined and theoretically determined  $U$ ; B) time residuals with respect to the observed temperature course of bulk temperature for water and cooling process with practically determined and theoretically determined  $U$

For heating the prediction calculated from the practically determined  $U$  the residues ranged from -0.82 min to 0.36 min. Prediction from the theoretically determined  $U$  yielded residues from -0.33 min to +8.07 min.

For cooling the prediction calculated from the practically determined  $U$  the residues ranged from -0.90 min to 0.19 min. Prediction from the theoretically determined  $U$  yielded residues from 0.00 min to +5.87 min.

## 6.2 Heat precipitation in small scale

### 6.2.1 Process

The starting material was 9.75 L of cell harvest with a CDM concentration of 36.88 g/L. The turbidity was 12240 NTU and the solid content was 11.25%.

The cell suspension was homogenized as described in 5.4.5.1.

The debris containing suspension had a GFP concentration of 747.2 mg/L at start and decreased only slightly to 729.1 mg/L after 3 h of heat treatment and separation. The formation of precipitate was observed by the increase of turbidity from 2640 NTU to 6720 NTU and the increase of solid content from 1.67% to 10.00%. After clarification the turbidity was 423 NTU and the solid content was 0.33%.

The debris free suspension had a concentration of 687.8 mg/L and increased slightly to 703.6 mg/L after 3 h of heat treatment and separation. The turbidity increased from 942 NTU to 4140 NTU and the solid content increased from 0.42% to 5.83%. After clarification the turbidity was 434 NTU and the solid content was 0.33%.

The losses of GFP were so small compared to the formation of precipitate, that the heat precipitation step was considered feasible. Since the precipitation increases the purity of GFP its activity also increases. This suggested that although the concentration measured by fluorescence stayed approximately constant, a small amount of GFP was lost during heat precipitation.

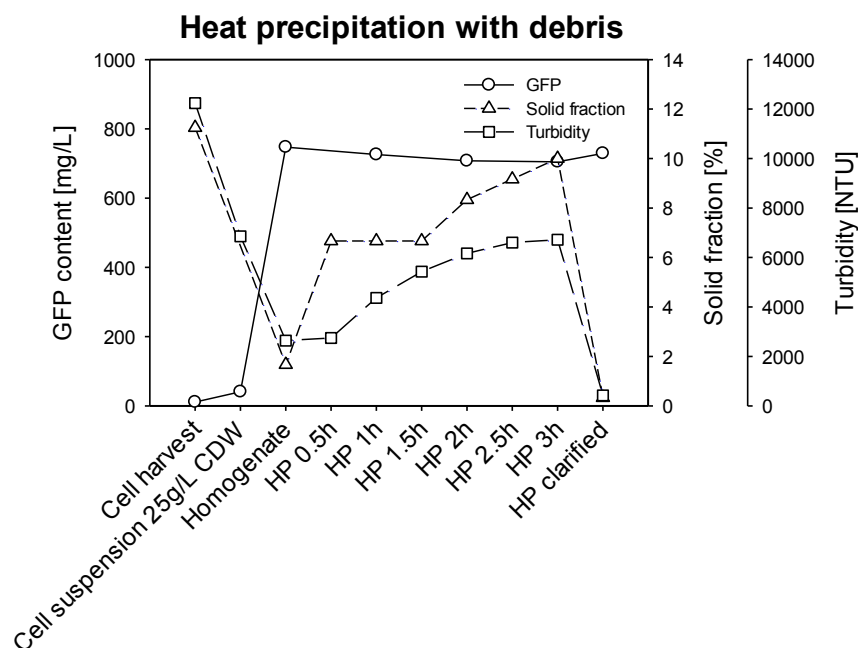


Figure 16: Small scale heat precipitation of homogenate containing 25 g/L CDM produced at 70/700 bar, 1 passage with debris

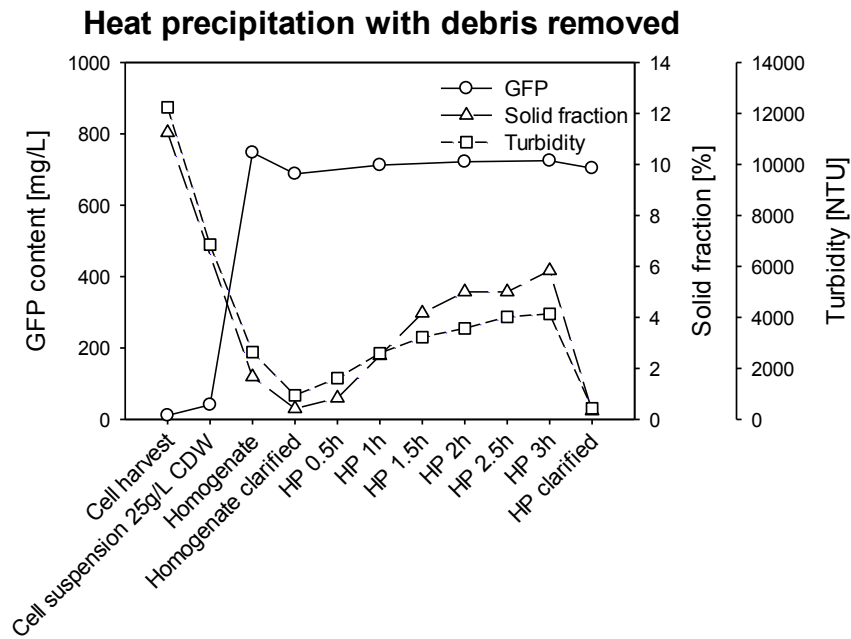


Figure 17: Small scale heat precipitation of homogenate produced from a cell suspension containing 25 g/L CDM at 70/700 bar, 1 passage with debris removed before the precipitation step

### 6.2.2 Particle sizes of process solutions

The cells had median particle size of 1283 nm. The resulting homogenate after 70/700 bar over one passage had a median particle size of 319 nm which was the starting material for heat precipitation of unclarified homogenate.

Clarified homogenate without heat treatment had a median particle size of 205 nm.

Heat precipitated clarified homogenate had a median particle size of 293 nm which decreased after separation to 211 nm.

The heat precipitation of unclarified homogenate increased its median particle size to 325 nm. After separation remaining particles had a median size of 226 nm.

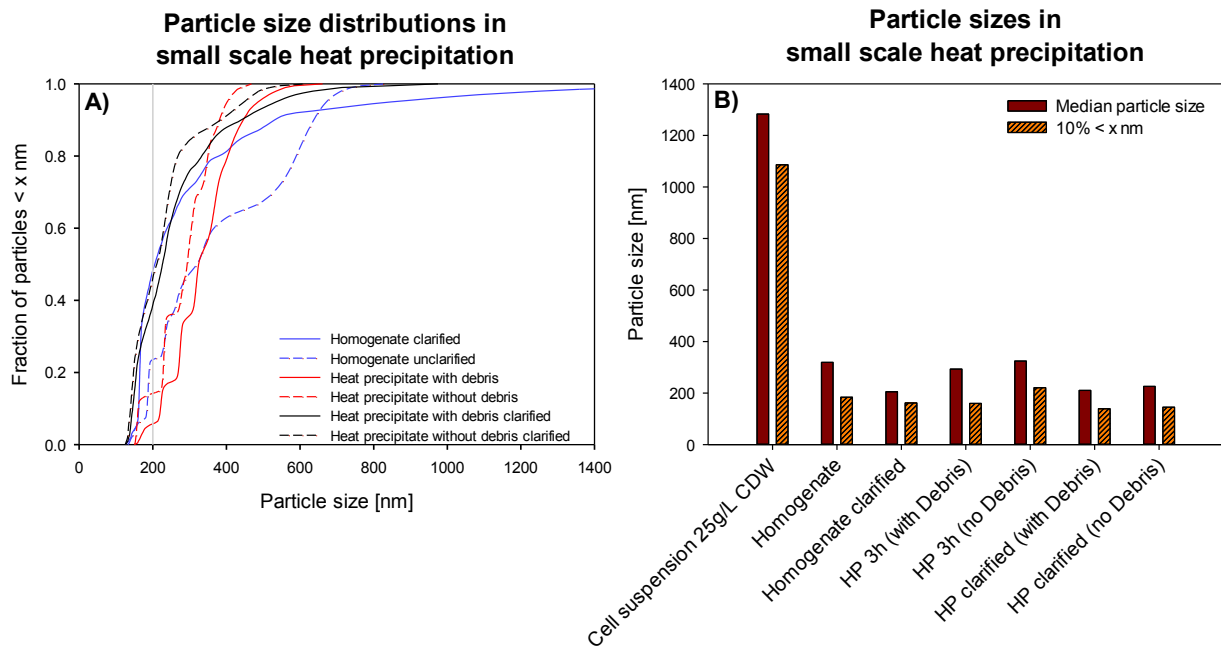


Figure 18: A) Particle size distributions of the homogenates and heat precipitates generated in small scale experiments; B) Median particle sizes of the homogenates and heat precipitates generated in small scale experiments

With respect to filtration as the next process step it was important to obtain particles which could be separated without blocking the sterile filters. The measurement of particle sizes showed, that all suspensions contained particles in the region of ~200 nm and the size distributions showed that there were up to 50% of particles smaller than 200 nm. This was problematic for filtration considering the typical pore size of sterile filters around 200 nm.

This was confirmed by filtration trials (see 6.7.1).

### 6.3 Heat precipitation in large scale

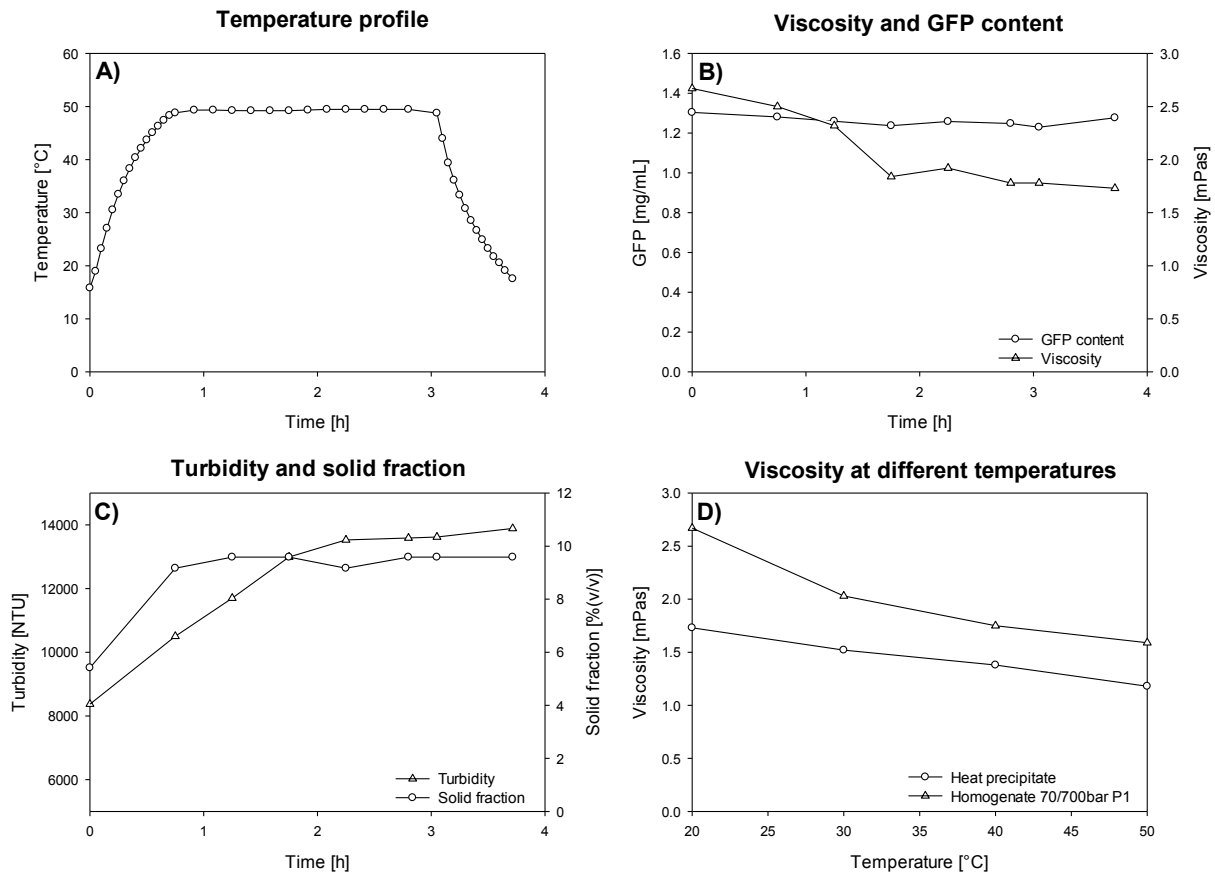


Figure 19: Large scale heat precipitation of homogenate obtained at 70/700 bar over one passage from a cell suspension with a CDM concentration of 25 g/L; A) temperature profile of the precipitation process; B) GFP content and viscosity during the precipitation process; C) turbidity and solid content during the precipitation process; D) viscosity of the homogenate and the heat precipitate at different temperatures in the range from 20°C to 50°C

The temperature course of the heat precipitation was in the range of the results of the model experiments with water. For heating from 11.87°C to 49.70°C a time of 40 min was observed which was comparable to the actual time needed of 42 min to heat from 15.83°C to 48.81°C. For maintaining the temperature, the tempering unit was sufficient. Cooling was also comparable to the model experiments, where cooling from 44.04°C to 11.91°C took 40 min. The actual time needed for cooling homogenate from 48.76°C to 17.57°C was 40 min.

Measured viscosity during the course of precipitation was significantly higher than that of water, although it was decreasing from 2.67 mPas to 1.73 mPas. Therefore the degree of turbulence was lower than it was the case in the experiments where water was used. The effect of turbulence was weakened by the change of specific heat capacity, because aqueous suspensions containing solids has got a lower specific heat capacity.

The viscosities were measured from the homogenate before heat precipitation and the heat precipitate at different temperatures. The viscosity of homogenate ranged from 2.67 mPas at 20°C to 1.59 mPas at 50°C. The viscosity of heat precipitate suspension ranged from 1.73 mPas at 20°C to 1.18 mPas at 50°C.

The GFP content was approximately constant. At start of heat precipitation it was 1.30 mg/mL and at the end it was 1.28 mg/mL. During the precipitation the measured values were ranging from 1.24 mg/mL to 1.30 mg/mL.

The turbidity increased from 8370 NTU to 13890 NTU and the solid content increased from 5.82% to 9.58%. These observations showed, that heat precipitate was formed during the heat treatment.

The particle sizes also were measured and can be found in Figure 25.

Figure 20 shows the difference between the observed temperature profile of the homogenate and the predicted temperature profile calculated from the practically determined overall heat transfer coefficients.

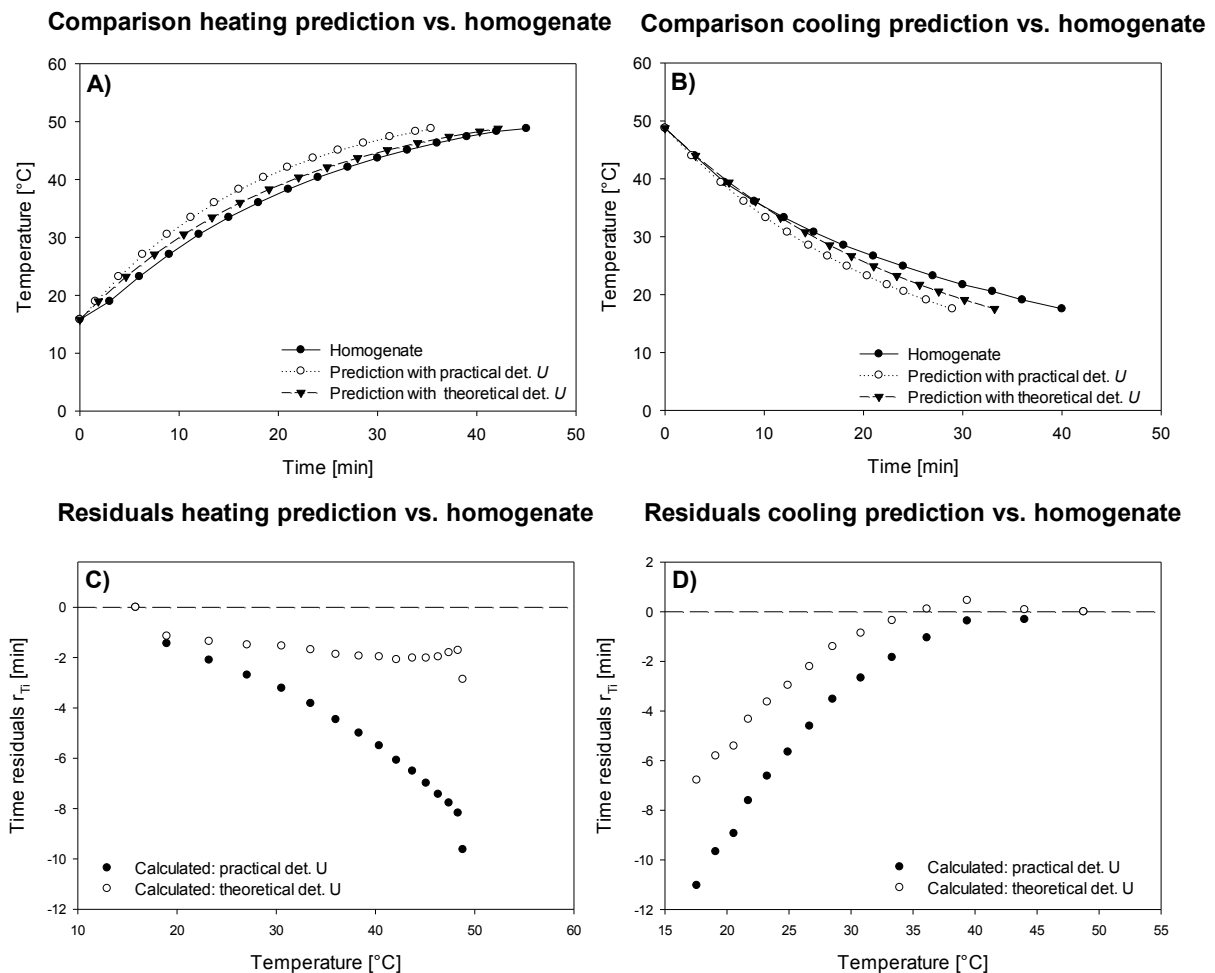


Figure 20: A) predicted course of homogenate heating with practical and theoretical determined  $U$  vs. observed course; B) predicted course of homogenate cooling with practical and theoretical determined  $U$  vs. observed course; C) time residuals between predicted course of homogenate heating with practical / theoretical determined  $U$  and observed course of homogenate; D) time residuals between predicted course of homogenate cooling with practical / theoretical determined  $U$  and observed course of homogenate

Table 23 shows the comparison of the observed heat precipitation process to the prediction of the process.

Table 23: Observed heat precipitation of homogenate 70/700 bar, one passage compared to prediction

Process	Heating	Cooling
Starting temperature [°C]	15.8	48.7
End temperature [°C]	48.8	17.6
Observed time [min]	45.0	40.0
Predicted time from practical U [min]	35.4	29.0
Temperature reached after predicted time [°C]	46.3 after 36 min	21.7 after 30 min
Difference to prediction [°C]	-2.5	4.1
Predicted time from theoretical U [min]	42.2	33.2
Temperature reached after predicted time [°C]	48.3 after 42 min	20.5 after 33 min
Difference to prediction [°C]	-0.5	2.9

Since the overall heat transfer coefficients were determined from the modelling fluid water, differences to the actual process suspension were expected.

It is noticeable, that the theoretically determined  $U$  delivered a better prediction of the observed temperature profile. Since the applied calculation procedure for  $U$  may have underestimated the actual  $U$ , this observation was reasonable.

Another fact was the difference in viscosities. If the viscosities at the mean temperatures ( $\sim 31^\circ\text{C}$ ) during precipitation were considered, the difference in turbulence in terms of the  $Re$  was obtained. Assuming a mean viscosity of 1.7 mPas during precipitation and using the density of water,  $Re$  for the homogenate was  $3.75 \cdot 10^4$ , while for water  $Re$  was  $8.50 \cdot 10^4$ . Both  $Re$  indicated turbulence, but the degree of turbulence was significantly different and therefore affected the thickness of the thermal boundary layer on the vessel side.

Also the isobaric heat capacity had an influence on the temperature profile, since it was used in the calculation in Eq.(4-10) and Eq.(4-11). The homogenate had a lower isobaric heat capacity than water due to the solids. This would increase the term on the right side, and therefore decrease the time  $\theta$  needed for heating and cooling. However the opposite was observed in the precipitation. The impact of this influence could not be evaluated, since the isobaric heat capacity of the homogenate was not determined.

The most reasonable explanation for the observed increase in time needed for heating is the activation energy. Transition of the proteins from the natural to the denatured state needs a certain amount of activation energy. This energy is supplied as heat and is consumed by the reaction. Due to this phenomenon consumed heat did not contribute to the increase of temperature leading to an increase of time needed to complete the heating process.

Since this argument was not valid for the cooling process, the difference for cooling had another cause. At lower temperatures, the heat transfer is worse because of the weaker transport due to the dependency on convective heat transfer. This could explain why the difference between prediction and observed cooling profile is higher than for the heating profile.

For the actual step of heat precipitation, the difference between the prediction and the real profile was unlikely to have big impact on the process, because the temperature differences were quite small.

## 6.4 Homogenization trials

As a consequence of the difficulties in filtration observed after separation in small scale the homogenization step was investigated. Different pressures and passage numbers were applied and the release of GFP, the particle size and the viscosity were determined. Besides calculation of the median particle size, also the size was determined which the smallest 10% of the particles do not exceed. Median size and 10% value together were used as an indicator for estimation, if a sterile filter with 200 nm pore size may be able to retain the remaining small particles remaining from homogenization and separation.

Table 24 shows which homogenization parameters were investigated.

Table 24: Pressures and passages for homogenization trials

Pressure [bar] 2 <sup>nd</sup> stage / 1 <sup>st</sup> stage	Number of passages	Concentration of CDM [g/L]
70/700	2	25; 50
0/700	2	25; 50
50/500	3	25; 50
0/500	3	25; 50
30/300	3	25; 50
0/400	1	25*

\*) Suspension was incubated at 4°C for 19 h with 2 % Triton-X100 prior to homogenization

The aim was to find the operating conditions which yield as big particles as possible, while keeping a reasonable high GFP release. This is important, because bigger particles can be separated easier by centrifugation.

Moreover viscosity should be not too high, as this was important for whether guaranteeing sufficient turbulence in the following heat precipitation step or successful separation in the disc stack centrifuge.

The results are shown in Table 25. The table shows the initial CDM concentrations, the GFP release obtained from homogenization, viscosity of the resulting suspension and the debris particle sizes resulting from the homogenization pressures investigated.

## 6.4.1 Overview of homogenization results

Table 25: Overview of results of homogenization trials

Parameter		GFP [mg/mL]		GFP release		Viscosity [mPas]		Median particle size [nm]		10% < x [nm]	
<b>Cell harvest</b>		-	-	-	-	1.73	1.72	1450	1,442	1297	1,277
<b>CDM [g/L]</b>		24.93	50.59	24.93	50.59	24.93	50.59	24.93	50.59	24.93	50.59
<b>Cell suspension</b>		-	-	-	-	1.66	1.72	1438	1,412	1333	1,258
Pressure [bar]	Passage number										
<b>70/700</b>	1	7.65	12.12	100%	92%	2.76	6.66	336.2	600.8	181.3	248.5
	2	7.65	13.14	100%	100%	2.13	4.48	260.2	397.1	162.7	204.7
<b>0/700</b>	1	5.95	12.80	78%	97%	2.24	9.32	268.7	544	164.7	248.6
	2	5.31	13.72	69%	104%	1.89	4.56	233.7	399.7	144.6	202.4
<b>50/500</b>	1	6.39	10.99	84%	84%	2.84	6.89	359.6	640.9	207.9	286.4
	2	7.03	13.79	92%	105%	2.35	5.74	343.1	549.6	174.4	258.1
	3	6.60	12.39	86%	94%	1.92	4.50	290.8	369.2	181.4	256.4
<b>0/500</b>	1	7.04	11.30	92%	86%	3.68	16.70	469.9	573.8	225.1	279.7
	2	7.35	13.25	96%	101%	2.30	5.49	335.9	425.4	153.5	229.6
	3	7.09	12.39	93%	94%	2.07	3.87	287.7	399.1	139.5	204.5
<b>30/300</b>	1	4.19	7.26	55%	55%	3.04	5.16	448.6	676.6	234.7	350.2
	2	5.26	9.36	69%	71%	2.42	5.13	373.4	662.1	254.1	298.8
	3	5.53	10.56	72%	80%	2.24	5.97	359.5	650.8	232.8	287.9
<b>0/400*</b>	incubated	1.60	-	21%	-	2.03	-	1333	-	1145	-
	1	6.14	-	80%	-	3.99	-	608.9	-	287.9	-
<b>2% Triton-X100 + 12.5 % KH<sub>2</sub>PO<sub>4</sub> **</b>		8.48	-	111%	-	11.40	-	-	-	-	-

\*) cell suspension was incubated with 2 % Triton-X100 for 19h at 4°C prior to homogenization at given pressure

\*\*\*) cell suspension was incubated with 2% Triton-X100 + 12.5 % KH<sub>2</sub>PO<sub>4</sub> and was not homogenized afterwards

## 6.4.2 Homogenization of 25 g/L CDM

For the release of GFP the second passage at 70/700 bar was chosen as a reference. It was defined as 100 % GFP release, to which the other passages were compared. The reference homogenate had a GFP concentration of 7.65 mg/mL.

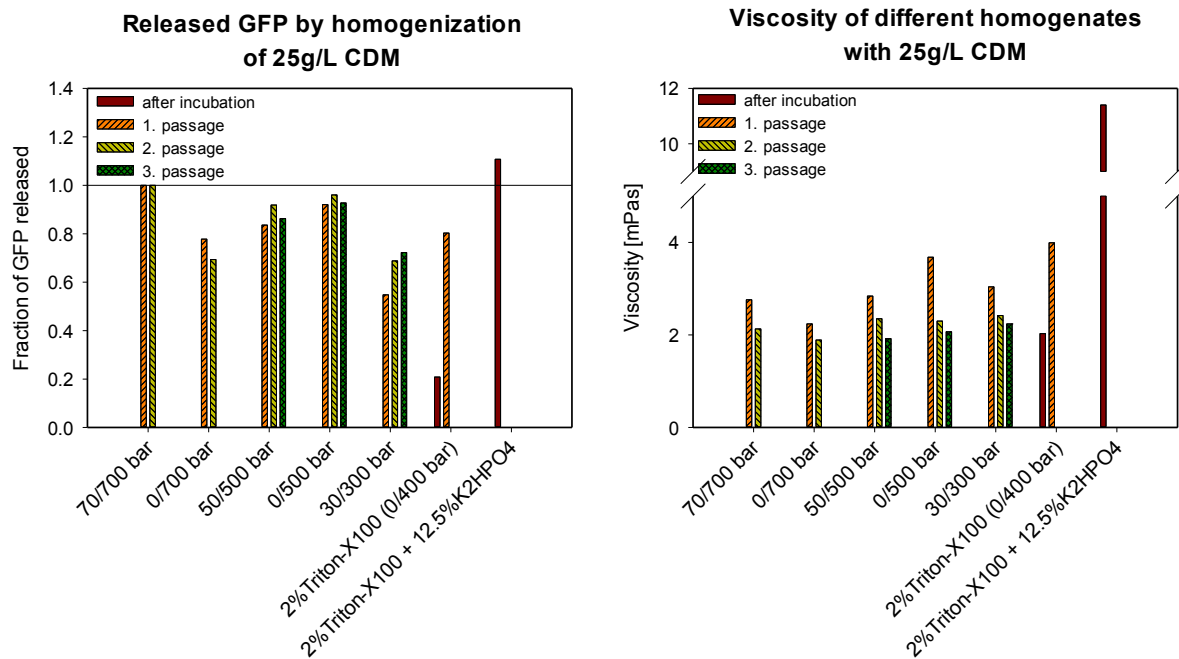


Figure 21: Release of GFP and viscosities after homogenization of 25 g/L CDM

Performing two passages at 70/700 bar did not increase the release. Therefore to reach the maximum release one passage at 70/700 bar is sufficient. At 0/700 bar the release decreased from 78 % to 69 %. This suggests, that GFP may be damaged to the mechanical stress induced by the instant expansion to a pressure of zero bar. A similar effect could be observed for the homogenizations at 50/500 bar and 0/500 bar respectively. The release increased from one passage to two passages, but drops after the third passage. For 50/500 bar the release was between 84 % and 92 %. For 0/500 bar the release was between 92 % and 96 %. At a pressure of 30/300 bar the release increased continuously from 55 % after the first passage to 69 % after the second passage and to 72 % after the third passage. The cell suspension containing 2 % Triton-X100 showed a release of 21 % after 19 h of incubation at 4°C. After homogenization of this solution at 0/400 bar the release was 80 %. Incubation with 2 % Triton-X100 and 12.5 % KH<sub>2</sub>PO<sub>4</sub> yielded a highly viscous slurry (11.40 mPas) with 111 % release. That suggests that most of the GFP is released.

For all homogenization pressures it was observed, that viscosity decreased with increasing passage number. The viscosity depends mostly on released DNA by disintegration of cells. With increasing passage number more DNA is fragmented than released by remaining cells, therefore reducing the viscosity of the homogenate. It was also observed, that with lower pressures the viscosity increased in comparison to homogenization at 70/700 bar. Moreover a significant increase of viscosity was observed for the cell suspension with both added Triton-X100 and KH<sub>2</sub>PO<sub>4</sub> after incubation at 4°C. The viscosity was 11.40 mPas. Therefore no homogenization was performed.

To decide which pressure is optimal for homogenization of 25 g/L CDM the particle sizes of the obtained homogenates were investigated.

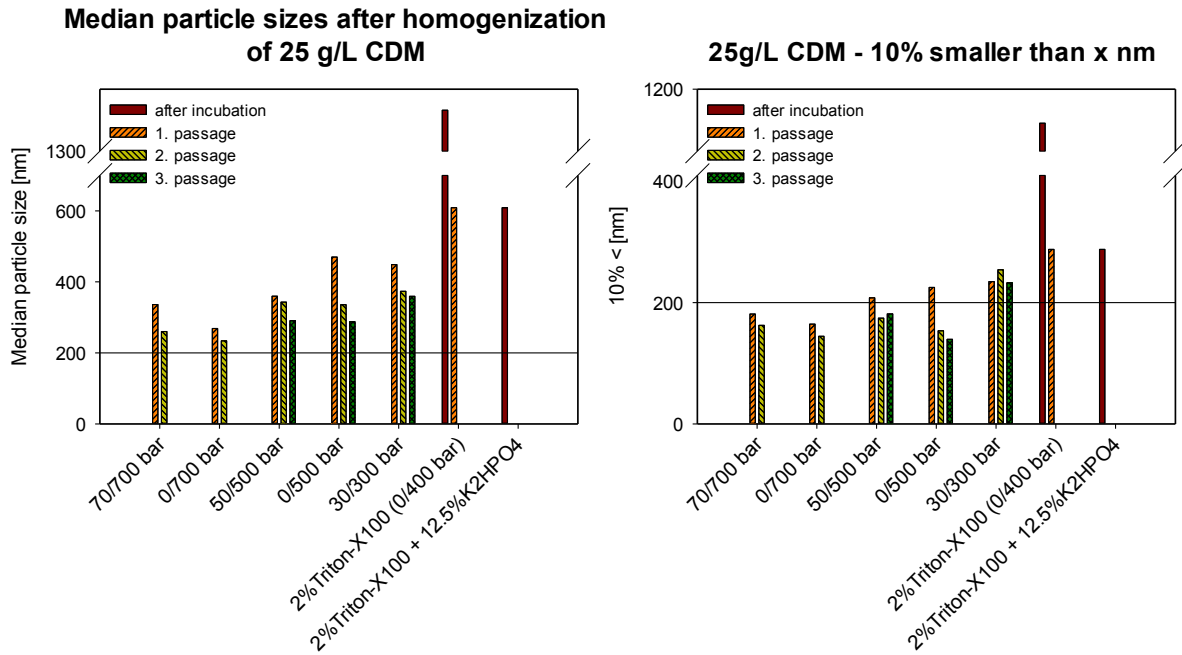


Figure 22: Particle sizes of homogenates with 25 g/L CDM

It was observed that the median particle size decreased with increasing passage number. This made sense because every passage breaks up more of the residual cells and decreased the size of debris further. The lower the applied pressure was, the bigger the particles. The smallest particles were obtained after the second passage at 0/700 bar with a median size of 233.7 nm. This size is comparable to the homogenization at 70/700 bar, which yielded 260.2 nm after the second passage. The biggest particles were found after homogenization of Triton-X100 treated cells with 608.9 nm.

The particle size for homogenization at 50/500 bar only slightly decreased from 359.6 nm after the first passage to 290.8 nm after the third passage, while providing a high GFP release, as mentioned above. The viscosity was in the range of 2.84 mPas after one passage to 1.92 mPas after three passages.

### 6.4.3 Cell suspension 50 g/L CDM

For the release of GFP the second passage at 70/700 bar was chosen as a reference. It was assigned with 100 % GFP release, to which the other passages were compared. The reference homogenate had a GFP concentration of 13.14 mg/mL.

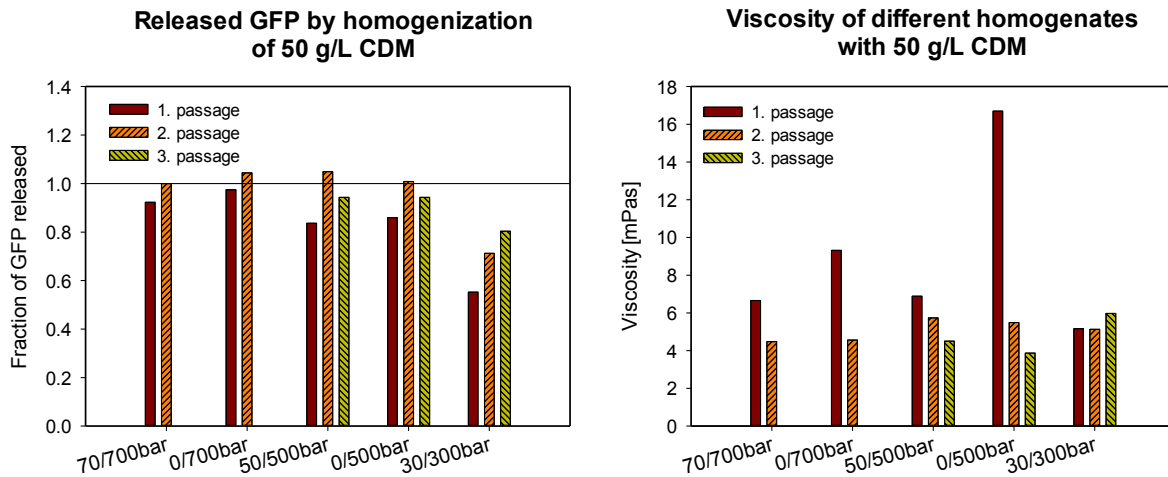


Figure 23: Release of GFP and viscosities after homogenization of 50 g/L CDM

At 70/700 bar the release increased from 92 % to 100 % from the first to the second passage. At 0/700 bar the release increased from 97 % after the first passage to 104 % after the second passage. Also at 50/500 bar, 0/500 bar and 30/300 bar an increase of release was observed from the first to the second passage. At 0/500 bar and 50/500 bar the release increased from 86 % to 101 % and from 84 % to 105 % respectively. Performing a third passage at these pressures lowered the release to 94 % because of mechanical stress applied the product. At 30/300 bar a continuous increase of release from 55 % after the first passage to 71 % after the second passage to 80 % after the third passage was observed. The smaller difference from the second passage to the third passage is also caused by mechanical stress.

In terms of GFP release homogenization at 30/300 bar seemed not to be feasible. At the other pressures a maximum of two passages seemed appropriate, since the release tended to be lowered by a third passage.

Main differences between the homogenates were observed in terms of viscosity. All pressures investigated yielded their highest viscosity after the first passage except of the homogenate produced at 30/300 bar. It should also be noted that its viscosity was the same after the first and the second passage (5.16 mPas and 5.13 mPas respectively) and only increased slightly to 5.97 mPas after the third passage. The viscosity of the other homogenates decreased continuously with the number of passages. The highest viscosity was observed after homogenization at 0/500 bar after the first passage. At 50 g/L CDM the pressure was sufficient to break up the cells but due to the instant expansion to zero bar the freed DNA was not fragmented. DNA fragmentation seemed to happen in the second passage, since the viscosity was reduced from 16.70 mPas to 5.49 mPas. The third passage again lowered the viscosity to 3.87 mPas. The lowest viscosities were observed after the second passage at 70/700 bar and 0/700 bar. After the first passage viscosities of 6.66 mPas and 9.32 mPas were measured while the second passage reduced them to 4.48 mPas and 4.56 mPas respectively. The higher viscosity after the first passage at 0/700 bar can be explained in the same way as it was the case at 0/500 bar. The difference in pressure of the one-stage homogenizations explains the difference in viscosity.

In terms of viscosity it seemed beneficial to perform two passages. After a third passage, the decrease in viscosity was minor or wasn't observed at all (30/300 bar).

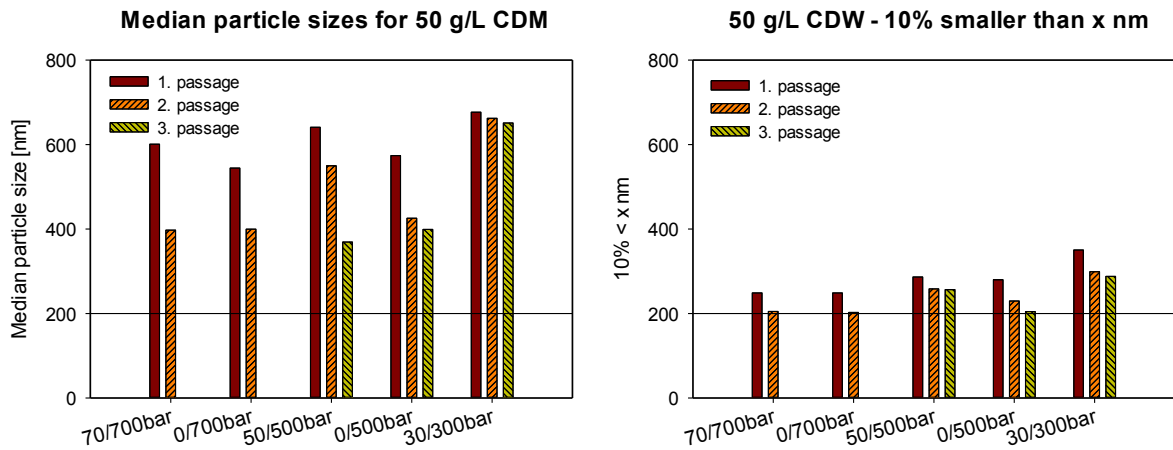


Figure 24: Particle sizes of homogenates with 25 g/L CDM

It was observed that the median particle size decreased with the increasing passage number. This was not the case at 30/300 bar, where it remained approximately constant (676.6 nm, 662.1 nm and 650.8 nm) and were the biggest particles in the trials. This could also be seen from the 10 % value. Generally it was observed, that the lower the applied pressure was, the bigger the particles remained. The smallest particles were obtained after the second passage at 0/700 bar and 70/700 bar with a median size of 399.7 nm and 397.1 nm respectively. At 50/500 bar every passage reduced the median size significantly from 640.9 nm after the first passage over 549.6 nm after the second passage to 369.2 nm after the third passage, while 10 % were smaller than 286.8 nm, 258.1 nm and 256.4 nm respectively. It was also observed, that the second passage of the two-stage homogenization at 50/500 bar produced a higher median particle size than its one-stage pendant with 425.4 nm. The difference was also observed at the 10 % value.

## 6.5 Separation

### 6.5.1 Cell separation

Cell separation was investigated from fermentation broth designed for 25 g/L CDM. 152.2 kg of the broth with a solid content of 11.67%, a viscosity of 2.02 mPas and a turbidity of 33570 NTU were separated with a disc stack centrifuge at 11390 rpm and a flow rate of 113 L/h.

Theoretical calculation yielded a required number of discharges of 22 and an estimated separation time of 81 min. This would have been a cycle time of 3.6 min.

From a WCM of 17.79 kg 15.11 kg were recovered in the form of cell paste with a solid content of ~65% and CDM concentration of 134.8 g/L. For separation 18 discharges with an average cycle time of 4.6 min were needed (83.6 min in total). The loss at each discharge was 1.28 kg of harvest suspension (0.15 kg of WCM) and therefore the yield of the separation step was 84.9%. The resulting pool of supernatant had a turbidity of 85.4 NTU. Assuming  $NTU_{min}$  is small, it was neglected and the clarification efficiency was calculated to be 99.75%.

The data of separation are listed in Table 26.

Table 26: Cell separation trial

Cycle number	Cycle time [s]	Turbidity of supernatant [NTU]	Notes
1	214		
2	242		
3	260		
4	270		
5	275		pressure drop from +0.25 bar to -0.25 bar during separation; after 12.cycle air flow was opened to restore a pressure of +0.25 bar
6	285	64.7	
7	300	27.4	
8	320	32.2	
9	340		
10	360		
11	380		
12	245		first cycle with corrected pressure
13	260		
14	255		
15	250		
16	250		
17	255		
18	255		full discharge
Summary	83.6 min	85.4 (pool)	

The transportation of suspension was carried out with closed air inlet during the first 11 cycles. Therefore a pressure drop occurred, which decreased the flow rate to the separator. Because of the pressure drop, the cycle times increased. After 11<sup>th</sup> cycle the air inlet was opened to restore pressure of 0.25 bar resulting in constant cycle times with ~245 to 260 s.

### 6.5.2 Separation of debris and heat precipitate

The cell paste obtained was used for homogenization and heat precipitation trials. The preparation of these suspensions is described in 5.4.5.2. The flow rate to the separator was 30 L/h and the speed was set to 13650 min<sup>-1</sup>.

Table 27: Cell separation trial

Parameter	70/700 bar 1Psg. heat precipitate 25 g/L CDM	50/500 bar 2Psg. 50 g/L 1:2 dil. 1x separated	50/500 bar 2Psg. 50 g/L 1:2 dil. 2x separated	0/400 bar 1Psg. 25 g/L 2% Triton-X100
Yield of supernatant	81.1%	83.7%	-	86.6%
Clarification Eff.	95.86%	96.40%	97.00%	95.86%
Turbidity before	13890 NTU	7800 NTU	281 NTU	7387 NTU
Turbidity after	173 NTU	281 NTU	234 NTU	306 NTU
Solid content before	9.60%	6.67%	-	9.20%
Mass before	48.10 kg	46.80 kg	-	20.20 kg
Mass after	39.00 kg	39.15 kg	4.95 kg	17.50 kg
Discharges	5	4	1	2
Loss per disch.	1.82 kg	1.91 kg	-	1.35 kg
Separation time	88.6 min	89.8 min	15.0 min	40.5 min
Discharges th.	5.77	3.90	1	2.32
Estimated time	96.2 min	93.6 min	9.9 min	40.4 min

The courses of separation were recorded.

Table 28: Separation of homogenate 25 g/L CDM, 70/700 bar, 1 passage, heat precipitated

Cycle number	Cycle time [s]	Turbidity at cycle start [NTU]	Turbidity at cycle end [NTU]
1	960	152	190
2	1120	164	189
3	1040	167	182
4	1120	157	179
5 (full discharge)	1080	181	163
Summary	88.6 min	-	173 (pool)

Table 29: 1x separated homogenate 50 g/L CDM, 50/500 bar, 2 passages, 1:2 diluted

Cycle number	Cycle time [s]	Turbidity at cycle start [NTU]	Turbidity at cycle end [NTU]
1	1320	245	280
2	1335	274	-
3	1350	264	-
4 (full discharge)	1380	245	287
Summary	89.8 min	-	281 (pool)

Table 30: 2x separated homogenate 50 g/L CDM, 50/500 bar, 2 passages, 1:2 diluted

Cycle number	Cycle time [s]	Turbidity at cycle start [NTU]	Turbidity at cycle end [NTU]
1	900	-	234 (pool)

Table 31: Separation of homogenate 25 g/L CDM, 0/400 bar, 1 passage, 2% Triton-X100 added

Cycle number	Cycle time [s]	Turbidity at cycle start [NTU]	Turbidity at cycle end [NTU]
1	1350	-	336
2	1080	-	302
Summary	40.5 min	-	306 (pool)

The experiment with Triton-X100 added homogenate showed the highest yield and the lowest loss per discharge, but the turbidity of its pool was the highest of all. Several disadvantages led to considering it being impracticable. The separator was hard to clean after the Triton-X100 containing suspension. With respect to filtration, the high final turbidity and the low particle size seemed unfavorable. This assumption was verified with filtration trials later.

The experiments with the homogenate generated at 50/500 bar over two passages showed better separability in terms of lower turbidity after separation and higher particle sizes compared to the Triton-X100 experiment. It was investigated, if a separation with two consecutive runs could improve separation and therefore make filtration easier. The turbidity could be decreased further. Particle size measurement suggested, that this reduction is caused by removal of remaining bigger particles, which may have passed the first separation. Both supernatants were problematic for sterile filtration, because the particle size is around 200 nm. This was the typical pore size of a sterile filter, making it vulnerable to pore blocking.

The last experiment was separation of homogenate obtained from 70/700 bar over one passage, which was heat precipitated prior to separation (see also 6.3). Particle size measurement showed, that particles were bigger after heat precipitation and also compared to the other experiments, improving separability of heat precipitate. This was verified by measurement of turbidity. The supernatant of heat precipitate had the lowest turbidity of all experiments after separation. Yield and loss per discharge, were comparable to the experiment without heat precipitation. Together with the investigated course of heat precipitation, showing that the product GFP is heat stable, suggested implementing the heat precipitation step into the downstream processing chain is beneficial.

All particle sizes were measured and are shown in Figure 25.

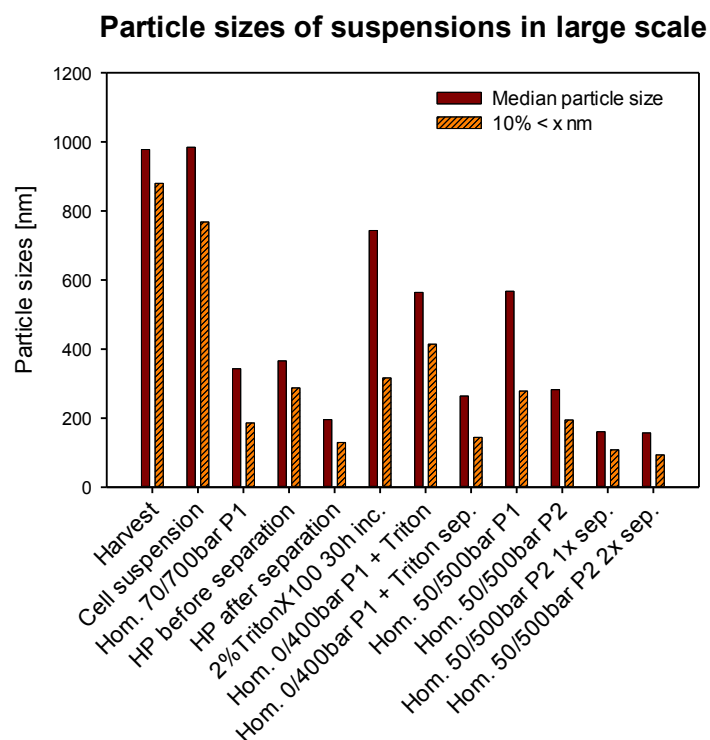


Figure 25: Particle sizes of large scale separation trials; the homogenates were obtained from a cell suspension containing 50 g/L CDM for homogenates produced at 50/500 bar and 25 g/L CDM for homogenates produced at 70/700 bar and the experiment with TritonX100; for heat precipitation the homogenate produced at 70/700 bar over one passage was used

## 6.6 SDS-PAGE of large scale trials

All solutions for large scale trials were analyzed by SDS-PAGE to evaluate the effect of heat precipitation compared to the processes without heat precipitation.

Table 32: Loaded samples onto SDS-PAGE from large scale trials

Lane	Loaded solution	Loading
1	-	-
2	Precision Plus Protein™ Dual Color Standards 500µL BIO-RAD (#161-0374)	5µL
3	-	-
4	Supernatant of heat precipitation of homogenate 70/700 bar Psg.1	0.75µg GFP
5	Supernatant of homogenate 50/500 bar; Psg.2; 2x separated	0.75µg GFP
6	Supernatant of homogenate with 2% TritonX100 0/400 bar; Psg.1	0.75µg GFP
7	-	-
8	Supernatant of heat precipitation of homogenate 70/700 bar Psg.1	0.50µg GFP
9	Supernatant of homogenate 50/500 bar; Psg.2; 2x separated	0.50µg GFP
10	Supernatant of homogenate with 2% TritonX100 0/400 bar; Psg.1	0.50µg GFP
11	leer	-
12	Supernatant of heat precipitation of homogenate 70/700 bar Psg.1	0.25µg GFP
13	Supernatant of homogenate 50/500 bar; Psg.2; 2x separated	0.25µg GFP
14	Supernatant of homogenate with 2% TritonX100 0/400 bar; Psg.1	0.25µg GFP
15	Supernatant of homogenate 70/700bar Psg.1 before heat precipitation	0.50µg GFP

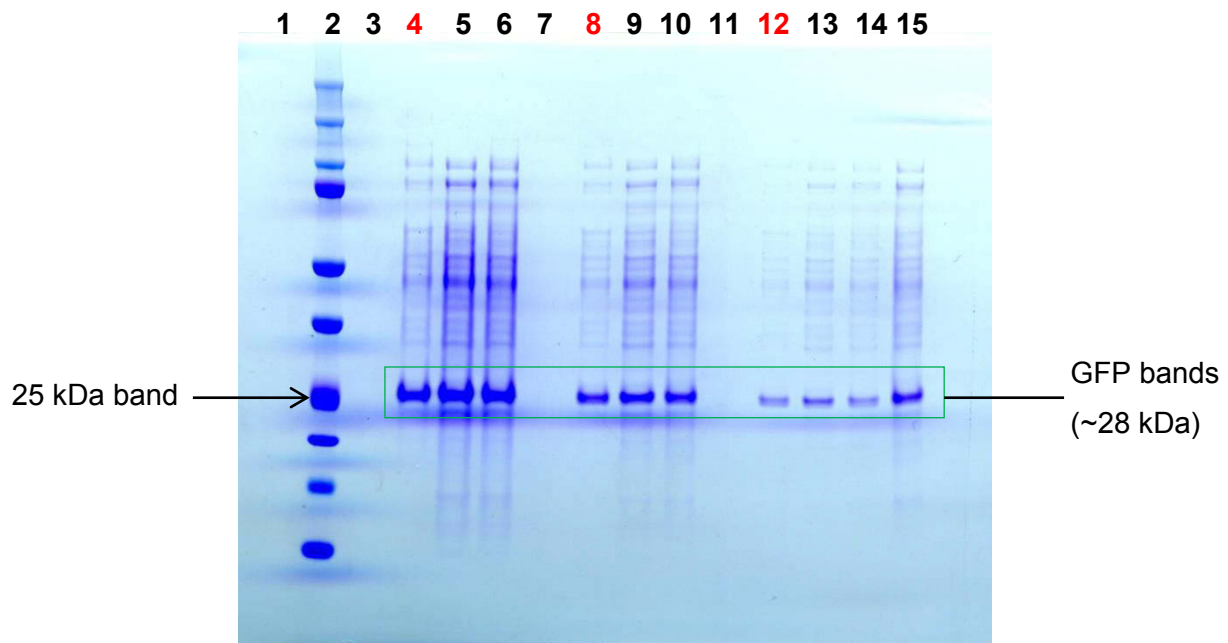


Figure 26: SDS-PAGE of large scale trials

The intensities of the bands other than GFP are significantly weaker in the supernatant of the heat precipitate (bands 4, 8 and 12), than in the other supernatants. The band patterns are the same for the supernatants of homogenates obtained from 50/500 bar, 70/700 bar and 0/400 bar. Compared to the band pattern from the supernatant of heat precipitate, it seems

that the heat treatment step mostly precipitates small proteins, because the bands below 25 kDa show the biggest difference in terms of intensity from the other experiments. Moreover the precipitation step did not remove a specific band from the pattern, but weakens all bands.

## 6.7 Filtration

### 6.7.1 Filtration after small scale precipitation

The filtration diagrams showing accumulated mass and mass flow vs. filtration time can be found in the appendix.

#### 6.7.1.1 Scale up of filter sizes

As a basis for scale up a batch volume of 35 L was assumed. The maximum allowable flux reduction  $J/J_0$  was fixed with 90%.

Table 33: Filter sizing based on small scale trials

Filter	NTU before	NTU after	blocking type	required area [m <sup>2</sup> ]	note
<b>Reference suspension</b>					
<i>PES 1.2 / 0.2 μm</i>	643	419	standard	8.59	
<i>PP3 0.65 μm</i>	643	-	-	-	instantly blocked*
<b>Heat precipitated clarified homogenate*</b>					
<i>PP3 0.45 μm</i>	502	415	complete	0.024	
<i>PP3 0.65 μm</i>	502	430	complete	0.020	
<b>Heat precipitated unclarified homogenate</b>					
<i>PP3 0.45 μm</i>	475	415	standard	0.16	
<i>PP3 0.65 μm</i>	475	413	complete	0.13	
<i>PES 1.2 / 0.2 μm</i>	475	169	standard	6.31	
<i>XLG 0.8 / 0.2 μm after PP3 0.65 μm</i>	415	-	-	20.7	instantly blocked*

\*too little filtrate for determination of turbidity

#### 6.7.1.2 Observations during filtration

##### Reference

Filtration of the reference suspension with the depth filter *Sartopure PP3 0.65 μm* resulted in a slight reduction of turbidity. The required filter area for the scale up was practically not feasible. *PES 1.2/0.2 μm* was instantly blocked, so the turbidity of the filtrate could not be measured.

##### Heat precipitated clarified homogenate

The depth filters *Sartopure PP3 0.65 μm* and *0.45 μm* resulted only in a small reduction of turbidity. The whole testing volume passed the filter with only slight flux reduction. This suggested, that the suspension passed the filter on the sides. An explanation could be a failure of the gasket in the apparatus. The other possible explanation could be, that the particles were so small that they passed through the filter without any holding back by the filter.

##### Heat precipitated unclarified homogenate

The depth filters *Sartopure PP3 0.65 μm* and *0.45 μm* were suitable for filtrating large volumes (~500 mL and ~300 mL), but resulted in insufficient reduction of turbidity. The filtrate of *Sartopure PP3 0.65 μm* was filtrated through the sterile filter *Sartopore2 XLG 0.8/0.2 μm*.

The immediate blocking of the filter after filtrating ~10 mL showed, that the performance of the depth filter wasn't sufficient. The last filter tested was *PES 1.2/0.2 μm*, which was also immediately blocked (~10 mL).

### 6.7.1.3 Particle sizes

The results of particle size measurement showed, that the used filters didn't have a significant impact on the sizes of remaining particles. The median particle sizes for all of the investigated filtrates is around 200 nm, while 10% of all particles are smaller than around 140 nm. Compared to the starting suspensions, the filtration step removed only few of the larger particles. Considering the high percentage of small particles of ~200 nm and rapid decay of filtrate flow indicated, that they went into the pores and therefore lead to fast blocking of the sterile filters. The depth filters were not blocked, but had no significant effect on the particle sizes.

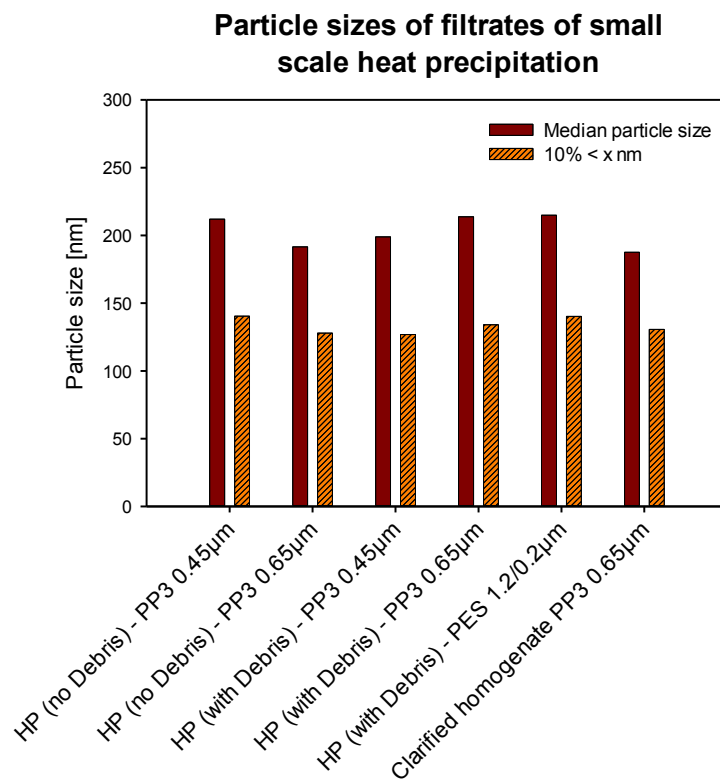


Figure 27: Particle sizes in small scale filtration after filtration of different supernatants of the respective suspensions

### 6.7.2 Filtration after large scale precipitation

The supernatants from the homogenates described in 6.5 were used for filtration trials. The results for different filters are listed in Table 34. As a basis for scale up a batch volume of 35 L was assumed. The maximum allowable flux reduction  $J/J_0$  was fixed with 90%.

Table 34: Required filter areas and performance of filters in large scale trials

Filter	Code	Type	Area [cm <sup>2</sup> ]	Turbidity before filtration [NTU]	Turbidity after filtration [NTU]	Turbidity reduction	r <sup>2</sup>	Required area [m <sup>2</sup> ]	Type of blocking
<b>Homogenate 70/700 bar with 25 g/L CDM, 1 passage, separated supernatant from heat precipitation</b>									
Sartopure PP3 0.45 µm	06P	Disc	13.5	207	184	11.1%	0.9950	0.052	standard
Sartopore 2 XLI 0.35 + 0.2 µm after Sartopure PP3 0.45 µm	07I	Disc	13.5	184	112	39.1%	0.9916	1.10	standard
Sartoguard GF 0.2 / 0.1 µm	58M	Disc	13.5	204	106	48.0%	0.9967	1.48	standard
Sartoguard PES 0.8 / 0.1 µm	58G	Disc	13.5	204	129	36.8%	0.9969	1.40	standard
Sartopore 2 XLG 0.8 + 0.2 µm	07G	Disc	13.5	204	118	42.2%	0.9997	0.694	standard
Sartopore 2 XLI 0.35 + 0.2 µm	07I	Disc	13.5	204	124	39.2%	0.9980	1.23	standard
Sartobran P 0.45 + 0.2 µm	07H	Disc	13.5	204	120	41.2%	0.9919	0.898	standard
Sartobran P150 0.45 + 0.2 µm	07H4--SS	Capsule	150	207	115	44.4%	0.9919	0.720	standard
<b>Homogenate 50/500 bar with 50 g/L CDM diluted 1:2, 2 passages, separated supernatant</b>									
Sartopure PP3 0.45 µm	06P	Disc	13.5	303	275	9.24%	0.9786	0.370	standard
Sartopure PP3 0.45 µm	06P4--SS	Capsule	150	330	241	23.9%	0.9988	1.45	standard
Sartoguard GF 0.2 / 0.1 µm	58M	Disc	13.5	303	122	59.7%	0.9695*	6.69	both
Sartopore 2 XLG 0.8 + 0.2 µm	07G	Disc	13.5	303		instantly blocked			
<b>Homogenate 50/500 bar with 50 g/L CDM diluted 1:2, 2 passages, 2x separated supernatant</b>									
Sartoguard GF 0.2 / 0.1 µm	58M	Disc	13.5	275	129	53.1%	0.9997*	6.44	both
Sartoguard PES 0.8 / 0.1 µm	58G	Disc	13.5	275		instantly blocked			
Sartoguard PES 0.8 / 0.1 µm	8G4--SS	Capsule	210	281	121	56.9%	0.9887	5.72	standard
Sartopure PP3 0.45 µm	06P	Disc	13.5	275	225	18.2%	0.9962	0.361	standard
Sartobran P 0.45 + 0.2 µm after PP3	07H	Disc	13.5	225	132	41.3%	0.9783	5.31	complete
Sartoguard GF 0.2 / 0.1 µm after PP3	58M	Disc	13.5	225	128	43.1%	0.9983	6.25	standard
<b>Homogenate 0/400 bar with 25 g/L CDM incubated with 2% TritonX-100 over night, 1 passage, separated supernatant</b>									
Sartoguard GF 0.2 / 0.1 µm	58M	Disc	13.5	325	79.4	75.6%	0.9745	6.14	standard
Sartoguard PES 0.8 / 0.1 µm	58G	Disc	13.5	325		instantly blocked			
Sartopore 2 XLG 0.8 + 0.2 µm	07G	Disc	13.5	318		instantly blocked			
Sartopure PP3 0.45 µm	06P	Disc	13.5	275	220	20.0%	0.9920	0.989	standard

\*) evaluation was done with the standard blocking model

Filtration trials after small scale precipitation were already described above (see 6.7.1). The results obtained from filtration trials after large scale precipitation seemed more reliable because the initial turbidities were lower and therefore allowed a greater volume to pass the test discs/capsules.

Supernatant of heat precipitated homogenate (70/700 bar, 25 g/L) was at first applied to a depth filter which didn't reduce the turbidity significantly (11.1%), therefore the focus was on the sterile filtration. All tested filters reduced the turbidity between 36.8% and 48.0%, but the *Sartopore 2 XLG 0.8+0.2 μm* needed the lowest area and is the most beneficial filter. The *Sartobran P 0.45+0.2 μm* performed only slightly worse (~0.7 – 0.9 m<sup>2</sup> needed) and would be another option.

Supernatants of 1x and 2x separated homogenates (50/500 bar, 50 g/L) showed similar behaviour in the filtration trials. A depth filtration step only reduced the initial turbidity by 9% to 18%. The required area of *Sartopure PP3 0.45 μm* was highly dependent on the testing device used. The scale up calculation from the data obtained from the filter disc yielded a required area of ~0.36 m<sup>2</sup> while the data obtained from the filter capsule yielded a required area of 1.45 m<sup>2</sup>. The sterile filters were blocked very fast so that a sterile filtration step would have required an area of ~6 m<sup>2</sup>, which is impracticable.

Supernatant of TritonX-100 treated separated homogenate (0/400 bar, 25 g/L) was impracticable for filtration. Depth filtration was possible, but for a reduction of initial turbidity by 20% already ~1 m<sup>2</sup> of filter area was needed. Tested sterile filters were either instantly blocked or needed impracticable filter area.

The results suggested, that a heat precipitation step is highly beneficial for filtration after centrifugation and a depth filtration step may not be necessary prior to sterile filtration.

## 6.8 Production of GFP with implemented heat precipitation

From the results of conducted trials in small scale and large scale the optimized process for GFP production was planned and conducted.

The process was performed within the framework of the lecture “Bioprocess Engineering Laboratory” in the summer semester of 2016. The focus during the process was on the heat precipitation step and on its influences on the following downstream steps.

Figure 28 shows the stepyields of each downstream step.

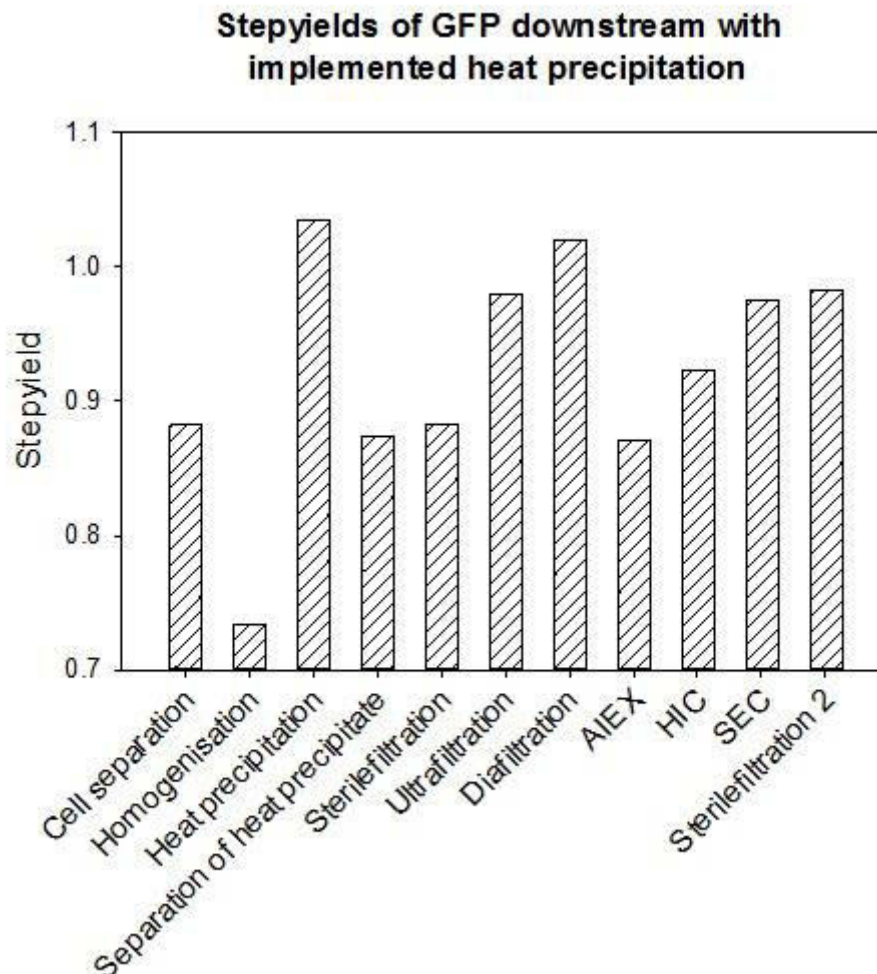


Figure 28: Stepyields of GFP production process with implemented heat precipitation

The starting material was 90.6 kg fermentation broth with 46.9 g/L CDM, which corresponded to 4.25 kg of absolute CDM. Considering a factor of 5 this corresponded to ~21.25 kg of WCM. Prior to separation in the disc stack centrifuge the broth was diluted with 42.35 kg water.

The separation was conducted with a flow rate of 65 L/h at 11392 min<sup>-1</sup>. After 21 discharges with an approximate cycle time of 3-4 min, the separation was complete. The broth had a turbidity of 61920 NTU, while the supernatant had a turbidity of 240 NTU. For the minimum turbidity 6 mL broth were diluted 1:2 with water and centrifugated in the desktop centrifuge for 30 min at 4500 rpm. NTU<sub>min</sub> was 200 and therefore the separation had a clarification efficiency of 99.94%. 25 kg of cell paste with a solid content of 75% were recovered, which

corresponded to 18.75 kg of WCM. This showed that 2.50 kg WCM were lost in total and 0.12 kg WCM were lost during each discharge. Thus the step yield of centrifugation was 88.3%.

For homogenization the cell paste was resuspended with homogenization buffer with pH 8.0 containing 50 mM Tris, 100 mM NaCl, 0.1% Tween20 (HCl was used for adjusting pH). 16.65 kg of cell paste were filled up to 50.00 kg with buffer to achieve a CDM concentration of ~50 g/L to avoid small cell debris. The suspension was splitted into 2x 25 L to investigate homogenization at 40/400 bar and 70/700 bar over two passages with respect to GFP release, viscosity, turbidity and solid content. Homogenization was performed with a flow rate of 75 L/h.

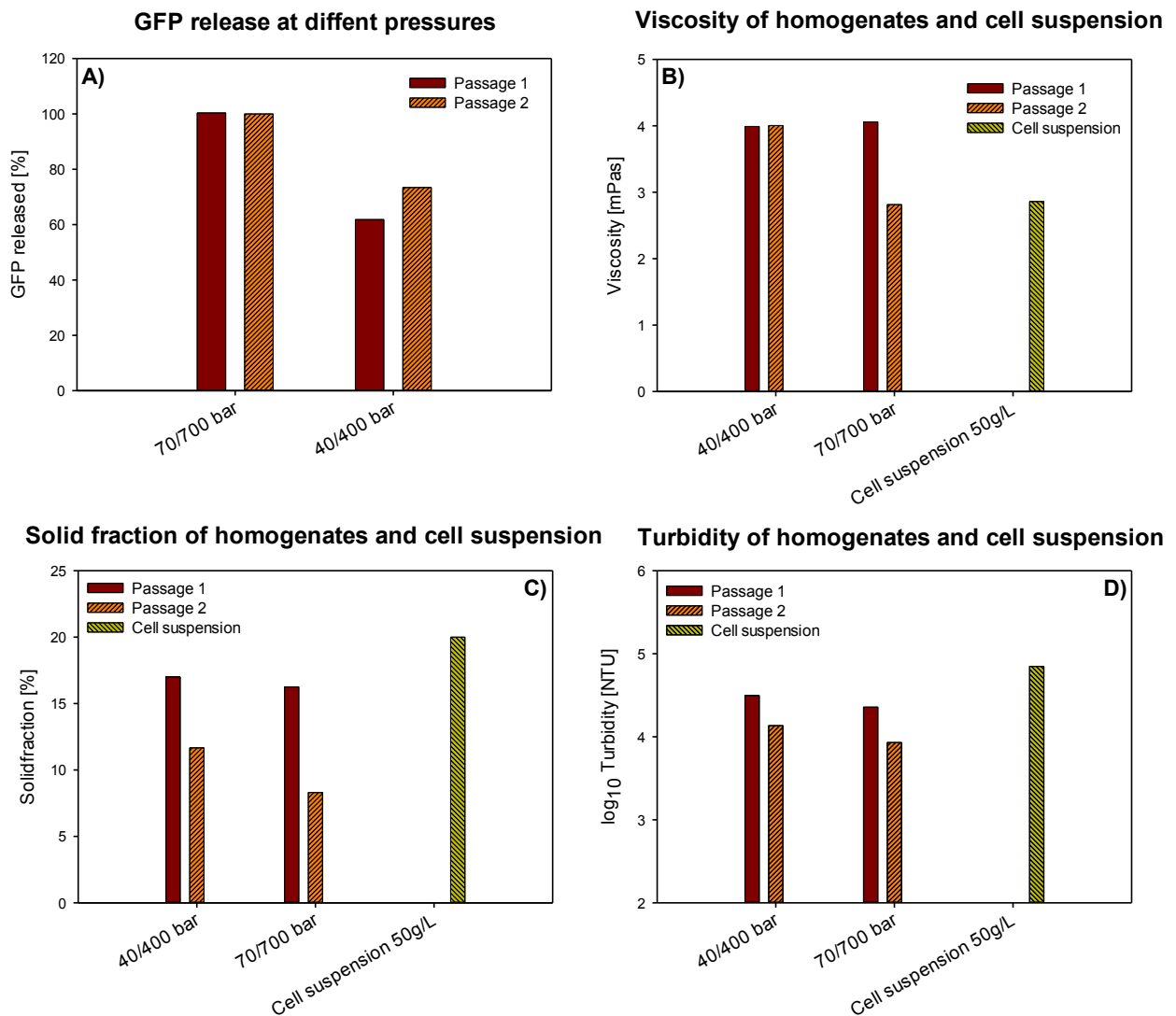


Figure 29: Optimized GFP production; A) GFP release (100% release = 70/700 bar / 2<sup>nd</sup> passage), B) viscosity, C) solid content and D) turbidity of homogenates and cell suspension containing 50 g/L CDM

Figure 29 shows, that the GFP release at 40/400 bar was lower than at 70/700 bar. The viscosity was approximately the same for all homogenates (~4 mPas) except the 2<sup>nd</sup> passage of 70/700 bar (2.86 mPas). A clear reduction was observed for the solid content and the turbidity from the first to the second passage at both pressures. It was chosen to continue

downstream processing with the second passage at 40/400 bar because from the homogenization trials, bigger debris were expected. This was verified by measurement of the particle sizes of the chosen homogenate and compared to the size of the cells (see Figure 29). The step yield of homogenization was 73.4%.

The homogenate was then diluted 1:2 with water (25 L homogenate + 25 L water) for heat precipitation at 50°C. The suspension had a GFP content of 2.97 mg/mL. During precipitation the temperature profile, GFP content, turbidity and solid content were monitored. The viscosity was measured at start and at the end of precipitation.

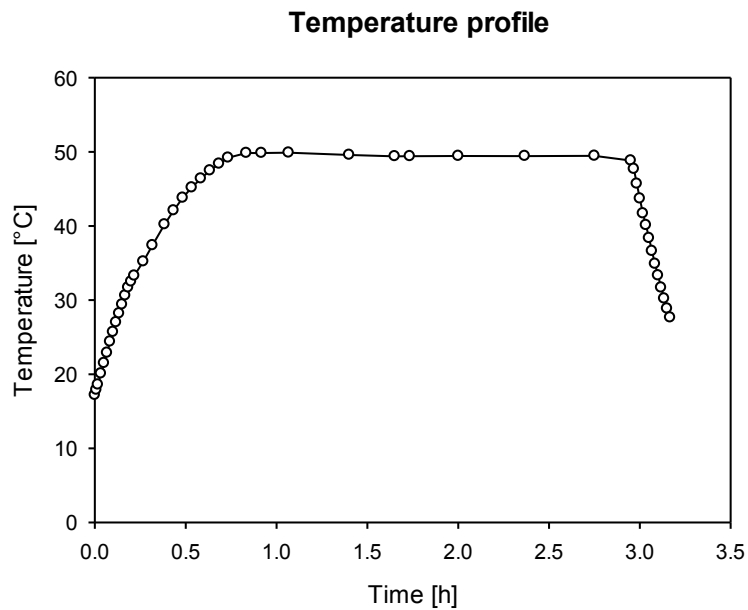


Figure 30: Optimized GFP production – temperature profile of heat precipitation; 50 L of diluted homogenate produced from homogenization at 40/400 bar over two passages with a CDM content of 25 g/L was used

Heating up of the suspension from 17.2°C to 50°C took 44 min. 50°C were held for 121 min. After the hold time, the jacket was emptied and connected to the ice water circuit. The cooling period took 25 min and was ended at 27.6°C.

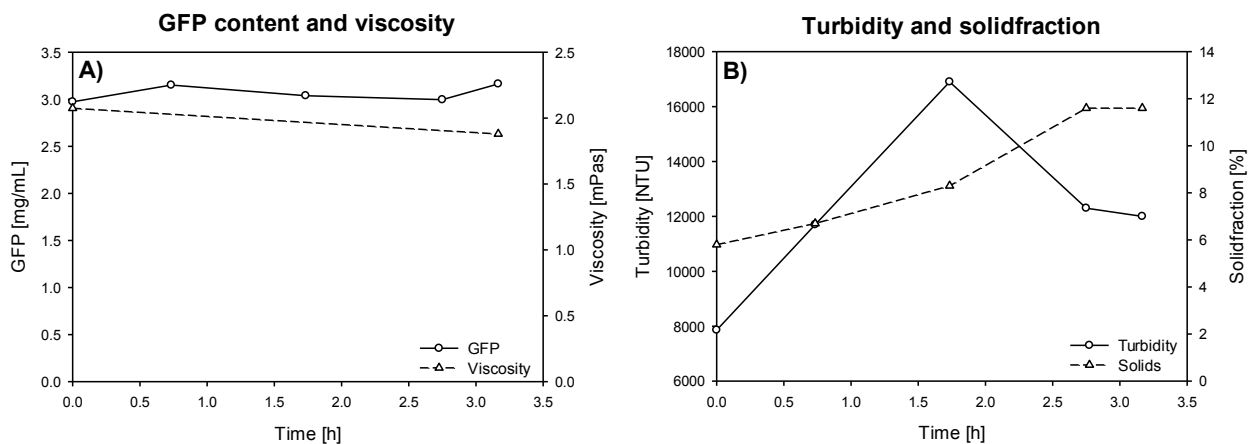


Figure 31: Optimized GFP production; A) GFP content and viscosity; B) turbidity and solid content of heat precipitation

The GFP content was approximately constant over process time. The solid content increased from 5.8% to 11.6%. Turbidity also increased from 7860 NTU to 12000 NTU and reached a peak of 16900 NTU after 1h of holding time. This could be explained by a continuously ongoing change of the nature of the heat precipitate during the heat treatment. Viscosity decreased slightly from 2.08 mPas to 1.88 mPas, which suggested, that a fraction of DNA is precipitated together with heat labile proteins. 48.65 kg of heat precipitated suspension with a GFP content of 3.16 mg/mL were obtained which corresponded to a stepyield of 103.5%. The cause for a yield >100% may be a break up of remaining intact cells or that the fluorescence of GFP increased due to the precipitation of other proteins resulting in reduced quenching during measurement.

After heat precipitation 5.80 kg of solids had to be removed from the suspension. For this task a disc stack centrifuge was used. Separation was done with a flow rate of ~20 L/h and a speed of 13650 min<sup>-1</sup>. The backpressure in the separator was set to 3-4 bar. After 5 discharges with a cycle time of 20-25 min the separation was completed. The turbidity of the suspension was reduced from 12000 NTU to 77 NTU in the supernatant which corresponded to a clarification efficiency of 99.4%. 42.55 kg of supernatant were obtained with a GFP concentration of 3.16 mg/mL. This corresponded to a stepyield of 87.5%, a loss of 1.22 kg during each discharge and a total loss of 6.10 kg. The supernatant was stored for three days at 4°C whereby the turbidity increased to 90.6 NTU.

The particle sizes were measured during these first steps of downstream.

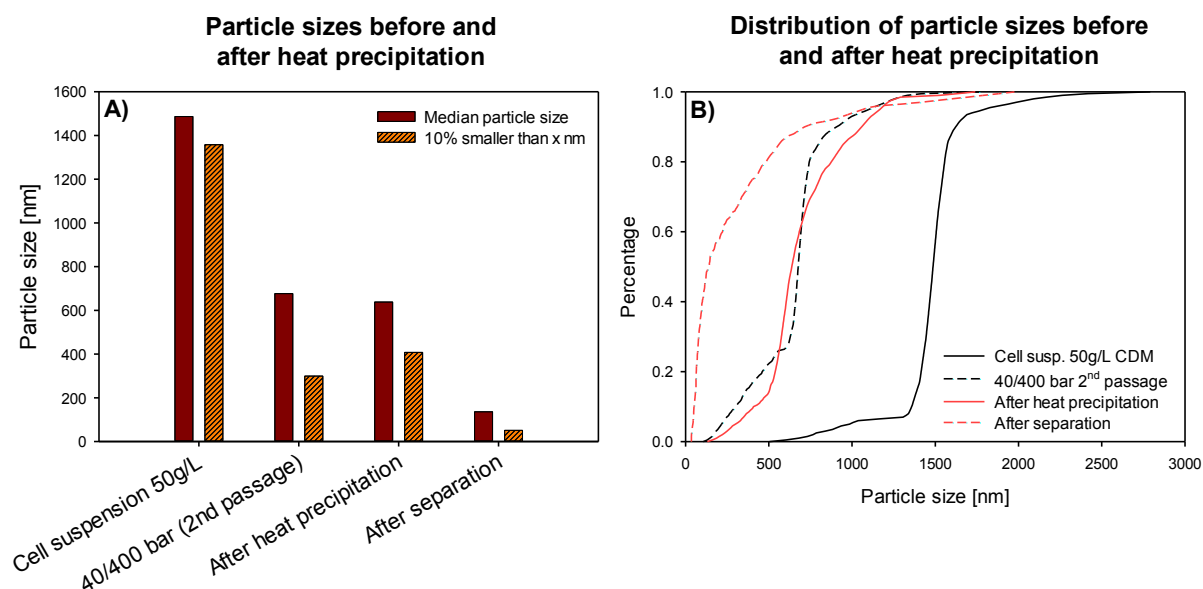


Figure 32: Optimized GFP production; A) median particle size of intact cells, homogenate (40/400 bar / 2<sup>nd</sup> passage), heat precipitated homogenate (40/400 bar / 2<sup>nd</sup> passage) and supernatant after centrifugation; B) particle size distributions of intact cells, homogenate (40/400 bar / 2<sup>nd</sup> passage), heat precipitated homogenate (40/400 bar / 2<sup>nd</sup> passage) and supernatant after centrifugation

The measured median particle size decreased from 1487 nm for the intact cells to 677 nm for the homogenate of the 2<sup>nd</sup> passage 40/400 bar. After heat precipitation a median particle size of 638 nm was measured, but a significant increase of the 10% < x nm value was observed (300 nm to 408 nm). This suggested that the particles in the precipitate aggregated together with cell debris and therefore reduced the number of small particles which are difficult to separate from the supernatant. This could also be seen in the high clarification efficiency of

the separation. The particles in the supernatant had a median particle size of 136 nm, which was measured before storage of the suspension.

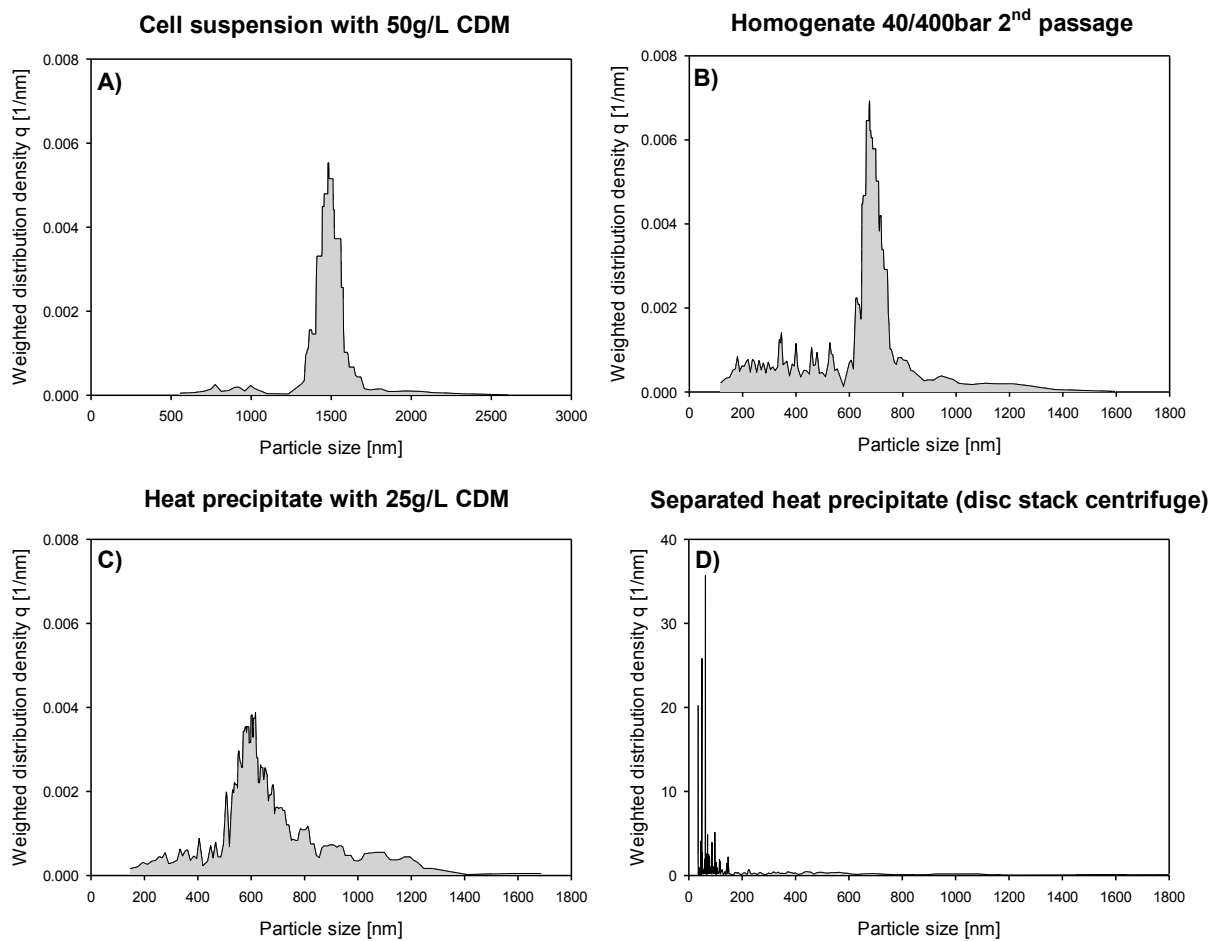


Figure 33: Optimized GFP production – particle size distributions of intact cells, homogenate (40/400 bar / 2<sup>nd</sup> passage), heat precipitated homogenate (40/400 bar / 2<sup>nd</sup> passage) and supernatant after centrifugation

The distributions of particle sizes were also determined. There is one clearly visible peak in the distribution of the cells, which showed that most of the cells were intact and there were almost no debris. The distribution broadened after homogenization and showed a dominant species of particles with a size of about 600 nm to 800 nm but also some particles with a size of <600 nm. After heat precipitation the distribution flattened out, which indicated that there were species of all sizes from 200 nm to 1400 nm. Since the area from 200 nm to 400 nm decreased, some small particles seemed to aggregate during heat treatment and therefore the 10% < x nm value increased. From the distribution of the supernatant after centrifugation it is clearly visible from the peaks in the range from 0 nm to 200 nm, that almost all particles >200 nm were removed.

After separation the supernatant was used for filtration trials to determine the appropriate filter. They showed, that a sterile filtration step was sufficient and no depth filter was required. For further downstream steps 30 L of process solution should be sterile filtrated. Therefore the scale up was calculated for 30 L and a maximum allowable flux reduction of 90%. All trials were conducted using a pressure of ~1.4 bar. For every tested filter the area required for the mentioned parameters was calculated (see Table 35).

Table 35: Required filter areas and performance of filters for optimized GFP production

Filter	Code	Type	Area [cm <sup>2</sup> ]	Turbidity before filtration [NTU]	Turbidity after filtration [NTU]	Turbidity reduction	r <sup>2</sup>	Required area [m <sup>2</sup> ]	Type of blocking
Sartopore 2 XLG 0.8 + 0.2 μm	07G	Disc	13.5	90.9	68.2	25.0%	0.9932	0.287	standard
Sartopore 2 XLI 0.35 + 0.2 μm	07I	Disc	13.5	90.9	64.1	29.5%	0.9973	0.375	standard
Sartoguard PES 0.8 / 0.1 μm	58G	Disc	13.5	90.9	83.4	8.25%	0.9382	0.100	standard
Sartobran P 0.45 + 0.2 μm	07H	Disc	13.5	90.9	62.5	31.2%	0.9951	1.69	standard
Sartobran P150 0.45 + 0.2 μm	07H--SS	Capsule	150	90.9	70.7	22.2%	0.9911	0.463	standard
Sartoguard GF 0.2/ 0.1 μm	58M	Disc	13.5	90.9	68.4	24.8%	0.9908	0.263	standard
Sartoguard GF 0.2/ 0.1 μm	58M4--SS	Capsule	150	90.9	45.7	49.7%	0.9908	2.606	standard
Sartopure PP3 0.45 μm	06P	Disc	13.5	90.9	82.5	9.24%	0.9954	0.053	complete
Sartobran P150 0.45 + 0.2 μm	07H4--SS	Capsule	4500	90.9	62.3	31.5%	-	-	-

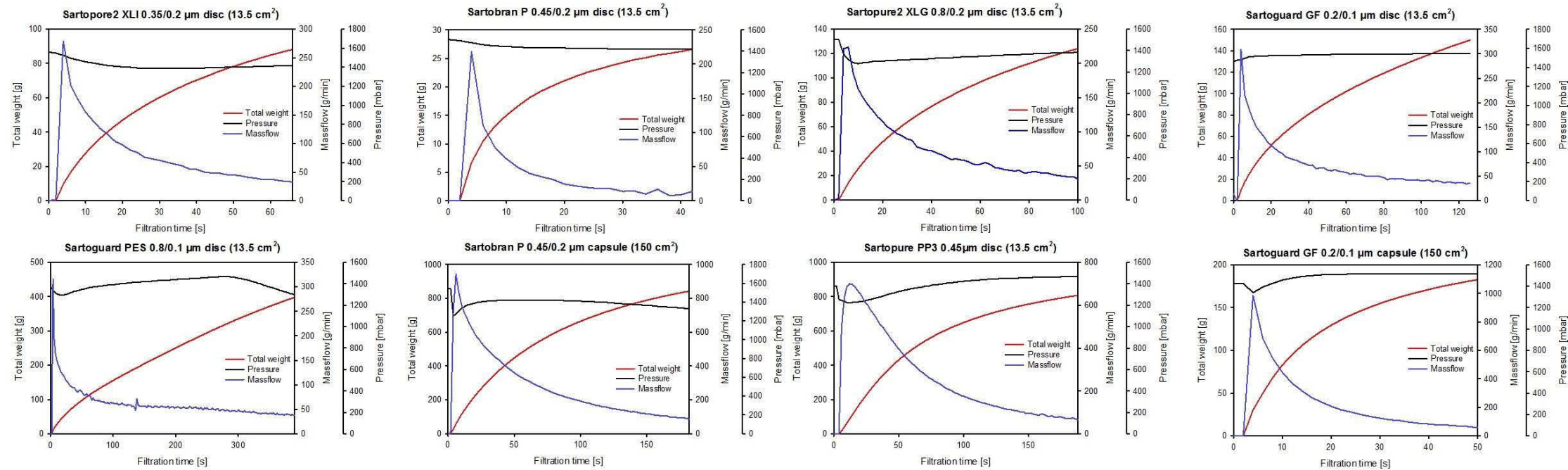


Figure 34: Filtration trials for optimized GFP production

Below only the trial which was scaled up is discussed.

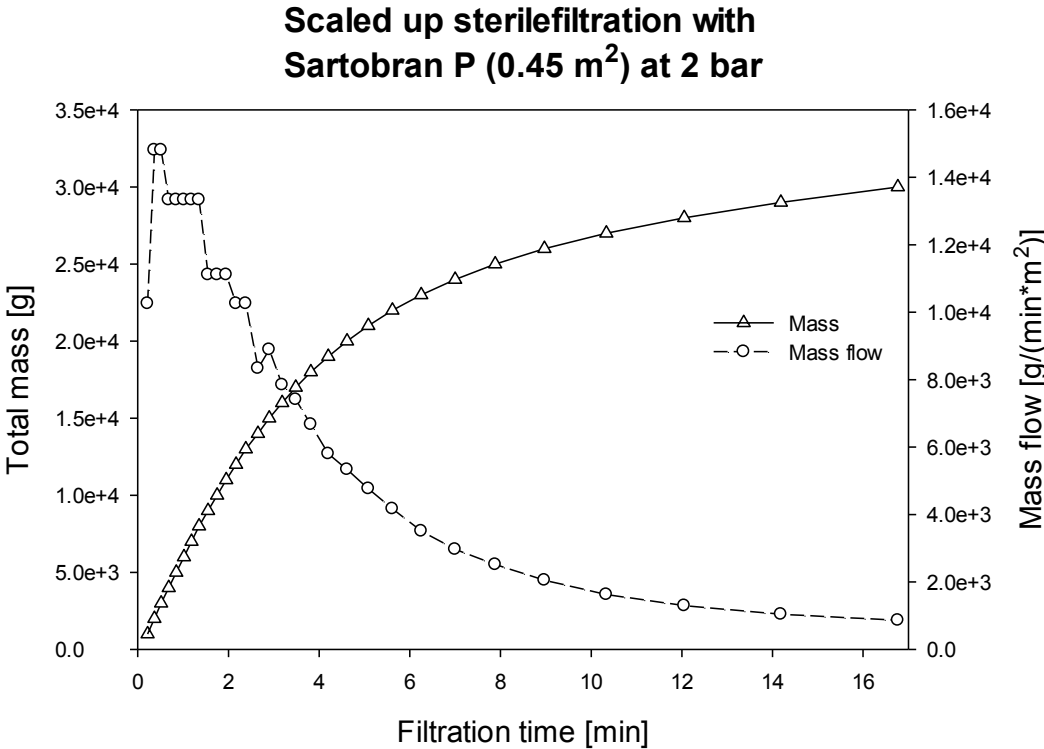
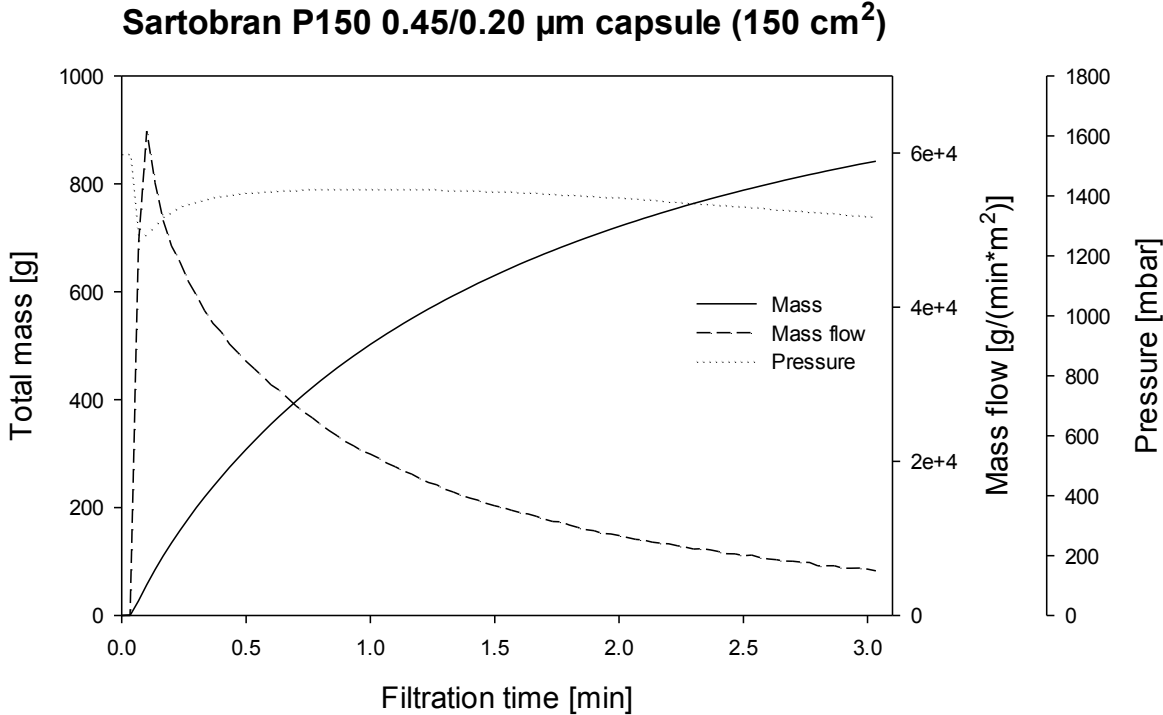


Figure 35: A) filtration trial with Sartobran P 0.45/0.2  $\mu\text{m}$  capsule (150  $\text{cm}^2$ ); B) scaled up filtration with Sartobran P 0.45/0.2  $\mu\text{m}$  capsule (0.45  $\text{m}^2$ )

The filtration trial using a Sartobran P 0.45/0.2  $\mu\text{m}$  capsule with an area of 150  $\text{cm}^2$  was used to calculate the scale up. Over 182 seconds 842 g of filtrate were collected. The filtration step

reduced the turbidity from 90.9 NTU to 70.7 NTU. This was a reduction of 22%. The evaluation was done by use of the standard blocking model. From the data a required area of 0.46 m<sup>2</sup> was obtained.

The scaled up filtration step was carried out with a *Sartobran P150 0.45/0.2 μm* capsule with an area of 4500 cm<sup>2</sup> and a constant pressure of ~2 bar.

The scaled up filtration step performed better than the trial in terms of turbidity reduction by reducing from 90.9 NTU to 62.3 NTU (31.5% reduction). 30.05 kg of solution were filtrated before filtration was broken up. The sterile filtrated solution had a GFP concentration of 2.79 mg/mL and therefore the stepyield was 88.3%.

For chromatographic steps, the material was concentrated by ultrafiltration. 27.00 L with a concentration of 2.79 mg/mL GFP were used and ultrafiltrated to a volume of 9.00 L with a concentration of 8.20 mg/mL which corresponded to a stepyield of 97.9%.

8 L of the ultrafiltrate were then diafiltrated with equilibration buffer with pH 7.5 for AIEX containing 10 mM TRIS/HCl. 8 L of diafiltrate were obtained with a concentration of 8.36 mg/mL, which corresponded to a stepyield of 101.9%. The stepyield > 100% could be explained by a combination of the change of buffer, further purification of GFP and the measurement's uncertainty.

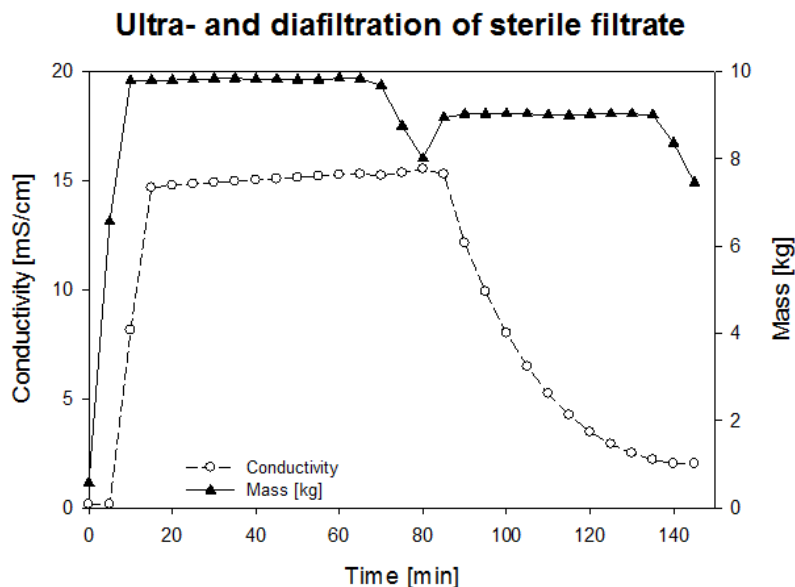


Figure 36: Ultra- and diafiltration of sterile filtrate

In Figure 36 the filling of the reservoir started at 0 min. The concentration step was performed during the first 90 min (increasing conductivity). Then the volume was adjusted to start the diafiltration. The diafiltration step lasted for further 55 min (decrease in conductivity from 15.5 mS/cm to 2.03 mS/cm). The decay after 140 min in total is because the draining was started there.

For capturing of GFP 7.5 L of diafiltrate were loaded to a *CaptoQ* column. The column had a column volume (CV) of 0.85 L. It was 13.3 cm high and had a diameter of 9 cm. For equilibration 10 mM Tris/HCl, pH 7.5 was used. For elution 10 mM Tris/HCl + 1 M NaCl, pH 7.5 was used. For regeneration 2 M NaCl + 0.5 M NaOH was used.

Table 36: Large scale capture step of GFP (AEX)

Step	Buffer	Volume / CV
Preparation	1 M NaCl	1 CV
Equilibration	Equilibration buffer	3 CV
Sample loading	Sample (residence time = 4 min)	7.5 L
Washing	Equilibration buffer	5 CV
Elution I	5% elution buffer	2 CV
Elution II (GFP)	30% elution buffer	3 CV
Elution III	100% elution buffer	3 CV
Regeneration	Regeneration buffer	1 CV
Washing	Equilibration buffer	until pH was neutral

1.54 kg of main fraction with a concentration of 35.5 mg/mL GFP were obtained. This corresponded to a step yield of 87.1%. The losses are due to the fact, that only the main fraction was collected thereby losing some of the GFP, which elutes within the tail of the main peak.

Ultrafiltrate, diafiltrate and AEX eluate were compared in terms of their adsorption behavior on *CaptoQ* gel. Adsorption isotherms were made for GFP and DNA. For DNA only the eluate from AEX and diafiltrate were used.

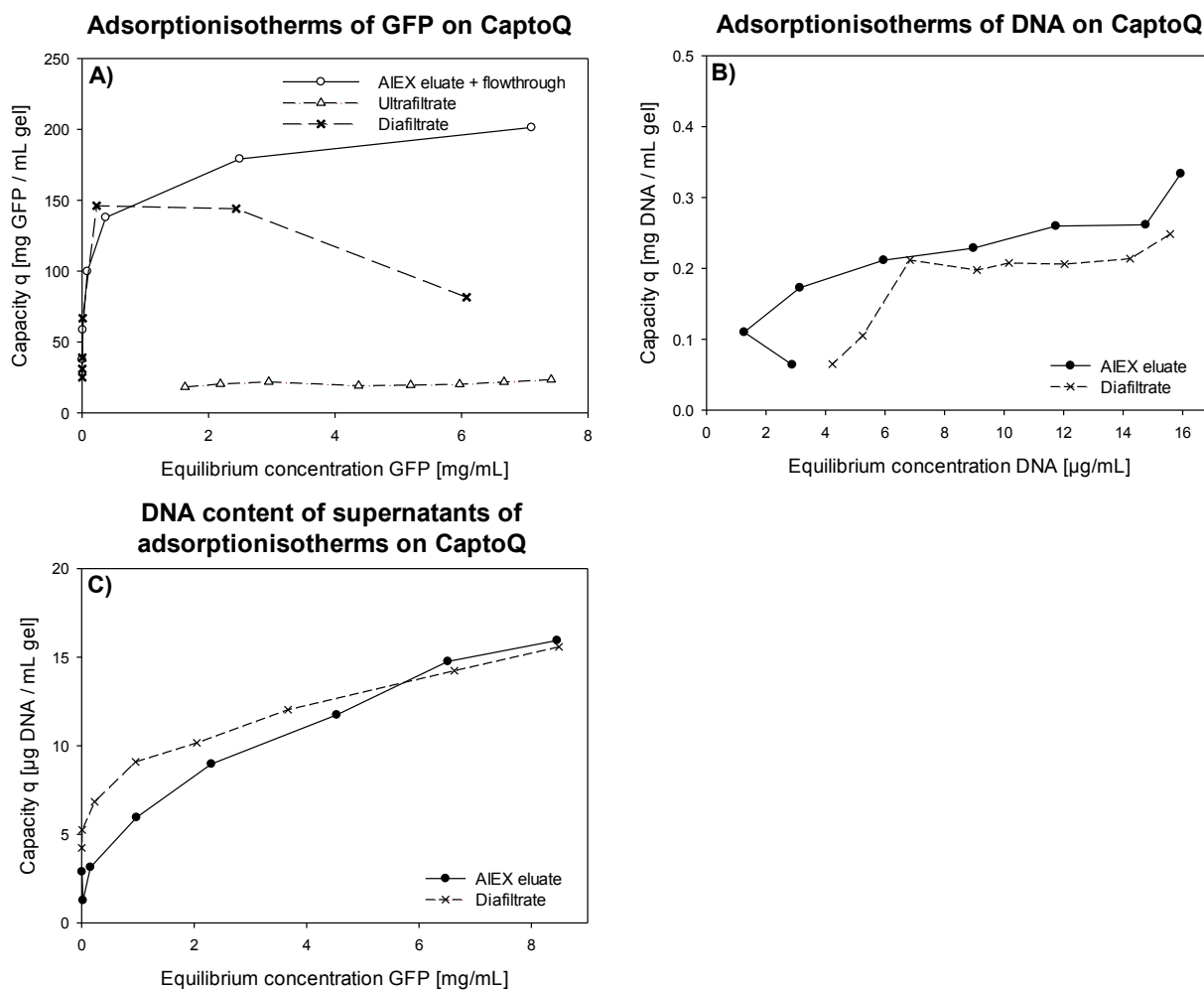


Figure 37: A) Adsorption isotherms of GFP and B) DNA and C) remaining DNA concentration as a function of GFP equilibrium concentration

For GFP the adsorption isotherm for the ultrafiltrate yielded a binding capacity of 18.35 mg/mL GFP at an equilibrium concentration of 1.63 mg/mL, which only slightly increased to a maximum load of 23.50 mg/mL at an equilibrium concentration of 7.42 mg/mL.

The GFP isotherm for the diafiltrate showed the maximum binding capacity of 146.2 mg/mL at an equilibrium concentration of 0.23 mg/mL. At higher equilibrium concentrations the binding capacity decreased to 81.63 mg/mL at 6.08 mg/mL. The form of the isotherm suggested, that there was occurring competitive binding to CaptoQ binding stronger at high concentrations. Since the DNA load was very low over the range investigated, it seemed not to be the cause for the form of the GFP adsorption behavior.

The GFP isotherm for the AIEX eluate showed the maximum binding capacity of 201.4 mg/mL at an equilibrium concentration of 7.71 mg/mL. To obtain comparable isotherms, the AIEX eluate was diluted 1:2 with AIEX flow through. Due to this the conductivities of ultrafiltrate, diafiltrate and AIEX eluate were approximately equal. Compared to the diafiltrate, the isotherm was not decreasing in the range from an equilibrium concentration of GFP of 0 to 7.71 mg/mL. Again the adsorption of DNA was neglectably small. Because there was no decrease of the GFP isotherm observed, this confirmed that not DNA was responsible for the form of the diafiltrate isotherm.

For further downstream the salt concentration of AIEX eluate increased to 3.3 M with 4.5 M NaCl to load it onto a HIC column. The bed of the HIC column was prepared with *Butyl-Sepharose-High-Performance* gel. It had a diameter of 10 cm and a height of 17.5 cm corresponding to a column volume of 1.4 L. For HIC 2.4 L of adjusted AIEX eluate with a concentration of 10.16 mg/mL GFP were loaded. For equilibration 10 mM Tris/HCl + 3.3 M NaCl, pH 7.5 was used. For elution 10 mM Tris/HCl, pH 7.5 was used. For regeneration 0.5 M NaOH + 0.5 M NaOH was used.

Table 37: Large scale purification of GFP (HIC)

Step	Buffer	Volume / CV
Preparation	Elution buffer	1 CV
Equilibration	Equilibration buffer	3 CV
Sample loading	Sample (residence time = 10.7 min)	2.4 L
Washing	Equilibration buffer	1 CV
Elution I	20% elution buffer	2 CV
Elution II (GFP)	80% elution buffer	3 CV
Elution III	100% elution buffer	3 CV
Regeneration	Regeneration buffer	1 CV
Washing	Equilibration buffer	until pH was neutral

From HIC 0.402 kg of GFP containing main fraction with a concentration of 55.85 mg/mL were collected. This corresponded to a yield of 92.3%. The HIC eluate was loaded onto a gel filtration column. The bed of the SEC column was prepared with *Superdex75 prep grade* gel. It had a diameter of 10 cm and a height of 45 cm corresponding to a column volume of 3.5 L. The column was operated with PBS, pH 7.4 as equilibration and running buffer. 2% of the volume of the SEC column were loaded from the HIC eluate main fraction (70 mL). 307 mL of SEC main eluate with a concentration of 11.52 mg/mL GFP and 130 mL of SEC peak shoulder eluate with a concentration of 2.14 mg/mL were obtained. This corresponded to a yield of 97.6%.

The final sterile filtration step was performed with a yield of 98.3%.

Calculating the product of all step yields, one gets the overall yield of the GFP downstream processing chain. The overall yield was **39.9%**. The downstream processing is summarized in Table 38.

Table 38: Downstream processing of optimized GFP production

Step	Basis	Mass [kg]	GFP [mg/mL]	GFP total [g]	GFP for next step [g]	Step yield
End of fermentation	Wet cells	21.25	-	549.0	549.0	-
Cell separation	Wet cells	18.75	-	484.5	322.7	88.3 %
Homogenization (40/400 bar, 2 psg.)	GFP	50.00	5.95	297.4	148.7	73.4 %*
Heat precipitation (homogenate 1:2 diluted)	Suspension	48.65	3.16	153.9	153.9	104 %
Separation of precipitate	Suspension	42.55	3.16	134.6	-	87.5 %
Sterile filtration (Sartobran P150)	Suspension	30.05	2.79	83.91	75.39	88.3 %
Ultrafiltration	Suspension	9.00	8.20	73.83	65.62	97.9 %
Diafiltration	Suspension	8.00	8.36	66.90	62.72	102 %
ALEX (main fraction)	Suspension	1.54	35.5	54.64	52.72	87.1 %
Salted ALEX eluate	Suspension	5.20	10.1	52.72	24.33	100 %
HIC (2.4 L salted ALEX eluate loaded)	GFP	0.402	55.9	22.45	3.91	92.3 %
SEC (main fraction)	GFP	0.307	11.5	3.54	-	-
SEC (shoulder)	GFP	0.130	2.14	0.28	3.81	97.6 %
Sterile filtration 2	GFP	-	-	-	-	98.3 %
Overall yield of downstream	-	-	-	-	-	39.9 %

\*) compared to 100% release = 8.10 mg/mL (70/700 bar, 2 passages)

In Table 38 the basis is the parameter from which the yield was calculated.

## 7 Summary and conclusion

It was shown that the downstream processing of recombinantly produced GFP can be significantly improved by implementing a heat precipitation step. The heat precipitation step implemented could be modelled with good accuracy with water as a modelling fluid. The overall yield of the combined downstream steps was 39.9% of the initially produced recombinant GFP. Compared to downstream processing without heat precipitation several advantages were identified. It was not necessary to conduct a centrifugation step after homogenization. Heat treatment of the cell debris containing homogenate increased the size of particles and therefore significantly improved the following centrifugation step. The obtained supernatant was purified from heat sensible substances and didn't even require a depth filtration step but could be filtered directly through a sterile filter. After ultra- and diafiltration the diafiltrate showed a significantly improved GFP binding capacity to the anion exchanger *CaptoQ*. Moreover there was no decrease of GFP binding capacity at higher equilibrium concentrations like it was observed in previous studies (Fink, 2015).

## 8 Symbols and mathematical notation

To refer to specific locations of the variable, indices were used as shown in Table 39.

Table 39: Indices used for applied mathematical notation

Index	Meaning
<i>c</i>	cold side during heating or cooling process
<i>h</i>	hot side during heating or cooling process
<i>m</i>	mean of the variable; specified in the text block of the respective variable
<i>W</i>	the variable refers to the wall separating hot and cold side
<i>J</i>	jacket side (if hot and cold assignment is not unambiguous)
<i>V</i>	vessel side (if hot and cold assignment is not unambiguous)
<i>heat</i>	the variable is associated with the heating process
<i>cool</i>	the variable is associated with the cooling process
<i>0</i>	variable is a reference
<i>1</i>	value of the variable refers to the starting point at $t = 0$
<i>2</i>	value of the variable refers to the end point at $t$
<i>+</i>	this index is only used superscript to temperatures indicating a reference point

Table 40: Mathematical symbols

Variable	Meaning	Unit
$A, A_m, A_c, A_h$	area involved in heat transfer or filter area in filtration trials	$m^2$
<i>B</i>	thickness of the wall separating hot and cold side of the heat precipitation vessel	m
<i>C</i>	equilibrium concentration in the supernatant in the Langmuir model	mg/mL
$C_P, c_P$	isobaric heat capacity, capital letter refers to the jacket side, minor letter refers to the vessel side	J/kgK
$d_o$	inlet diameter for heating/cooling media into the heat precipitation vessel's jacket	m
$d_g$	characteristic diameter of the annular space of the heat precipitation vessel's jacket	m
$D_T, D_i$	T = inner diameter of heat precipitation vessel, i = impeller diameter	m
$D_P$	particle diameter	m
<i>Ec</i>	Eckhoff number	-
<i>g</i>	gravitational acceleration	$m/s^2$
$h_S$	height of the annular space of the heat precipitation vessel's jacket	m
<i>h</i>	individual heat transfer coefficients	$W/m^2K$
$H_L$	height of the liquid filled into the heat precipitation vessel	m
$J_0$	initial filtration flux at $t = 0$	$m^3/s$
$J_{min}$	fixed minimum allowable filtration flux	$m^3/s$
<i>J</i>	filtration flux	$m^3/s$
<i>k</i>	resistance coefficient in filtration	depends
$K_a$	association constant in the Langmuir model	mL/mg
$K_S$	kinetic flux decline constant	$s^{-1}$
$K_1$	supporting variable in the calculation of the overall heat transfer coefficient	-
$L_0$	reference length	-
<i>M</i>	mass	kg
<i>n</i>	blocking index	-
$N_i$	impeller speed	$s^{-1}$
<i>Nu</i>	general Nusselt number / Nusselt number on the vessel inside	-
$Nu_{S,L}$	Nusselt number of the jacket side of the heat precipitation vessel	-
<i>Pr</i>	Prandtl number	-
<i>q</i>	binding capacity in the Langmuir model	mg/mL
$q_m$	maximum binding capacity in the Langmuir model	mg/mL

$Q$	heat energy	kJ
$R$	resistance to heat transfer	K/W
$r$	radius	m
$r^2$	coefficient of determination	-
$Re, Re_i$	general Reynolds number / Reynolds number in stirred liquids	-
$Re_s$	Reynolds number in the jacket of the heat precipitation vessel	-
$T, t$	temperatures in Perry's notation	°C
$U$	overall heat transfer coefficient	W/m <sup>2</sup> K
$uA$	fluid velocity due to natural convection	m/s
$u_c$	settling velocity of a particle in centrifugal field	m/s
$u_g$	settling velocity of a particle in gravitational field	m/s
$u_h$	characteristic fluid velocity in the jacket of the heat precipitation vessel	m/s
$u_o$	fluid velocity at the inlet to the jacket of the heat precipitation vessel	m/s
$u_s$	fluid velocity in the annular space of the jacket of the heat precipitation vessel	m/s
$u_o$	characteristic velocity	-
$V_{max}$	maximum filterable volume with the chosen filter	m <sup>3</sup> /s
$V_{cap}$	filterable volume until the specified flux decline is reached	m <sup>3</sup> /s
$V_B$	batch volume to be filtrated	m <sup>3</sup> /s
$\dot{V}_M$	volumetric flow of heating or cooling media into the jacket of the heat precipitation vessel	m <sup>3</sup> /s
$W$	mass flow of heating or cooling media into the jacket of the heat precipitation vessel	kg/s
$\frac{d^2t}{dv^2}, \frac{dt}{dv}$	1 <sup>st</sup> order and 2 <sup>nd</sup> order filtration time derivative with respect to filtration volume	-
$dJ/dt$	derivative of filtration flux with respect to time	-
$r_{Ti}$	time residuals in the theoretical/practical heating/cooling course	min
$\delta$	width of the annular space of the jacket of the heat precipitation vessel	m
$\rho$	density	kg/m <sup>3</sup>
$\mu$	viscosity	kg/ms
$\Delta$	difference	-
$\lambda$	thermal conductivity	W/mK
$\omega$	angular velocity	s <sup>-1</sup>
$\vartheta$	temperature used for derivation of the Nusselt number	°C
$\theta$	time interval	s
$(d\vartheta/dy)_w$	temperature gradient near the wall	-

## 9 Abbreviations

Table 41: Glossary of abbreviations used

Abbreviation	Meaning
AIEX	anionic exchange chromatography
CDM	cell dry mass
CV	column volume
CFD	computational fluid dynamics
DNA	deoxyribonucleic acid
HIC	hydrophobic interactions chromatography
NTU	nephelometric turbidity unit
PBS	phosphate buffered saline
SEC	size exclusion chromatography
SDS-PAGE	sodium dodecylsulfate polyacrylamide gel electrophoresis
VDI	Verein deutscher Ingenieure
WCM	wet cell mass
mM, M	concentration units – mmol/L or mol/L
µg, mg, g, kg	units of mass – microgram, milligram, gram, kilogram
nm, µm, mm, cm, m	units of length – micrometer, millimetre, centimetre, metre
µs, s, min, h	units of time – microsecond, second, minute, hour
rpm	revolutions per minute
mL, L, m <sup>3</sup>	units of volume – millilitre, litre, cubic metre
mA	milli ampere
V	volt
rfu	relative fluorescence unit
mPas	unit of viscosity
mS/cm	unit of conductivity
kDa	unit of protein mass – kilo dalton
°C	unit of temperature – degrees celsius
K	unit of temperature – degrees kelvin
J, kJ	unit of energy - joule, kilojoule
W	unit of power – energy per time

## 10 Tables

Table 1: Base quantities .....	10
Table 2: Geometry of the stirred tank reactor .....	25
Table 3: Data of tempering unit K20 DC10 .....	25
Table 4: Properties of water.....	27
Table 5: GFP calibration - parameters.....	30
Table 6: GFP calibration – calibration curve .....	30
Table 7: Parameters for the determination of particle sizes .....	32
Table 8: Adsorptionisotherm of AIEX eluate diluted 1:2 with AIEX flow through on CaptoQ ..33	
Table 9: Adsorptionisotherm of ultrafiltrate on CaptoQ .....	33
Table 10: Adsorptionisotherm of diafiltrate on CaptoQ .....	33
Table 11: Samples for SDS-PAGE in large scale trials .....	34
Table 12: Solutions for SDS-PAGE .....	34
Table 13: Flow and temperature of heating/cooling media.....	36
Table 14: Flow and temperature of heating/cooling media.....	36
Table 15: Values for estimation of individual heat transfer resistances .....	37
Table 16: Properties of water for calculation of individual heat transfer resistances.....	38
Table 17: Jacket side – individual heat transfer - heating .....	38
Table 18: Jacket side – individual heat transfer - cooling.....	38
Table 19: Vessel side – individual heat transfer - heating .....	39
Table 20: Vessel side – individual heat transfer - cooling .....	39
Table 21: Theoretical overall heat transfer coefficient U .....	39
Table 22: Overall heat transfer coefficients – tempering unit .....	41
Table 23: Observed heat precipitation of homogenate 70/700 bar, one passage compared to prediction.....	52
Table 24: Pressures and passages for homogenization trials .....	53
Table 25: Overview of results of homogenization trials .....	54
Table 26: Cell separation trial .....	59
Table 27: Cell separation trial .....	60
Table 28: Separation of homogenate 25 g/L CDM, 70/700 bar, 1 passage, heat precipitated .....	60
Table 29: 1x separated homogenate 50 g/L CDM, 50/500 bar, 2 passages, 1:2 diluted .....	60
Table 30: 2x separated homogenate 50 g/L CDM, 50/500 bar, 2 passages, 1:2 diluted .....	60
Table 31: Separation of homogenate 25 g/L CDM, 0/400 bar, 1 passage, 2% Triton-X100 added .....	60
Table 32: Loaded samples onto SDS-PAGE from large scale trials.....	62
Table 33: Filter sizing based on small scale trials .....	64
Table 34: Required filter areas and performance of filters in large scale trials .....	66
Table 35: Required filter areas and performance of filters for optimized GFP production.....	73
Table 36: Large scale capture step of GFP (AIEX) .....	76
Table 37: Large scale purification of GFP (HIC) .....	78
Table 38: Downstream processing of optimized GFP production.....	79
Table 39: Indices used for applied mathematical notation .....	81
Table 40: Mathematical symbols .....	81
Table 41: Glossary of abbreviations used.....	83

## 11 Figures

Figure 1: Structure of wild-type GFP (taken from PDB database, Code: 1GFL).....	6
Figure 2: A) Structure of the chromophore of the S65T variant of GFP (red = oxygen, blue = nitrogen, other interactions = yellow, dashed); B) emission wavelengths of and their chromophore structure at the emission peaks of natural GFP .....	6
Figure 3: Tubular bowl centrifuge (Doran, 2 <sup>nd</sup> , edition p.461, Figure 11.6).....	16
Figure 4: Disc stack centrifuge (Doran, 2 <sup>nd</sup> edition, p.463, Figure 11.8).....	16
Figure 5: Homogenization valve ( <a href="https://en.wikipedia.org/wiki/Homogenization_(chemistry)#/media/File:Homogenizing_valve.svg">https://en.wikipedia.org/wiki/Homogenization_(chemistry)#/media/File:Homogenizing_valve.svg</a> ; 06.12.2016).....	17
Figure 6: (A) Influence of the number of passages on cell break up; (B) influence of the number of passages on particle size .....	18
Figure 7: Scheme of an ultrafiltration/diafiltration process.....	20
Figure 8: GFP calibration in PBS .....	31
Figure 9: Theoretical thermal resistances of the tested system of heat transfer.....	40
Figure 10: Heating trials with tempering unit. The red line is the temperature of heating media at the inlet; the blue line is the temperature of the heating media at the outlet; the black line is the temperature of the bulk. A) 20 kg of water heated; B) 50 kg of water heated; C) 80 kg of water heated .....	41
Figure 11: Heating of 50 kg of water; heating media was tap water with a temperature of 54.3°C and a flow through the annular space of 21.8 L/min.....	42
Figure 12: Heating of 50 kg of water; cooling media was ice water with a temperature of 4.5°C and a flow through the annular space of 45.3 L/min.....	43
Figure 13: Comparison of theoretical and practical determined overall heat transfer coefficient U for heating and cooling process .....	44
Figure 14: A) prediction of the course of bulk temperature for water and heating process with practically determined and theoretically determined U; B) prediction of the course of bulk temperature for water and cooling process with practically determined and theoretically determined U.....	45
Figure 15: A) time residuals with respect to the observed temperature course of bulk temperature for water and heating process with practically determined and theoretically determined U; B) time residuals with respect to the observed temperature course of bulk temperature for water and cooling process with practically determined and theoretically determined U.....	46
Figure 16: Small scale heat precipitation of homogenate containing 25 g/L CDM produced at 70/700 bar, 1 passage with debris .....	47
Figure 17: Small scale heat precipitation of homogenate produced from a cell suspension containing 25 g/L CDM at 70/700 bar, 1 passage with debris removed before the precipitation step .....	48
Figure 18: A) Particle size distributions of the homogenates and heat precipitates generated in small scale experiments; B) Median particle sizes of the homogenates and heat precipitates generated in small scale experiments.....	49
Figure 19: Large scale heat precipitation of homogenate obtained at 70/700 bar over one passage from a cell suspension with a CDM concentration of 25 g/L; A) temperature profile of the precipitation process; B) GFP content and viscosity during the precipitation process; C) turbidity and solid content during the precipitation process; D) viscosity of the homogenate and the heat precipitate at different temperatures in the range from 20°C to 50°C .....	50
Figure 20: A) predicted course of homogenate heating with practical and theoretical determined U vs. observed course; B) predicted course of homogenate cooling with practical and theoretical determined U vs. observed course; C) time residuals between predicted course of homogenate heating with practical / theoretical determined U and observed course of homogenate; D) time residuals between predicted course of homogenate cooling with practical / theoretical determined U and observed course of homogenate .....	51
Figure 21: Release of GFP and viscosities after homogenization of 25 g/L CDM .....	55

Figure 22: Particle sizes of homogenates with 25 g/L CDM.....	56
Figure 23: Release of GFP and viscosities after homogenization of 50 g/L CDM .....	57
Figure 24: Particle sizes of homogenates with 25 g/L CDM.....	58
Figure 25: Particle sizes of large scale separation trials; the homogenates were obtained from a cell suspension containing 50 g/L CDM for homogenates produced at 50/500 bar and 25 g/L CDM for homogenates produced at 70/700 bar and the experiment with TritonX100; for heat precipitation the homogenate produced at 70/700 bar over one passage was used	61
Figure 26: SDS-PAGE of large scale trials .....	62
Figure 27: Particle sizes in small scale filtration after filtration of different supernatants of the respective suspensions .....	65
Figure 28: Stepyields of GFP production process with implemented heat precipitation.....	68
Figure 29: Optimized GFP production; A) GFP release (100% release = 70/700 bar / 2 <sup>nd</sup> passage), B) viscosity, C) solid content and D) turbidity of homogenates and cell suspension containing 50 g/L CDM.....	69
Figure 30: Optimized GFP production – temperature profile of heat precipitation; 50 L of diluted homogenate produced from homogenization at 40/400 bar over two passages with a CDM content of 25 g/L was used.....	70
Figure 31: Optimized GFP production; A) GFP content and viscosity; B) turbidity and solid content of heat precipitation.....	70
Figure 32: Optimized GFP production; A) median particle size of intact cells, homogenate (40/400 bar / 2 <sup>nd</sup> passage), heat precipitated homogenate (40/400 bar / 2 <sup>nd</sup> passage) and supernatant after centrifugation; B) particle size distributions of intact cells, homogenate (40/400 bar / 2 <sup>nd</sup> passage), heat precipitated homogenate (40/400 bar / 2 <sup>nd</sup> passage) and supernatant after centrifugation .....	71
Figure 33: Optimized GFP production – particle size distributions of intact cells, homogenate (40/400 bar / 2 <sup>nd</sup> passage), heat precipitated homogenate (40/400 bar / 2 <sup>nd</sup> passage) and supernatant after centrifugation .....	72
Figure 34: Filtration trials for optimized GFP production .....	73
Figure 35: A) filtration trial with Sartobran P 0.45/0.2 µm capsule (150 cm <sup>2</sup> ); B) scaled up filtration with Sartobran P 0.45/0.2 µm capsule (0.45 m <sup>2</sup> ).....	74
Figure 36: Ultra- and diafiltration of sterile filtrate.....	75
Figure 37: A) Adsorption isotherms of GFP and B) DNA and C) remaining DNA concentration as a function of GFP equilibrium concentration.....	77

## 12 Literaturverzeichnis

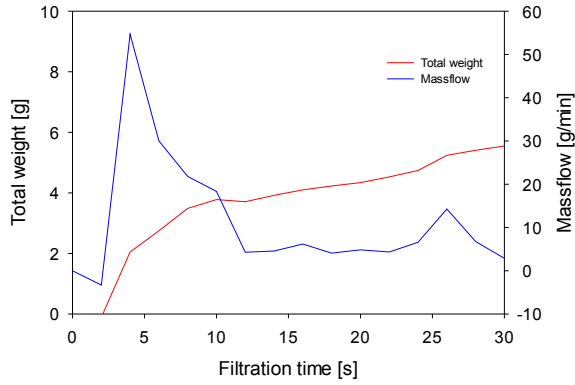
- Alkaabi, K. M., Yafea, A., & Ashraf, S. S. (2005). Effect of pH on thermal- and chemical-induced denaturation of GFP. *Appl Biochem Biotechnol*, 126(2), S. 149-156.
- Baehr, H. D., & Stephan, K. (2013). *Wärme- und Stoffübertragung* (8. Ausg.). Springer-Verlag Berlin Heidelberg.
- Brejč, K., Sixma, T. K., Kitts, P. A., Kain, S. R., Tsien, R. Y., Ormö, M., et al. (March 1997). Structural basis for dual excitation and photoisomerization of the *Aequorea victoria* green fluorescent protein. *Proc. Natl. Acad. Sci.*(94), S. 2306-2311.
- Daxhelet, G. A., Coene, M. M., Hoet, P. P., & Cocito, C. G. (1989). *Anal. Biochem.*, 179, S. 401-403.
- Doran, P. M. (2013). *Bioprocess Engineering Principles* (2. Ausg.). Elsevier.
- Doran, P. M. (2013). *Bioprocess Engineering Principles* (2 Ausg.). Elsevier, Ltd.
- Fink, M. (2015). *Clarification of E. coli homogenates*. University of Natural Resources and Life Sciences, Department of Biotechnology, Vienna.
- Honig, E. S., & Schwartz, P. D. (February 1997). Impact of Design and Selection of Prefilters on Operating Cost. *Filtration & Separation*, S. 73-78.
- Inouye, S., & Tsuji, F. I. (1994). *Aequorea* green fluorescent protein. *FEBS Lett.*(341), S. 277-280.
- Kelly, W. J., & Muske, K. R. (December 2004). Optimal operation of high-pressure homogenization for intracellular product. *Bioprocess Biosyst Eng*, 27(1), S. 25-37.
- Kleinig, A. R., & Middelberg, A. P. (1998). On the mechanism of microbial cell disruption in high-pressure homogenisation. *Chemical Engineering Science*, 53(5), S. 891-898.
- Labarca, C., & Paigen, K. (1980). *Anal. Biochem.*, 102, S. 344-352.
- Lehrer, I. H. (1970). Jacket-side Nusselt number. *Ind Eng Chem Process Des Develop* 9(4), S. 553-558.
- Moe, D., Garbarsch, C., & Kirkeby, S. J. (1994). *Biochem. Biophys. Methods*, 28, S. 263-276.
- Morise, H., Shimomura, O., Johnson, F. H., & Winant, J. (1974). Intermolecular Energy Transfer in Bioluminescent systems of *aequorea*. *Biochemistry*, 13, S. 2656-2662.
- Perry, R. H. (2007). Heat-Transfer Equipment. In R. H. Perry, & D. W. Green, *Perry's Chemical Engineers' Handbook* (8 Ausg., S. 11-18). McGraw-Hill.
- Prasher, D. C., Eckenrode, V. K., Ward, W. W., & Prendergast, F. G. (1992). Primary structure of the *Aequorea victoria* green-fluorescent protein. (E. S. B.V., Hrsg.) *ASFA: Aquatic Sciences and Fisheries Abstracts*, 111, S. 229-233.
- Remington, J. S. (2011). Green fluorescent protein: A perspective. *Protein Science*, 20, S. 1509-1519.
- Roda, A. (March 2010). Discovery and development of the green fluorescent protein, GFP: the 2008 Nobel Prize. *Anal Bioanal Chem*, 396(5), S. 1619-1622.
- Sanders, J. K., & Jackson, S. E. (2009). The discovery and development of the green fluorescent protein, GFP. *Chem. Soc. Rev.*, 38, S. 2821-2822.
- Shimomura, O. (August 1979). Structure of the Chromophore of *Aequorea* Green Fluorescent Protein. (Elsevier, Hrsg.) *FEBS Letters*, 4(2).
- Shimomura, O. (January 2005). The discovery of aequorin and green fluorescent protein. *Journal of Microscopy*, 217(1), S. 3-15.

- Tsien, R. Y. (2010). Nobel lecture: constructing and exploiting the fluorescent protein paintbox. *Integr. Biol.*, 2, S. 77-93.
- Verein deutscher Ingenieure. (2013). *VDI-Wärmeatlas* (11. Ausg.). Heidelberg: Springer-Verlag Berlin Heidelberg.
- Vessoni, P. T., Ishii, M., Cholewa, O., & de Souza, L. C. (2004). Thermal characteristics of recombinant green fluorescent protein (GFPuv) extracted from *Escherichia coli*. *Letters in Applied Microbiology*, 38, S. 135-139.
- von Böckh, P., & Wetzel, T. (2014). *Wärmeübertragung - Grundlagen und Praxis; 5.Auflage*. Springer-Verlag Berlin Heidelberg.
- Wong, H. H., O'Neill, B. K., & Middelberg, A. J. (March 1997). A mathematical model for *Escherichia coli* debris size reduction during high pressure homogenisation based on grinding theory. *Chemical Engineering Science*, 52(17), S. 2883-2890.
- Zimmer, M. (2002). Green Fluorescent Protein (GFP): Applications, Structure, and Related Photophysical Behavior. *Chem. Rev.*, 102(3), S. 759-781.
- Zydney, A. L., & Ho, C.-C. (February 2002). Scale-up of microfiltration systems: fouling phenomena and Vmax analysis. *Desalination*, 146, S. 75-81.

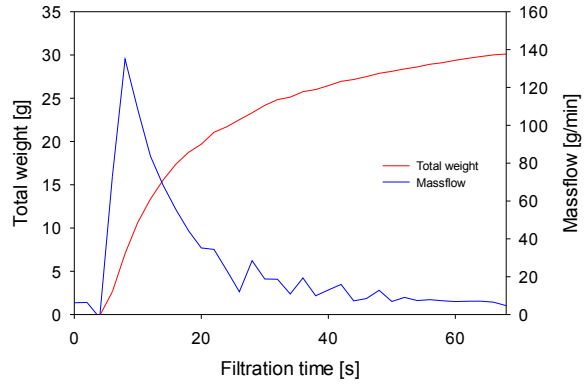
# 13 Appendix

## 13.1 Filtration trials in small scale

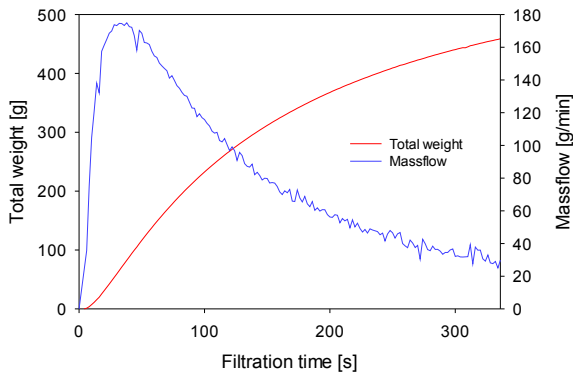
**Sartoguard PES 1.2 / 0.2 $\mu$ m disc (13.5 cm<sup>2</sup>)  
clarified homogenate, not heat precipitated**



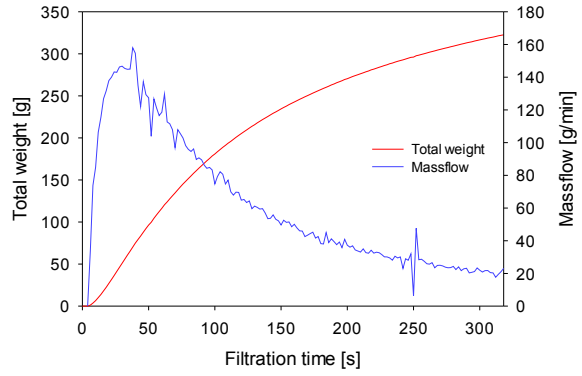
**Sartopure PP3 0.65 $\mu$ m disc (13.5 cm<sup>2</sup>)  
clarified homogenate, not heat precipitated**



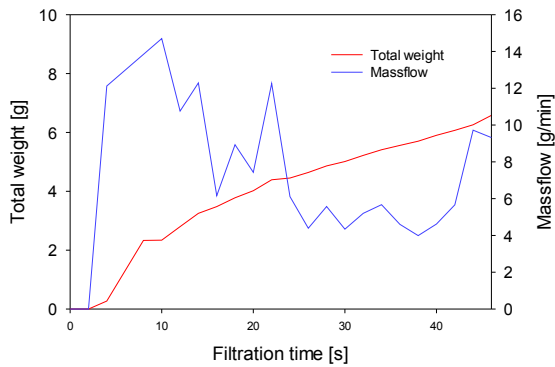
**Sartopure PP3 0.65 $\mu$ m disc (13.5 cm<sup>2</sup>)  
unclarified homogenate**



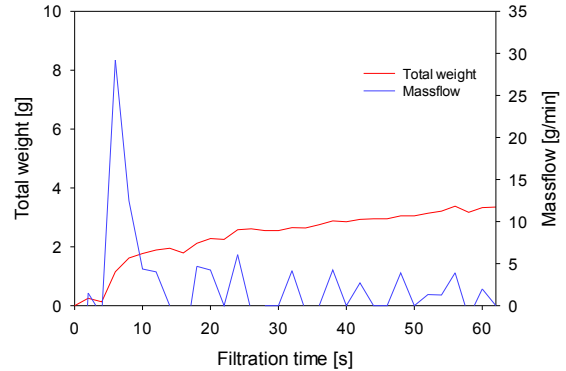
**Sartopure PP3 0.45 $\mu$ m disc (13.5 cm<sup>2</sup>)  
unclarified homogenate**



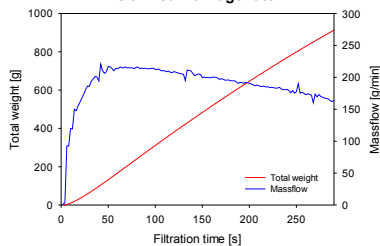
**Sartoguard PES 1.2 / 0.2 $\mu$ m disc (13.5 cm<sup>2</sup>)  
unclarified homogenate**



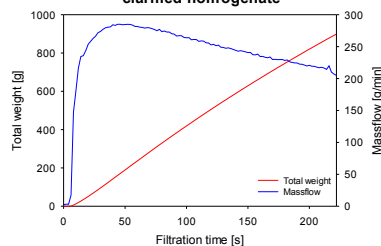
**Sartopure2 XLG 0.8 / 0.2 $\mu$ m after  
Sartopure PP3 0.45 $\mu$ m discs (13.5 cm<sup>2</sup>)  
unclarified homogenate**



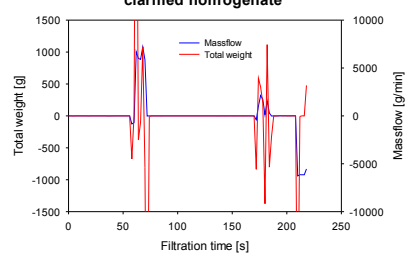
**Sartopure PP3 0.65 $\mu$ m disc (13.5 cm<sup>2</sup>)  
clarified homogenate**



**Sartopure PP3 0.45 $\mu$ m disc (13.5 cm<sup>2</sup>)  
clarified homogenate**



**Sartoguard PES 1.2 / 0.2 $\mu$ m disc (13.5 cm<sup>2</sup>)  
clarified homogenate**



As shown in Figure 4 the feed is supplied continuously from the upper side and is transported to the bottom of the bowl. From there it travels upwards through several metal discs. They are conically shaped and stacked above each other with a clearance of about around 3 mm. The discs fulfill the purpose to separate the suspension in many thin liquid films to enhance separation. By centrifugation the lighter liquid phase is travelling towards the inside and can be drained from there. The heavier solids slip down the discs and accumulate at the bottom of the centrifuge bowl.

#### 4.6 Homogenization

Since many products (like antibodies, medicinal proteins,... or GFP) obtained by fermentation are intercellular this step is necessary to free them in order to make them available for further downstream. This is achieved by breaking up the cell wall to free the desired product (Kelly & Muske, 2004). A typical homogenization valve is shown in Figure 5. For homogenization, the feed is promoted axially in the direction of the valve through the valve seat. From there the feed is distributed radially onto the impact ring and is forced through the gap between the seat and the impact ring. The width of the gap determines the pressure applied to the cells and therefore is one key parameter determining the yield.

Generally there are four different types of force responsible for cell break up. These are the inlet pressure gradient, channel shear stress, post channel turbulence and impact ring impingement forces. They are all a form of mechanical stress. Another important effect causing cell disruption is cavitation. Due to high pressure gradients arising during homogenization it is possible, that small zones emerge, which are free of liquid and under low pressure. These cavities are susceptible to collapsing under the surrounding high pressure, therefore creating a shock wave leading to cell disruption (Kelly & Muske, 2004) (Kleinig & Middelberg, 1998). When performing homogenization it is important to find a compromise between applied pressure and obtained yield. Too much mechanical stress may cause thermal degradation or mechanical damage of the product. Moreover it can introduce cell debris, which may be so small, that they interfere with further downstream steps like centrifugation and filtration. Depending on the flow velocity one distinguishes between acting viscous forces, which dominate at low  $Re$  number and acting inertial forces, which dominate at high  $Re$ . The latter are arising due to the high inlet pressure gradient at higher flow velocity (Kleinig & Middelberg, 1998).

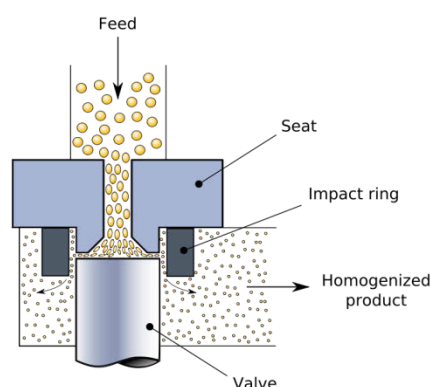


Figure 5: Homogenization valve

[https://en.wikipedia.org/wiki/Homogenization\\_\(chemistry\)#/media/File:Homogenizing\\_valve.svg](https://en.wikipedia.org/wiki/Homogenization_(chemistry)#/media/File:Homogenizing_valve.svg); 06.12.2016)

Homogenization is usually performed over one stage or two stages. If one e.g. homogenizes with 70/700 bar pressure, this means that the cell suspension is forced through a ring slit applying 700 bar pressure on the cells, which is called the first stage. In the example the

solution is not expanded to zero bar directly but undergoes an applied pressure of 70 bar afterwards, which is called the second stage. Using two stages provides the advantage, that firstly cell walls are disrupted at high pressure and by not expanding directly to zero bar freed DNA is fragmented. Due to the fragmentation of DNA viscosity is lowered, making processing of the solution easier.

The last screw, one can adjust for homogenization is the number of passages. It may be more favorable to apply less pressure, but to do this twice or more in a row (Wong, O'Neill, & Middelberg, 1997).

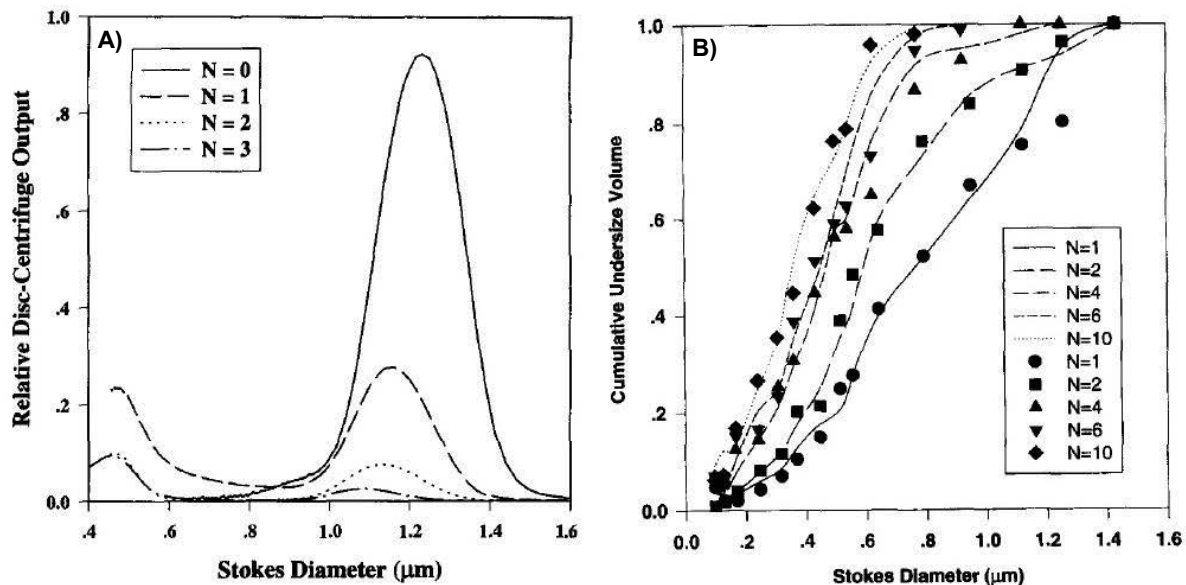


Figure 6: (A) Influence of the number of passages on cell break up; (B) influence of the number of passages on particle size

Figure 6 shows, that the fewer passages are applied, the fewer cells are broken up (large peak at  $\sim 1.2 \mu\text{m}$  in A) represent intact cells). In B) it is indicated, that the more passages are performed, the particle size distribution shifts to particles of smaller size.

## 4.7 Quantification of GFP

### 4.7.1 Fluorescence

Fluorescence is the physical phenomenon used for quantification of GFP.

Electrons are organized in atoms in the form of different discrete energy levels. This means an electron can only have the energy of  $E_1$  or  $E_2$ , but it could never have an energy level in between  $E_1$  and  $E_2$ .

It is possible, that an electron takes up a certain amount of energy to jump from  $E_1$  to  $E_2$ . This energy is supplied in the form of light. This process is called excitation. When the electron after excitation falls back down from  $E_2$  to its original energy level  $E_1$  the energy difference  $E_2 - E_1$  is dissipated. To the dissipation the emission of light of a higher wavelength (less energy than the excitation wavelength) is associated. The intensity of the emitted light can be measured.

- resistance of filter device (depending on the filter material)
- resistance of filter cake (depending on nature of filtrated particles, pressure,..)

Dead-end-filtration can therefore only be operated in a discontinuous fashion.

Cross-flow-filtration means that the suspension is pumped tangentially to the filtration area. This can be performed with different kinds of membrane modules. Due to the tangential flow mode, filter cake is building up only to a certain degree. It can't get thicker because it is removed by the flow velocity of the stream. Therefore long operation intervals and cleaning of the filter devices by flushing backwards is possible. Cross-flow-filtrations are used for e.g.:

- desalting of solutions (diafiltration)
- concentration of a product (ultrafiltration)

For ultrafiltration (UF) the solution to be concentrated is continuously pumped through a membrane. The concentrate is then collected again in the reservoir, while the ultrafiltrate is discarded. The UF is conducted at a constant level of liquid. To achieve this fresh solution is continuously added to the reservoir to maintain the level. The membrane used has a cut-off, which only allows impurities to cross, but retains the product within the concentrate. An important parameter in UF is the factor of concentration.

For diafiltration (DF) the mode of operation is principally the same as in UF. The difference lies in the buffer which is added to keep the liquid level constant. DF is often used to prepare the product containing solution for e.g. a chromatographic step like ALEX. For this purpose ALEX equilibration buffer is used to achieve low conductivity to allow the product to bind to the resin. In DF the salt is crossing the membrane and is discarded with the diafiltrate, while the product is retained in the retentate. An important parameter in DF is the number of changes of volume.

Both modes are characterized by the trans-membrane pressure (TMP), which is calculated from the pressures before and after the membrane (Doran P. M., 2013).

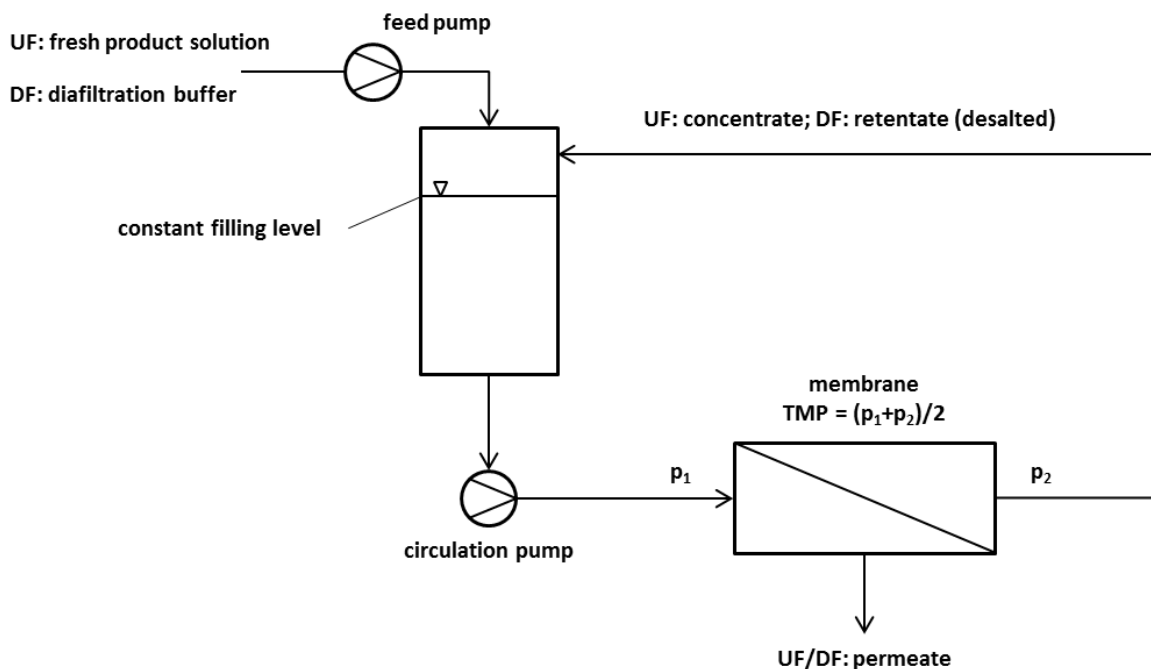


Figure 7: Scheme of an ultrafiltration/diafiltration process

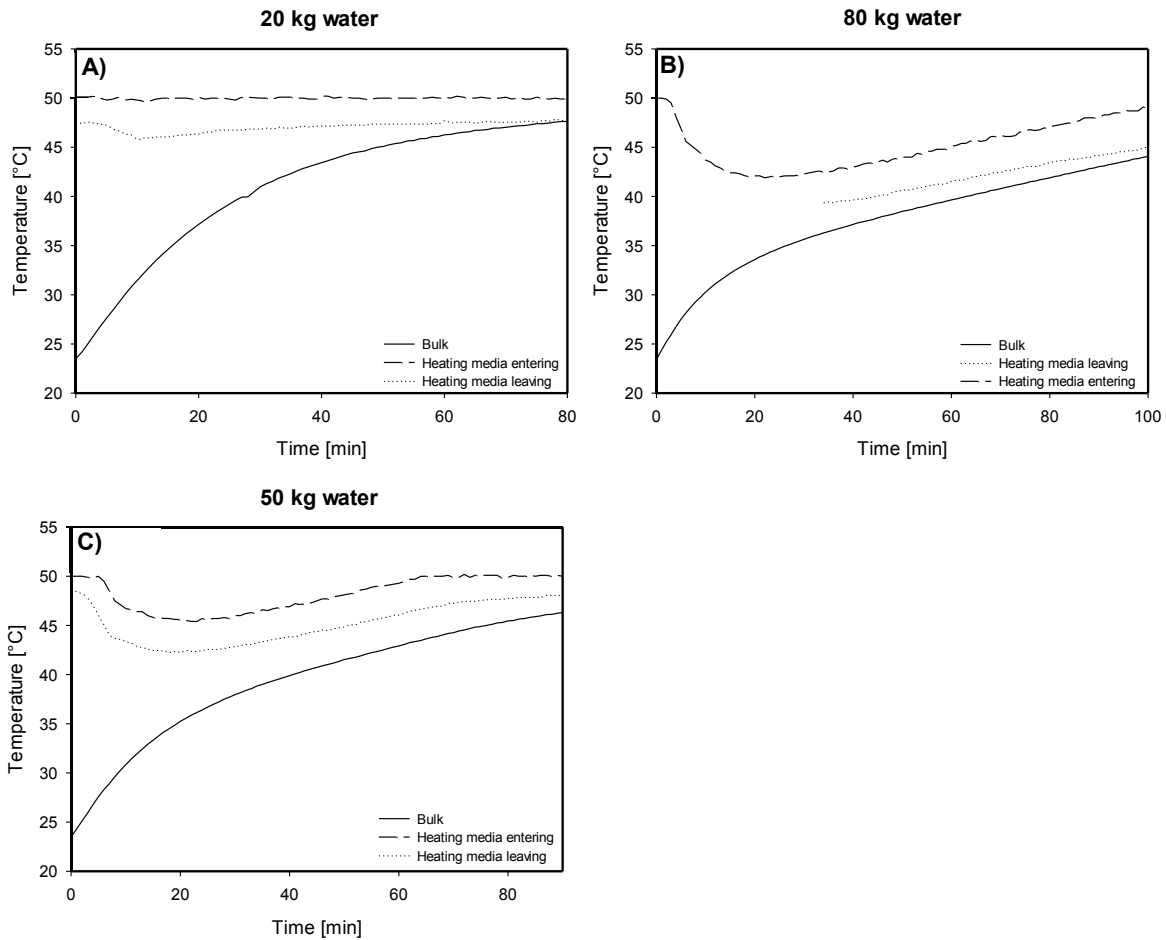


Figure 10: Heating trials with tempering unit. The red line is the temperature of heating media at the inlet; the blue line is the temperature of the heating media at the outlet; the black line is the temperature of the bulk. A) 20 kg of water heated; B) 50 kg of water heated; C) 80 kg of water heated

Figure 10 shows, that the temperature of leaving heating media was a function of time, when applying 50 or 80 kg of water. For 20 kg of water the temperature of leaving heating media was constant. With 50 kg and 80 kg of water respectively the device couldn't compensate for the loss of heat due to transfer. Therefore the temperature of heating media entering the jacket became lower. As a result the process of heating took longer.

The overall heat transfer coefficients were calculated. Trials with 50 kg and 80 kg water were evaluated by Eq.(4-10) and Eq.(4-11) because of the time dependent outlet temperature. As the mean temperature of the heating media an average of one minute time increments was used. The trial with 20 kg water was evaluated by Eq.(4-13) because the outlet temperature was constant.

Table 22: Overall heat transfer coefficients – tempering unit

Mass of water [kg]	Start temperature [°C]	End temperature [°C]	Temperature heating media [°C]	Time [min]	$U$ [W/m <sup>2</sup> K]
20	24.49	47.00	50.00	70	210.1
50	23.49	46.31	48.15	90	216.3
80	23.45	44.07	45.14	100	241.9

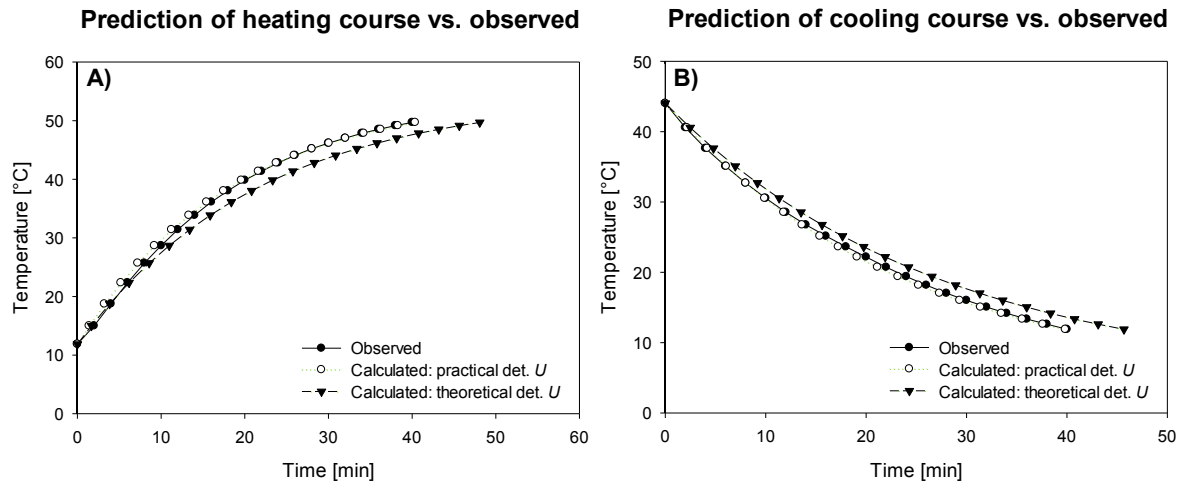


Figure 14: A) prediction of the course of bulk temperature for water and heating process with practically determined and theoretically determined  $U$ ; B) prediction of the course of bulk temperature for water and cooling process with practically determined and theoretically determined  $U$

Figure 14 the profiles of heating and cooling are shown. The profiles, which were obtained in the practical determination of the overall heat transfer coefficients were compared to the predicted profiles. Therefore two ways of prediction were used:

- 1) The values for  $U$  from the practical determination were used to predict the profile.
- 2) The theoretical calculated values for  $U$  from the correlations were used to predict the profile.

For both, heating and cooling, the differences from the obtained profiles and the predicted profiles were small, when the practically determined  $U$  was used. Calculation using the theoretically determined  $U$  estimated a longer time for heating and cooling, than the observed time. This is shown in Figure 15, where the residues calculated by Eq.(6-7), are shown.

$$r_{T_i} = t_{T_i,calc} - t_{T_i,obs} \quad Eq.(6-7)$$

The index  $T_i$  refers to the temperature, which was reached after the observed time interval. The index  $calc$  refers to the predicted time to reach  $T_i$ , the index  $obs$  refers to the measured time to reach  $T_i$ .

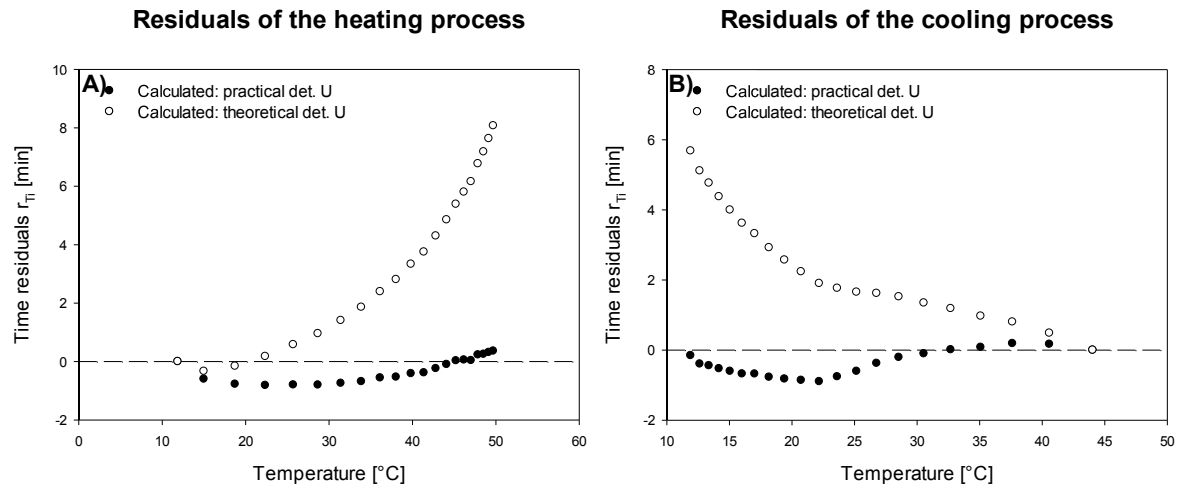


Figure 15: A) time residuals with respect to the observed temperature course of bulk temperature for water and heating process with practically determined and theoretically determined  $U$ ; B) time residuals with respect to the observed temperature course of bulk temperature for water and cooling process with practically determined and theoretically determined  $U$

For heating the prediction calculated from the practically determined  $U$  the residues ranged from -0.82 min to 0.36 min. Prediction from the theoretically determined  $U$  yielded residues from -0.33 min to +8.07 min.

For cooling the prediction calculated from the practically determined  $U$  the residues ranged from -0.90 min to 0.19 min. Prediction from the theoretically determined  $U$  yielded residues from 0.00 min to +5.87 min.

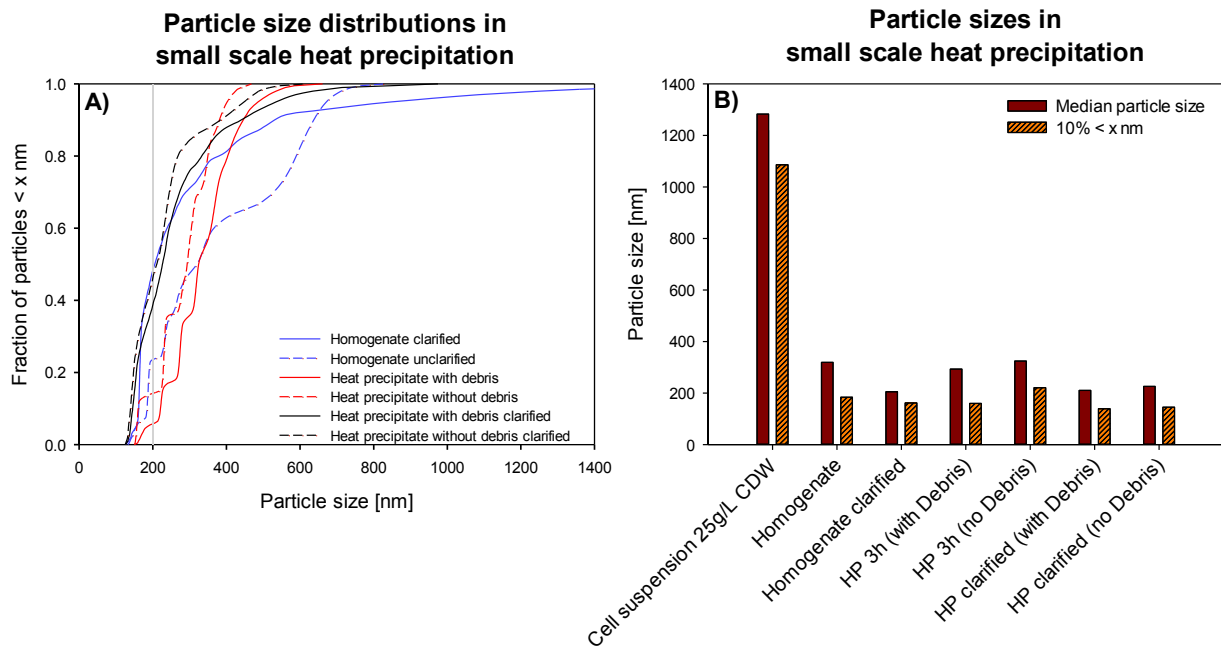


Figure 18: A) Particle size distributions of the homogenates and heat precipitates generated in small scale experiments; B) Median particle sizes of the homogenates and heat precipitates generated in small scale experiments

With respect to filtration as the next process step it was important to obtain particles which could be separated without blocking the sterile filters. The measurement of particle sizes showed, that all suspensions contained particles in the region of ~200 nm and the size distributions showed that there were up to 50% of particles smaller than 200 nm. This was problematic for filtration considering the typical pore size of sterile filters around 200 nm.

This was confirmed by filtration trials (see 6.7.1).

### 6.3 Heat precipitation in large scale

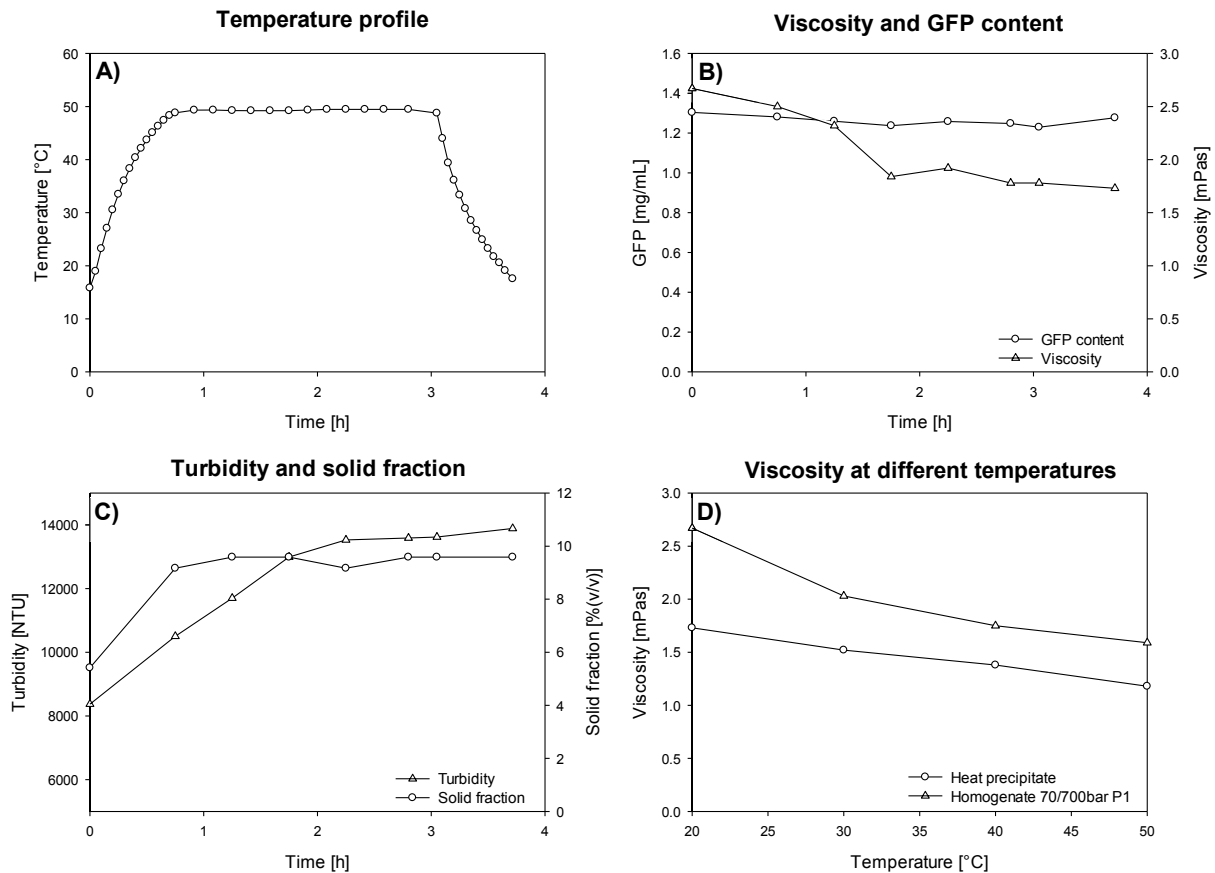


Figure 19: Large scale heat precipitation of homogenate obtained at 70/700 bar over one passage from a cell suspension with a CDM concentration of 25 g/L; A) temperature profile of the precipitation process; B) GFP content and viscosity during the precipitation process; C) turbidity and solid content during the precipitation process; D) viscosity of the homogenate and the heat precipitate at different temperatures in the range from 20°C to 50°C

The temperature course of the heat precipitation was in the range of the results of the model experiments with water. For heating from 11.87°C to 49.70°C a time of 40 min was observed which was comparable to the actual time needed of 42 min to heat from 15.83°C to 48.81°C. For maintaining the temperature, the tempering unit was sufficient. Cooling was also comparable to the model experiments, where cooling from 44.04°C to 11.91°C took 40 min. The actual time needed for cooling homogenate from 48.76°C to 17.57°C was 40 min.

Measured viscosity during the course of precipitation was significantly higher than that of water, although it was decreasing from 2.67 mPas to 1.73 mPas. Therefore the degree of turbulence was lower than it was the case in the experiments where water was used. The effect of turbulence was weakened by the change of specific heat capacity, because aqueous suspensions containing solids has got a lower specific heat capacity.

The viscosities were measured from the homogenate before heat precipitation and the heat precipitate at different temperatures. The viscosity of homogenate ranged from 2.67 mPas at 20°C to 1.59 mPas at 50°C. The viscosity of heat precipitate suspension ranged from 1.73 mPas at 20°C to 1.18 mPas at 50°C.

The GFP content was approximately constant. At start of heat precipitation it was 1.30 mg/mL and at the end it was 1.28 mg/mL. During the precipitation the measured values were ranging from 1.24 mg/mL to 1.30 mg/mL.

The turbidity increased from 8370 NTU to 13890 NTU and the solid content increased from 5.82% to 9.58%. These observations showed, that heat precipitate was formed during the heat treatment.

The particle sizes also were measured and can be found in Figure 25.

Figure 20 shows the difference between the observed temperature profile of the homogenate and the predicted temperature profile calculated from the practically determined overall heat transfer coefficients.

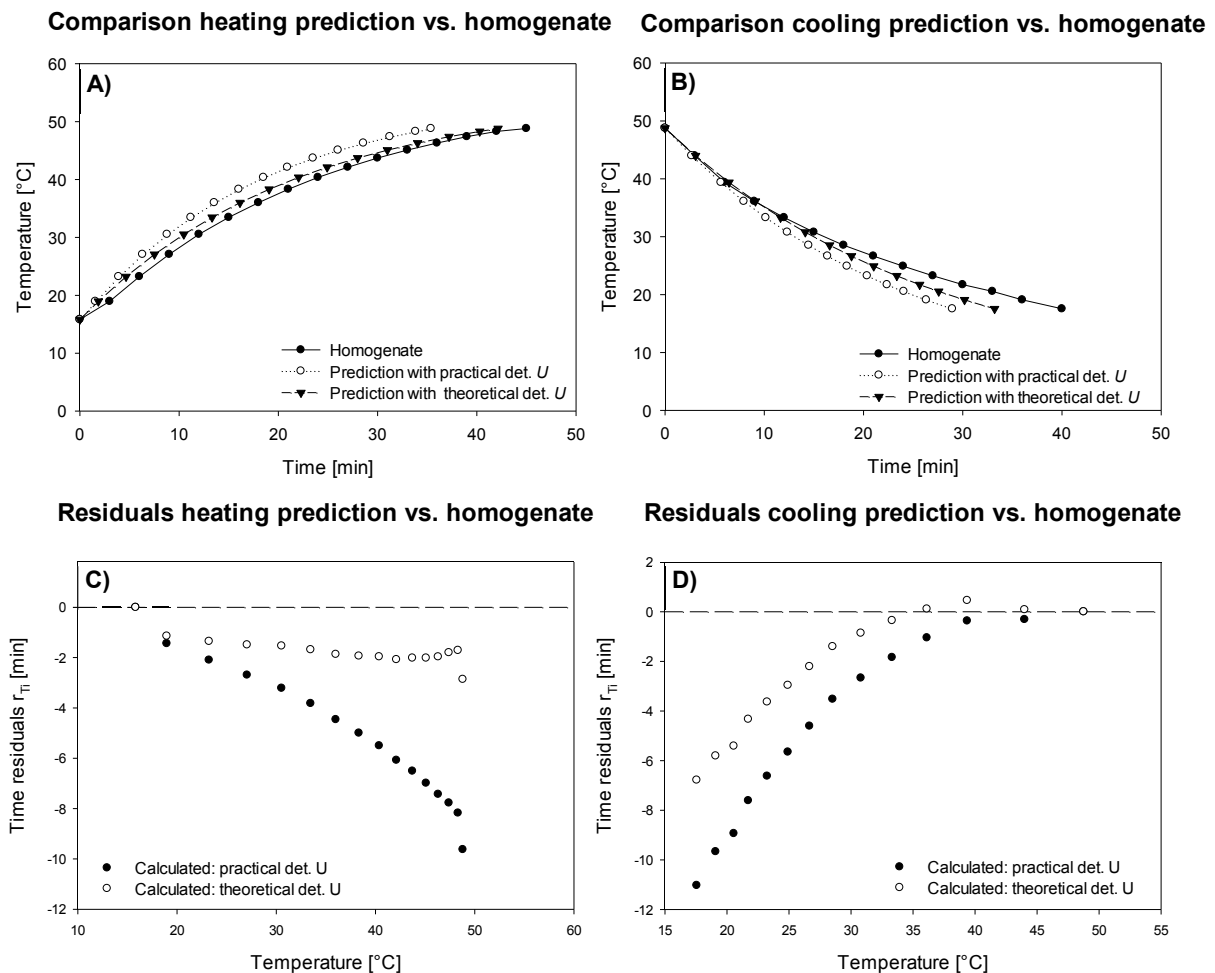


Figure 20: A) predicted course of homogenate heating with practical and theoretical determined  $U$  vs. observed course; B) predicted course of homogenate cooling with practical and theoretical determined  $U$  vs. observed course; C) time residuals between predicted course of homogenate heating with practical / theoretical determined  $U$  and observed course of homogenate; D) time residuals between predicted course of homogenate cooling with practical / theoretical determined  $U$  and observed course of homogenate

## 6.6 SDS-PAGE of large scale trials

All solutions for large scale trials were analyzed by SDS-PAGE to evaluate the effect of heat precipitation compared to the processes without heat precipitation.

Table 32: Loaded samples onto SDS-PAGE from large scale trials

Lane	Loaded solution	Loading
1	-	-
2	Precision Plus Protein™ Dual Color Standards 500µL BIO-RAD (#161-0374)	5µL
3	-	-
4	Supernatant of heat precipitation of homogenate 70/700 bar Psg.1	0.75µg GFP
5	Supernatant of homogenate 50/500 bar; Psg.2; 2x separated	0.75µg GFP
6	Supernatant of homogenate with 2% TritonX100 0/400 bar; Psg.1	0.75µg GFP
7	-	-
8	Supernatant of heat precipitation of homogenate 70/700 bar Psg.1	0.50µg GFP
9	Supernatant of homogenate 50/500 bar; Psg.2; 2x separated	0.50µg GFP
10	Supernatant of homogenate with 2% TritonX100 0/400 bar; Psg.1	0.50µg GFP
11	leer	-
12	Supernatant of heat precipitation of homogenate 70/700 bar Psg.1	0.25µg GFP
13	Supernatant of homogenate 50/500 bar; Psg.2; 2x separated	0.25µg GFP
14	Supernatant of homogenate with 2% TritonX100 0/400 bar; Psg.1	0.25µg GFP
15	Supernatant of homogenate 70/700bar Psg.1 before heat precipitation	0.50µg GFP

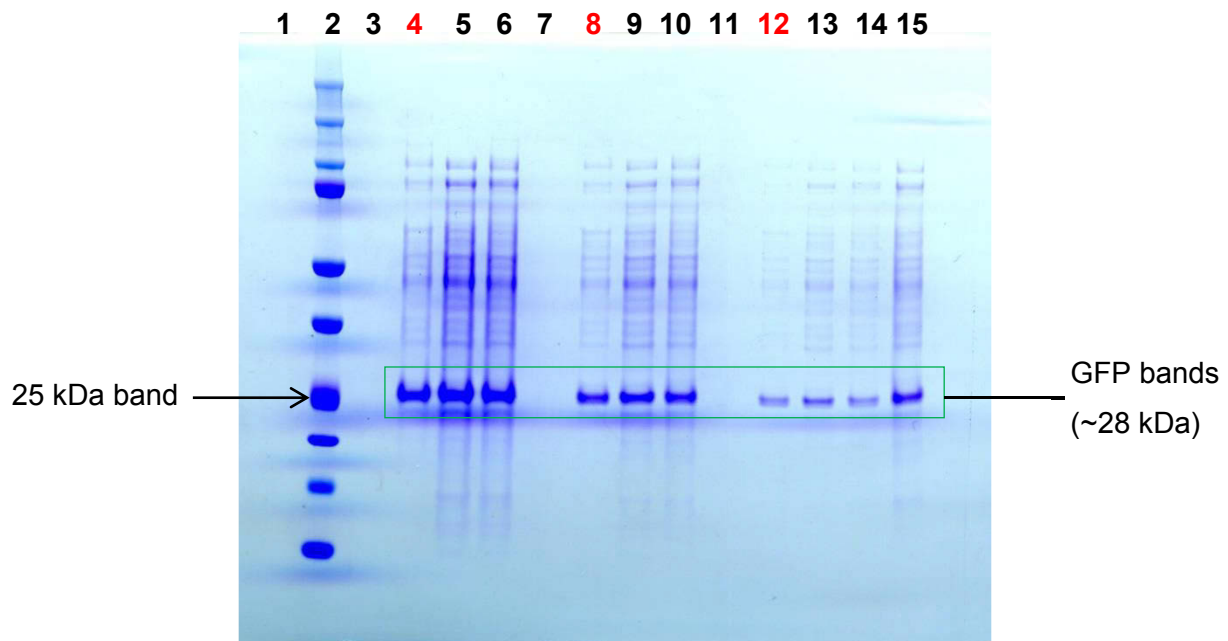


Figure 26: SDS-PAGE of large scale trials

The intensities of the bands other than GFP are significantly weaker in the supernatant of the heat precipitate (bands 4, 8 and 12), than in the other supernatants. The band patterns are the same for the supernatants of homogenates obtained from 50/500 bar, 70/700 bar and 0/400 bar. Compared to the band pattern from the supernatant of heat precipitate, it seems

downstream processing with the second passage at 40/400 bar because from the homogenization trials, bigger debris were expected. This was verified by measurement of the particle sizes of the chosen homogenate and compared to the size of the cells (see Figure 29). The step yield of homogenization was 73.4%.

The homogenate was then diluted 1:2 with water (25 L homogenate + 25 L water) for heat precipitation at 50°C. The suspension had a GFP content of 2.97 mg/mL. During precipitation the temperature profile, GFP content, turbidity and solid content were monitored. The viscosity was measured at start and at the end of precipitation.

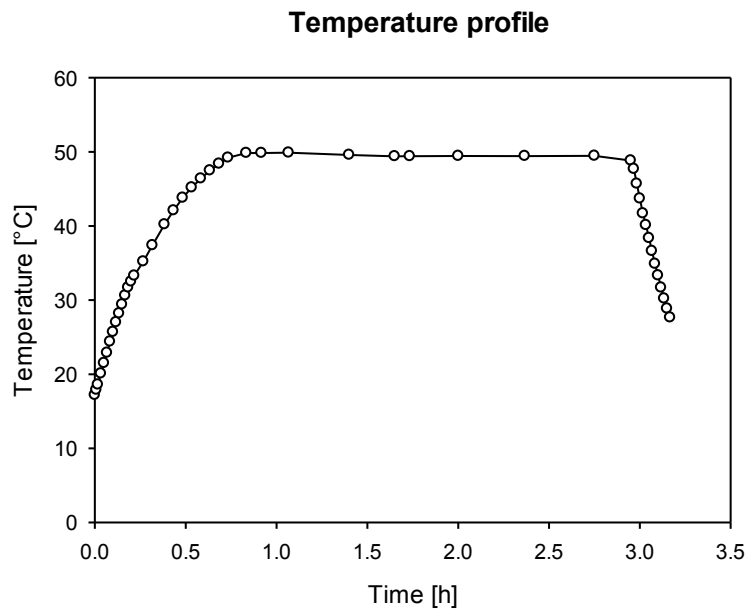


Figure 30: Optimized GFP production – temperature profile of heat precipitation; 50 L of diluted homogenate produced from homogenization at 40/400 bar over two passages with a CDM content of 25 g/L was used

Heating up of the suspension from 17.2°C to 50°C took 44 min. 50°C were held for 121 min. After the hold time, the jacket was emptied and connected to the ice water circuit. The cooling period took 25 min and was ended at 27.6°C.

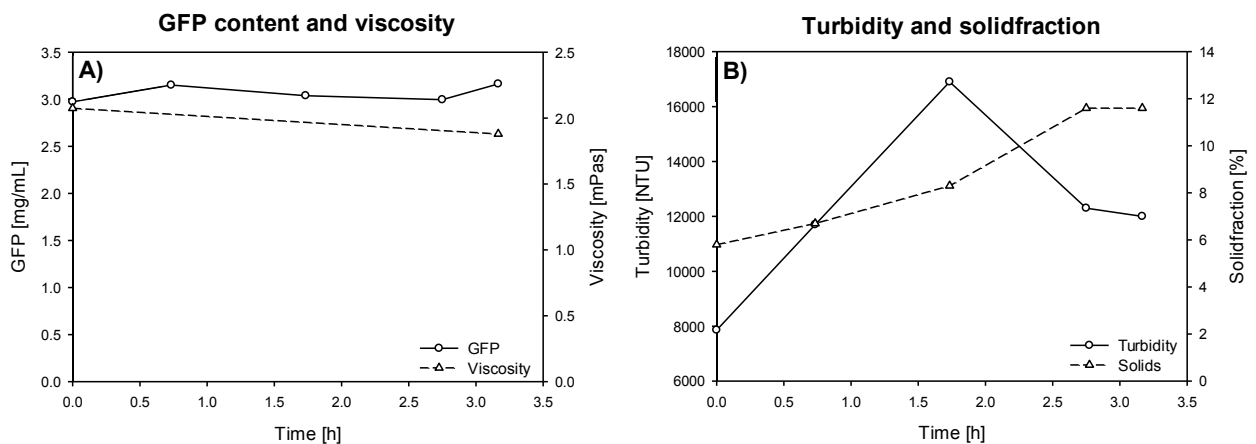


Figure 31: Optimized GFP production; A) GFP content and viscosity; B) turbidity and solid content of heat precipitation

the separation. The particles in the supernatant had a median particle size of 136 nm, which was measured before storage of the suspension.

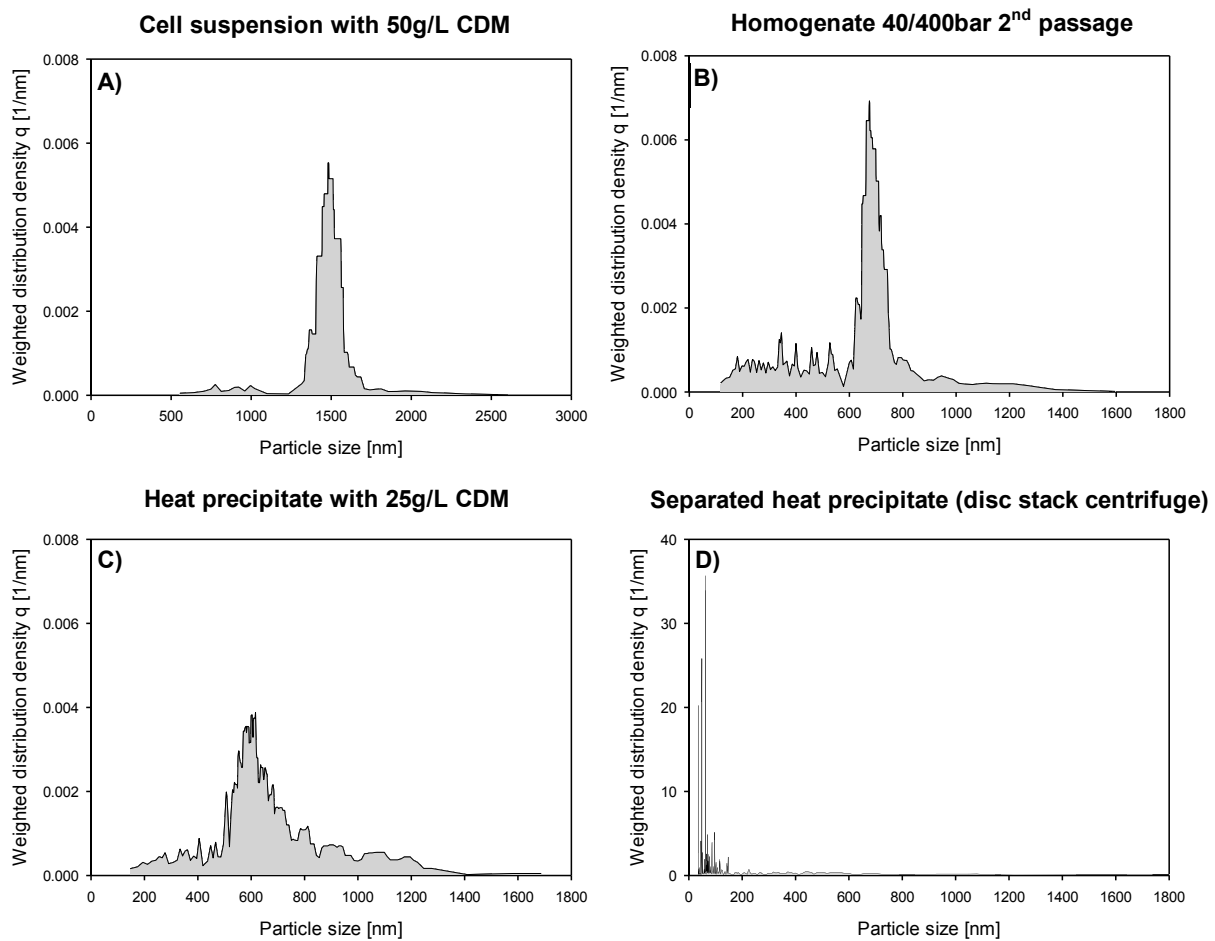


Figure 33: Optimized GFP production – particle size distributions of intact cells, homogenate (40/400 bar / 2<sup>nd</sup> passage), heat precipitated homogenate (40/400 bar / 2<sup>nd</sup> passage) and supernatant after centrifugation

The distributions of particle sizes were also determined. There is one clearly visible peak in the distribution of the cells, which showed that most of the cells were intact and there were almost no debris. The distribution broadened after homogenization and showed a dominant species of particles with a size of about 600 nm to 800 nm but also some particles with a size of <600 nm. After heat precipitation the distribution flattened out, which indicated that there were species of all sizes from 200 nm to 1400 nm. Since the area from 200 nm to 400 nm decreased, some small particles seemed to aggregate during heat treatment and therefore the 10% < x nm value increased. From the distribution of the supernatant after centrifugation it is clearly visible from the peaks in the range from 0 nm to 200 nm, that almost all particles >200 nm were removed.

After separation the supernatant was used for filtration trials to determine the appropriate filter. They showed, that a sterile filtration step was sufficient and no depth filter was required. For further downstream steps 30 L of process solution should be sterile filtrated. Therefore the scale up was calculated for 30 L and a maximum allowable flux reduction of 90%. All trials were conducted using a pressure of ~1.4 bar. For every tested filter the area required for the mentioned parameters was calculated (see Table 35).

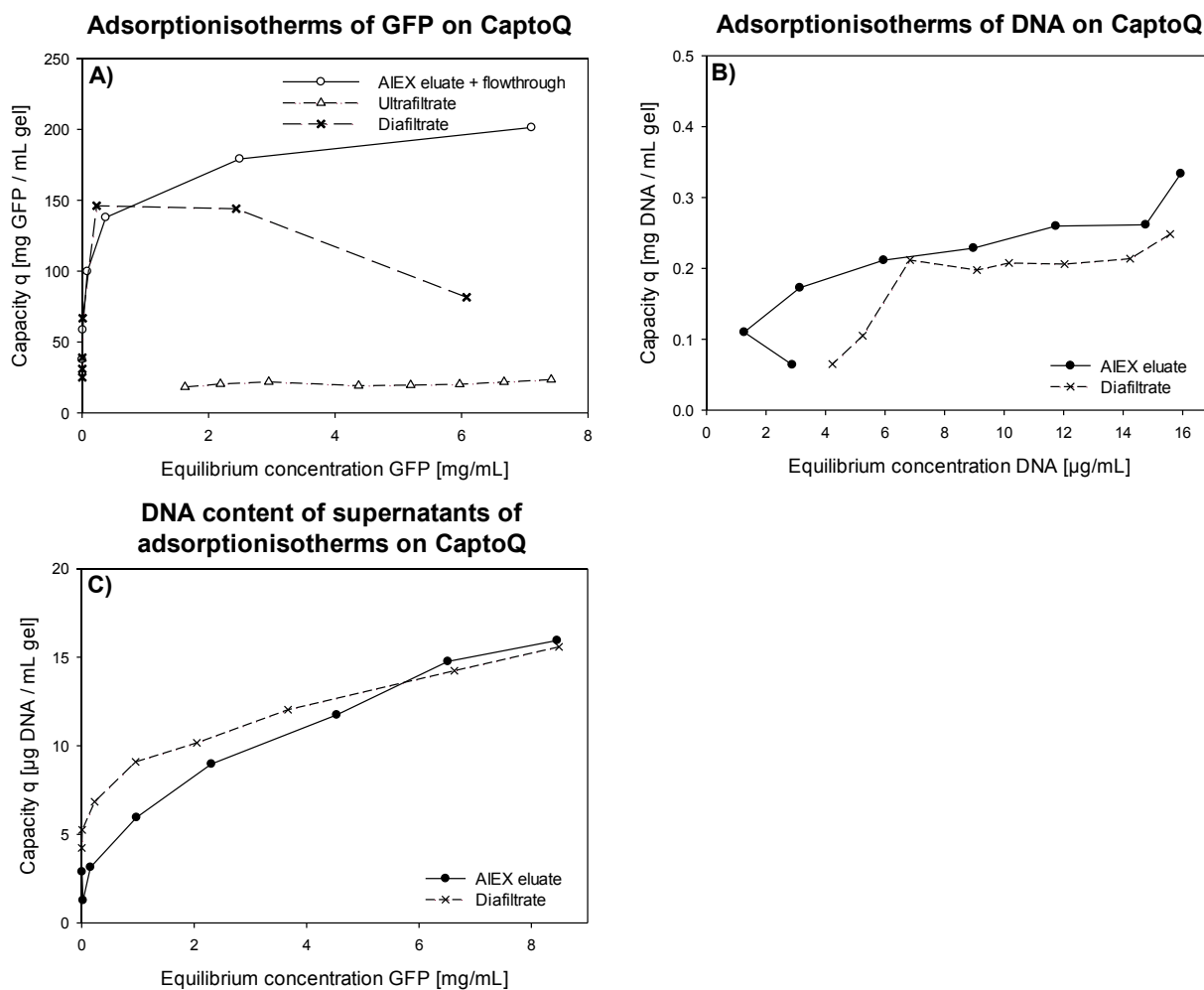


Figure 37: A) Adsorption isotherms of GFP and B) DNA and C) remaining DNA concentration as a function of GFP equilibrium concentration

For GFP the adsorption isotherm for the ultrafiltrate yielded a binding capacity of 18.35 mg/mL GFP at an equilibrium concentration of 1.63 mg/mL, which only slightly increased to a maximum load of 23.50 mg/mL at an equilibrium concentration of 7.42 mg/mL.

The GFP isotherm for the diafiltrate showed the maximum binding capacity of 146.2 mg/mL at an equilibrium concentration of 0.23 mg/mL. At higher equilibrium concentrations the binding capacity decreased to 81.63 mg/mL at 6.08 mg/mL. The form of the isotherm suggested, that there was occurring competitive binding to CaptoQ binding stronger at high concentrations. Since the DNA load was very low over the range investigated, it seemed not to be the cause for the form of the GFP adsorption behavior.

The GFP isotherm for the AIEX eluate showed the maximum binding capacity of 201.4 mg/mL at an equilibrium concentration of 7.71 mg/mL. To obtain comparable isotherms, the AIEX eluate was diluted 1:2 with AIEX flow through. Due to this the conductivities of ultrafiltrate, diafiltrate and AIEX eluate were approximately equal. Compared to the diafiltrate, the isotherm was not decreasing in the range from an equilibrium concentration of GFP of 0 to 7.71 mg/mL. Again the adsorption of DNA was neglectably small. Because there was no decrease of the GFP isotherm observed, this confirmed that not DNA was responsible for the form of the diafiltrate isotherm.